

AN ABSTRACT OF THE THESIS OF

Randall A. Keller for the degree of Doctor of Philosophy in Oceanography presented  
on February 1, 1996. Title: The Petrology, Geochemistry, and Geochronology of  
Hotspot Seamounts in the North Pacific and Arc/Backarc Volcanism on the Northern  
Antarctic Peninsula. *Redacted for Privacy*

Abstract approved: \_\_\_\_\_

Martin R. Fisk

Volcanic rocks from hotspots and island arcs/backarcs typically have enriched trace element and isotopic compositions that contain a contribution from subducted oceanic crust. Isotopic and trace element data suggest that the enriched components in hotspot volcanism are ancient subducted sediment and crust, and the enriched components in arc/backarc volcanism are hydrous fluids and melts from the subducting slab. This thesis examines the origins of these enriched components, and how they change in time and space.

The Hawaiian-Emperor seamount chain records over 81 million years of volcanism from the Hawaiian hotspot. Seamounts at the old (northern) end of the chain have isotopic compositions more depleted than anything previously reported from the Hawaiian hotspot. Detroit seamount (81 Ma) has the most depleted composition, and was created while an active spreading ridge was close to the hotspot. Proximity to a spreading ridge must have caused the hotspot to entrain and melt more of the depleted upper mantle.

The Patton-Murray seamount platform, at the old end of the Cobb hotspot track in the Gulf of Alaska, was volcanically active at 33 Ma, 27 Ma, and 17 Ma. The 33 Ma tholeiitic phase and 27 Ma alkalic phase are related to passage over the hotspot. The 17 Ma phase erupted too late to be directly related to the hotspot, but may have been caused by minor extension along a zone of weakness originally created by passage over the hotspot.

On the northern Antarctic Peninsula, volcanism occurred above a subducting slab up to 360 km from the South Shetland Trench. Volcanism on the South Shetland Arc has enriched trace element and isotopic compositions that can be modeled by mixing of subducted sediments and depleted mantle. Backarc basin volcanism in Bransfield Strait contains less of the subducted component, and the most depleted samples are distinguishable from MORB only by their slightly elevated Cs and Pb concentrations. Extreme-backarc volcanism on James Ross Island (360 km from the trench) shows no evidence for the subducted component in its trace element compositions, but its Pb isotopic ratios are affected by Pb from subducted sediment.

**The Petrology, Geochemistry, and Geochronology of Hotspot  
Seamounts in the North Pacific and Arc/Backarc Volcanism  
on the Northern Antarctic Peninsula**

by

Randall A. Keller

A THESIS

submitted to

Oregon State University

in partial fulfillment of  
the requirements for the  
degree of

Doctor of Philosophy

Presented February 1, 1996

Commencement June 16, 1996

Doctor of Philosophy thesis of Randall A. Keller presented on February 1, 1996.

APPROVED:

*Redacted for Privacy*

---

Major Professor, representing Oceanography

*Redacted for Privacy*

---

Dean of College of Oceanic and Atmospheric Sciences

*Redacted for Privacy*

---

Dean of Graduate School

I understand that my thesis will become part of the permanent collection of Oregon State University libraries. My signature below authorizes release of my thesis to any reader upon request.

*Redacted for Privacy*

---

Randall A. Keller, Author

## Acknowledgments

I am grateful to all of my committee members (Dave Christie, Bob Duncan, Martin Fisk, Dave Graham, and Anita Grunder) for participating in numerous insightful discussions on the thoughts and results in this thesis, and for providing helpful comments on various drafts of this thesis. Bob Duncan helped me convince the Ocean Drilling Program that I should participate in Leg 145 across the North Pacific. Anita Grunder led many fun and interesting fieldtrips that greatly improved my enjoyment and understanding of geology. Martin Fisk planted, nurtured, and pruned many of the ideas presented herein. Drawing on his own character-building experience as an advisee, he managed to fashion himself into an ideal advisor.

My three expeditions to Antarctica were made possible by the kindness of other scientists. Krzysztof Birkenmajer took me to Deception Island and King George Island in 1991. Jorge Strelin took me to James Ross Island in 1992, and also assisted with dredging and sampling in Bransfield Strait in 1993. Larry Lawver took me on his cruise to Bransfield Strait in 1993, and provided assistance and shiptime for dredging.

Lew Hogan, Roger Nielsen, and Andy Ungerer, all at OSU, are largely responsible for the fine quality of the argon, microprobe, and ICP-MS data (respectively) in this thesis. Bill White generously opened up his isotope lab to me during several visits to Cornell, and was always good for a discussion on the magic of isotopic analyses and interpretation. Mike Cheatham made sure that each time I left Cornell after two nearly-sleepless months of labwork, I had the most and best data my samples could provide.

I am grateful to the many students at OSU and Cornell with whom I shared laughs and learnings, especially Lance Forsythe, Bill Gallahan, Matt Gorring, Karen Harpp, Christine Orgren, Doug Pyle, and Chris Sinton. And I am especially grateful to Carol Chin for her love and support, and for making sure that I occasionally paused to have fun.

Finally, I would like to thank my parents for their patience, understanding, and support over my career as a student; a career that turned out to be far longer than they ever could have imagined.

## Contributions of Co-authors

This thesis is a collection of manuscripts that include comments and contributions by co-authors. The exceptions are Chapters 1 (Introduction) and 7 (Summary and Conclusions), which are entirely my writing, but incorporate comments from my Ph.D. committee members (D. Christie, R. Duncan, M. Fisk, D. Graham, and A. Grunder). For Chapters 2 through 6, I wrote the first draft of a manuscript and then incorporated comments and contributions from the co-authors and my Ph.D. committee members. Co-authors contributions to Chapters 2 through 6 are as follows:

Chapter 2: R. Duncan provided the opportunity and impetus for me to participate in ODP Leg 145, and contributed to interpretation of the dating results and their significance to Pacific plate motion models. M. Fisk contributed to interpretation of the geochemical results.

Chapter 3: M. Fisk suggested studying the isotopic evolution of the Hawaiian hotspot, and contributed to models of hotspot evolution and ridge-hotspot interaction. W. White contributed to interpretation of the isotopic results, and to the models of hotspot melting dynamics and ridge-hotspot interaction.

Chapter 4: R. Duncan contributed to interpretation of the dating results and the unusual temporal and geochemical aspects of the northeast Pacific seamounts, and suggested the possible models for the youngest phase of volcanism on the Patton-Murray seamount platform. M. Fisk contributed to interpretation of the geochemical results and the unusual geochemical aspects of the northeast Pacific seamounts. W. White is reviewing the manuscript.

Chapter 5: M. Fisk contributed to interpretation of the geochemical results and to the modeling. J. Smellie contributed the British Antarctic Survey dredge samples and the South Shetland Arc samples (except LH-1), and will review the manuscript. J. Strelin provided the opportunity and guidance for fieldwork on James Ross Island, and assisted with dredging, description, and sorting of the Bransfield Strait samples. W. White is reviewing the manuscript. I. Millar contributed some Sr and Nd isotopic analyses of the South Shetland Arc samples. L. Lawver contributed shiptime for the Bransfield Strait dredging and assisted with dredging operations.

Chapter 6: M. Fisk contributed to interpretation of the geochemical results. J. Smellie contributed the British Antarctic Survey dredge samples, the South Shetland Arc samples (except LH-1), and the XRF analyses, and will review the manuscript. J. Strelin assisted with dredging, description, and sorting of the Bransfield Strait samples. L. Lawver contributed shiptime for the dredging and assisted with dredging operations.

## Table of Contents

	<u>Page</u>
I. Chapter 1: Introduction .....	1
II. Chapter 2: Geochemistry and $^{40}\text{Ar}/^{39}\text{Ar}$ Geochronology of Basalts from ODP Leg 145 (North Pacific Transect).....	5
ABSTRACT.....	6
INTRODUCTION.....	6
DESCRIPTIONS OF THE SAMPLES.....	7
METHODS.....	9
RESULTS.....	13
DISCUSSION.....	27
CONCLUSIONS.....	30
ACKNOWLEDGMENTS.....	31
III. Chapter 3: Isotopic Characteristics of Cretaceous Volcanism at the Hawaiian Hotspot.....	32
ABSTRACT.....	33
INTRODUCTION.....	33
SAMPLES AND DATA.....	36
DISCUSSION AND INTERPRETATION .....	39
CONCLUSIONS.....	44
ACKNOWLEDGMENTS.....	44
IV. Chapter 4: Sixteen Million Years of Volcanism on the Patton-Murray Seamount Platform, Gulf of Alaska .....	45
ABSTRACT.....	46
INTRODUCTION.....	46
SAMPLES AND DATA.....	48
DISCUSSION .....	54
CONCLUSIONS.....	56
ACKNOWLEDGMENTS.....	56
V. Chapter 5: An Isotopic Profile Across the Northern Antarctic Peninsula: Relationships Between Subduction History and Geochemical Components .....	57
ABSTRACT.....	58
INTRODUCTION AND BACKGROUND.....	58
DISCUSSION .....	65
CONCLUSIONS.....	70
ACKNOWLEDGMENTS.....	71

## Table of Contents (Continued)

VI. Chapter 6: Geochemistry of Backarc Basin Volcanism in Bransfield Strait, Antarctica: Subducted Contributions and Along-Axis Variations .....	72
ABSTRACT.....	73
INTRODUCTION.....	73
SAMPLE LOCATIONS AND DESCRIPTIONS .....	77
RESULTS.....	79
DISCUSSION .....	90
CONCLUSIONS.....	99
ACKNOWLEDGMENTS.....	99
ANALYTICAL TECHNIQUES APPENDIX .....	99
VII. Chapter 7: Summary and Conclusions.....	101
Bibliography .....	106

## List of Figures

<u>Figure</u>	<u>Page</u>
I.1 Generalized crustal and upper mantle cross-section .....	2
II.1 Index map of the North Pacific Ocean showing Leg 145 drill sites.....	8
II.2 MgO vs. FeO*, TiO <sub>2</sub> , Zr, and Sr for samples from Detroit Seamount (Sites 883 and 884) and Meiji seamount (DSDP Site 192) .....	15
II.3 Apparent age spectrum (plateau) diagrams for: (A) Sample 145-883F-1R-3, 37–41 cm, and (B) Sample 145-883F-2R-3, 129–133 cm.....	17
II.4 Apparent age spectrum (plateau) diagram for Sample 145-884E-10R-4, 6–10 cm (plagioclase separate) .....	19
II.5 Radiometric dating results for Sample 145-884E-10R-4, 6–10 cm, (plagioclase-free) .....	20
II.6 Apparent age spectrum (plateau) diagram for Sample 145-884E-10R-6, 136–140 cm.....	21
II.7 MgO vs. FeO*, TiO <sub>2</sub> , Zr, and Sr for samples from Chinook Trough (Site 885) and Patton-Murray seamount platform (Site 887).....	22
II.8 Radiometric dating results for Sample 145-885A-8X-1, 38–42 cm .....	23
II.9 Stratigraphy for the basement portion of Hole 887D interpreted from downhole logging data and core recovery data .....	24
II.10 Radiometric dating results for Sample 145-887D-4R-4, 47–39 cm .....	25
II.11 Radiometric dating results for Sample 145-887D-7R-3, 67–70 cm .....	26
II.12 Distance (measured along seamount chain) from Kilauea vs. age for islands and seamounts in the Hawaiian-Emperor chain.....	27
III.1 Locations of samples from the Hawaiian-Emperor island/seamount chain that have been dated.....	34
III.2 Plot of sample age vs. <sup>87</sup> Sr/ <sup>86</sup> Sr for tholeiitic basalts from the Hawaiian-Emperor island/seamount chain.....	36
III.3 <sup>206</sup> Pb/ <sup>204</sup> Pb versus other isotopic ratios for tholeiitic basalts from the Hawaiian-Emperor island/seamount chain .....	40
IV.1 Locations of seamounts and spreading ridges in the northeast Pacific/Gulf of Alaska region .....	47

## List of Figures (Continued)

IV.2 Stratigraphy and geochemical characteristics of the basement portion of Hole 887D .....	50
IV.3 Sample 10R-2 dating results.....	51
IV.4 Sr/Y vs. Zr/Nb for the Hole 887D samples compared to other data from the northeast Pacific .....	52
IV.5 $^{206}\text{Pb}/^{204}\text{Pb}$ vs. other isotopic ratios for the Hole 887D samples compared to other data from the northeast Pacific .....	53
V.1 Map of the northern Antarctic Peninsula showing locations of volcanism discussed in this study.....	59
V.2 Generalized crustal and upper mantle cross-section of the northern Antarctic Peninsula .....	60
V.3 $^{87}\text{Sr}/^{86}\text{Sr}$ vs. Ba/Nb for northern Antarctic Peninsula basalts.....	61
V.4 $^{206}\text{Pb}/^{204}\text{Pb}$ vs. other isotopic ratios for northern Antarctic Peninsula basalts.....	63
VI.1 Generalized tectonic map of the northern Antarctic Peninsula.....	75
VI.2 Bathymetric map of the Bransfield Rift axis.....	76
VI.3 Major element plots of Bransfield Strait glass analyses by electron microprobe .....	81
VI.4 Major element plots of Bransfield Strait whole rock analyses by x-ray fluorescence.....	83
VI.5 Whole rock MgO vs. trace element plots for Bransfield Strait volcanism.....	86
VI.6 NMORB-normalized element-ratio plots of South Shetland Island Arc and Bransfield Strait samples .....	87
VI.7 $^{206}\text{Pb}/^{204}\text{Pb}$ vs. $^{87}\text{Sr}/^{86}\text{Sr}$ and $^{143}\text{Nd}/^{144}\text{Nd}$ of South Shetland Island Arc and Bransfield Strait samples compared to other backarc basins .....	91
VI.8 Ba/Nb vs. Ce/Pb, and $\text{K}_2\text{O}/\text{Rb}$ vs. Ba/Rb of South Shetland Island Arc and Bransfield Strait samples .....	93
VI.9 Longitude vs. $\text{K}_2\text{O}/\text{Rb}$ and $\text{K}_2\text{O}/\text{P}_2\text{O}_5$ of Bransfield Strait samples .....	95
VII.1 Evolution of Sr isotopic ratios of hotspots over time.....	102

## List of Tables

<u>Table</u>	<u>Page</u>
II.1 Whole rock major and trace element concentrations by XRF.....	10
II.2 $^{40}\text{Ar}/^{39}\text{Ar}$ plateau and isochron ages for basalts from Leg 145 .....	12
II.3 Representative analyses of minerals in Sample 145-884E-10R-4, 0–4 cm .....	13
II.4 Representative analyses of minerals in samples from Site 887 .....	14
III.1 Measured and initial isotopic ratios and trace element ratios.....	38
IV.1 Trace element and isotopic data for ODP Hole 887D basalts .....	49
V.1 Isotopic data for basalts from the South Shetland Island Arc.....	62
V.2 Isotopic data for samples dredged from Bransfield Strait.....	65
V.3 Isotopic data for basalts from the James Ross Island Volcanic Group .....	66
V.4 Comparison of sediment, arc, depleted mantle, and JRVG data .....	67
V.5 Isotopic characteristics and possible identities of mixing components .....	68
VI.1 Electron microprobe analyses of Bransfield Strait glass samples .....	80
VI.2 Representative XRF analyses of whole rock samples from Bransfield Strait ....	82
VI.3 Representative ICP-MS whole rock analyses of Bransfield Strait and South Shetland Islands samples .....	85
VI.4 Representative isotopic analyses of Bransfield Strait samples.....	89

# The Petrology, Geochemistry, and Geochronology of Hotspot Seamounts in the North Pacific, and Arc/Backarc Volcanism on the Northern Antarctic Peninsula

## Chapter 1

### Introduction

One of the basic tenets of modern igneous petrology is that there is a relationship between the geochemistry of a volcanic rock and the tectonic setting in which it erupted (Pearce and Cann, 1973). Volcanism at divergent plate boundaries (i.e., mid-ocean ridge basalts) has depleted trace element and radiogenic isotope signatures that require derivation from a source that has had very low concentrations of incompatible elements for a long time (White and Hofmann, 1982). The accepted identity of this depleted source is the convective upper mantle.

Volcanism within plates (hotspots, rifts) is enriched in incompatible trace element and radiogenic isotopes relative to mid-ocean ridge basalts (MORBs). The enriched signatures of many ocean island (hotspot) basalts, even those far from any subduction zone, are consistent with a component of recycled sediment or altered basaltic crust in their sources (Hofmann and White, 1982). Exactly how this subducted component makes its way into a mantle plume that creates a hotspot is unclear. Some suggest that the deeply subducted crust is the initial source of the mantle plume (Hofmann and White, 1982; Hart, 1988), while others believe that the subducted component resides somewhere above the plume source, and is picked up by the plume as it ascends through the mantle (Han and Graham, submitted).

Volcanism at convergent plate boundaries (arcs/backarcs) is enriched (relative to MORB) in incompatible elements that are mobile in hydrous solutions (e.g., Sr, Cs, Ba, and Pb), but is depleted (again relative to MORB) in the elements that are relatively immobile under hydrous conditions (e.g., Nb and Ta; Figure I.1) (Tatsumi et al., 1986). The lack of enrichment in Nb and Ta sets convergent-margin volcanic rocks apart from those from intraplate settings. Based upon these characteristics, and isotopic mixing arguments, the source of convergent-margin volcanism is thought to be depleted

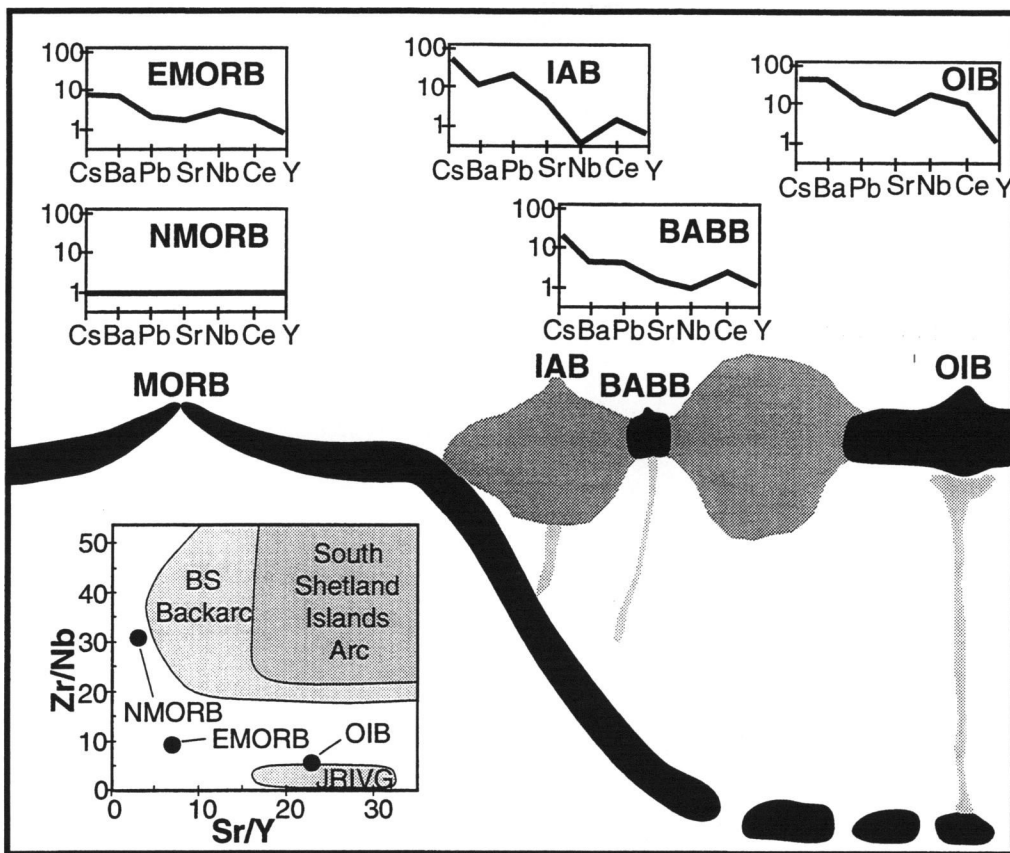


Figure I.1. Generalized crustal and upper mantle cross-section of spreading ridge, subduction zone, and ocean island, showing possible paths of crustal recycling. Basalts in each tectonic setting are abbreviated: MORB = mid-ocean ridge basalt, IAB = island arc basalt, BABB = backarc basin basalt, OIB = ocean island basalt. Typical NMORB-normalized element-ratio diagrams are shown for each environment. Normal MORB (NMORB), enriched MORB (EMORB), and OIB values are from Sun and McDonough (1989). IAB and BABB values are representative analyses from the South Shetland Islands and Bransfield Strait, respectively (see Chapter 6). The Sr/Y vs. Zr/Nb compositions of the South Shetland Arc, Bransfield Strait backarc, and James Ross Island Volcanic Group (JRIVG) extreme backarc are shown compared to oceanic basalt values of Sun and McDonough (1989).

upper mantle mixed with a few percent or less of a recycled component derived from subducted oceanic crust (sediments and/or altered basalt) (Armstrong, 1971; Kay, 1980).

Thus, both intraplate and subduction-zone volcanism contain recycled components that, though different from one another, are both derived from subducted oceanic crust.

We refer to this recycled component as the 'enriched' component because it is rich in incompatible trace elements and radiogenic isotopes. The behavior of this enriched component in hotspot and subduction zone volcanism over time and space is the unifying theme of this thesis. First, I examine the long-term history of two hotspots (Chapters 2, 3, and 4) in an attempt to determine what role an enriched component might play in their chemical and isotopic evolution. Then, by identifying the nature and amount of enriched component in subduction zone volcanism (Chapters 5 and 6), I attempt to determine how the interaction between a subducted slab and the upper mantle varies over time and space. Once this is determined, I will be able to constrain the nature of the enriched component in the slab that makes it through the subduction zone and into the deeper mantle to contribute to hotspot volcanism. This introduction provides some background on crustal recycling, and poses some of the questions that I eventually hope to answer in this thesis.

To examine the long-term behavior of hotspots, I studied basalts recovered by ocean drilling from the old end of two hotspot-created, linear seamount chains in the North Pacific: Detroit seamount platform in the northwest Pacific near the old end of the Hawaiian hotspot track (Chapters 2 and 3), and Patton-Murray seamount platform in the northeast Pacific at the old end of the Cobb hotspot track (Chapters 2 and 4). These two hotspot tracks are compositionally distinct from one another, but both show evidence for having more enriched signatures now than in the past. The Hawaiian hotspot has a primitive mantle signature now (Stille et al., 1986), but during the Late Cretaceous it had a depleted upper mantle signature very similar to mid-ocean ridge basalt (Chapter 3 and Keller et al., 1994, 1995). The Cobb hotspot has had a depleted upper mantle signature for at least the past 33 million years (Chapter 4 and Keller et al., 1995), although the oldest products of the hotspot may be slightly more depleted than the more recent ones (Keller et al., 1995). Other hotspot tracks that have been sampled in sufficient detail to determine their long-term chemical evolution (Réunion and Kerguelen: White et al., 1990; Weis et al., 1992) also became more enriched with time. In Chapters 2 through 4, I discuss whether this trend toward more enriched compositions is a phenomenon within the mantle plume itself, or is it that depleted upper mantle played a more important role in hotspot volcanism in the past.

By the time oceanic crust reaches a subduction zone, it includes sediments and hydrothermal-alteration products that are enriched (relative to fresh MORB) in incompatible elements. If the enriched components in subducted crust are entirely extracted in the subduction zone and erupted in the arc and backarc, then there is no net

flux of the enriched components to the mantle. There is considerable evidence in the geochemical signature of convergent margin volcanism that at least some of the enriched components of the subducted crust are indeed extracted and recycled to the surface at the arc and backarc (e.g., Armstrong, 1971). It is still controversial as to whether these enriched components are removed mechanically (i.e., sediment underplating), extracted by partial melting, extracted in a fluid phase from dehydration reactions and metamorphism, or that different combinations of these mechanisms occur at different depths and temperatures in the subduction zone (Tatsumi et al., 1986; Morris et al., 1990). The approach taken here is to determine which of these processes are important at a single subduction zone by carefully examining across-axis and along-axis variations in the trace element and isotopic characteristics of the arc and backarc volcanism. After determining the amount of enriched component that is subducted and the amount of enriched component that is recycled to the overlying volcanism, the amount of enriched component available to contribute to the deeper mantle may be calculated by subtraction (e.g., White and Patchett, 1984). This is one objective of the project on the northern Antarctic Peninsula subduction zone (Chapters 5 and 6).

Tertiary-Quaternary volcanic rocks on the northern Antarctic Peninsula erupted above a subducted slab at a wide range of distances (100–360 km) from the active South Shetland Trench. The wide spatial dispersion of the volcanism makes it possible to determine which elements are removed from the downgoing slab to contribute to volcanism at the subduction zone, and which elements remain with the slab that is carried deeper into the mantle. In Chapter 5, I present isotopic data from volcanic rocks from three distances from the trench, and show that there is almost no subducted component in the volcanism 360 km from the trench. Chapter 6 examines in more detail the composition of the volcanism between 100 and 150 km from the trench, and how that composition varies along strike of the subduction zone.

This thesis is in manuscript format. Chapter 1 (this chapter) is a common introduction, and Chapter 7 is a common conclusion. Chapters 2 through 6 contain contributions by co-authors (see Contributions of Co-authors section). Chapter 2 was published in the Ocean Drilling Program Leg 145 Scientific Results volume (Keller et al., 1995). Chapters 3 through 6 are manuscripts in various stages of preparation for publication in scientific journals.

## Chapter 2

### Geochemistry and $^{40}\text{Ar}/^{39}\text{Ar}$ Geochronology of Basalts from ODP Leg 145 (North Pacific Transect)

Randall A. Keller, Robert A. Duncan, and Martin R. Fisk

Published in D.K. Rea, I.A. Basov, D.W. Scholl, and J.A. Allan (Eds.), 1995,  
Proceedings of the Ocean Drilling Program, Scientific Results, vol. 145, p. 333–344.

## ABSTRACT

Leg 145 of the Ocean Drilling Program recovered basalts at three locations in the North Pacific. Drilling at Sites 883 and 884 on Detroit Seamount, near the northern end of the Emperor seamount chain, penetrated altered pillow basalts that may be of transitional composition (Site 883) and thick flows of tholeiitic composition (Site 884). The Site 883 basalts did not yield a reliable crystallization age, but a basalt from Site 884 yielded an age of 81 Ma. This is the first reliable radiometric age determination for the northern end of the Emperor seamounts, and lengthens the period of known activity of the Hawaiian-Emperor seamount chain by approximately 15 million years. Published Pacific-plate-motion models predict an age for Detroit Seamount of approximately 65 to 75 Ma. Either the 81 Ma tholeiite is from very early in the history of an unusually long-lived volcano, or the velocity of the Pacific plate relative to the Hawaiian hotspot increased some time between 81 and 65 Ma.

Drilling at Site 885 was expected to reach Lower(?) Cretaceous oceanic crust near the Chinook Trough in the central North Pacific. Basalt was contacted beneath less than one-half of the expected thickness of sediments. The basalt is altered, but appears to have a mid-ocean ridge tholeiite composition. It yielded a concordant  $^{40}\text{Ar}/^{39}\text{Ar}$  plateau age of only 80 Ma, suggesting that volcanism associated with the Late Cretaceous plate reorganization and formation of the Chinook Trough affected a wider area than previously thought.

Drilling at Site 887 on the Patton-Murray seamount platform in the Gulf of Alaska recovered transitional basalts overlain by two chemically-distinct types of alkalic basalts. The Site 887 basalts are chemically similar to samples dredged from other seamounts in the northeast Pacific.  $^{40}\text{Ar}/^{39}\text{Ar}$  dating of an alkalic basalt midway in the section yielded an age of 27 Ma. The uppermost basalt recovered is a sediment-bounded sill that yielded an  $^{40}\text{Ar}/^{39}\text{Ar}$  age of 17 Ma. Thus, volcanic activity at this seamount platform spanned at least 10 million years.

## INTRODUCTION

Leg 145 of the Ocean Drilling Program (ODP) sampled basalts at the old ends of two seamount chains in the North Pacific. Sites 883 and 884 penetrated basalt at two locations on Detroit Seamount, at the northern end of the Hawaiian-Emperor seamounts

(Figure II.1). Before this expedition no samples suitable for radiometric dating existed from the Emperor seamounts north of Suiko Seamount (750 km south of Detroit Seamount). Basalts recovered from Meiji seamount (240 km northwest of, and the only Emperor seamount older than, Detroit Seamount) during Leg 19 of the Deep Sea Drilling Project (DSDP) did not yield a reliable  $^{40}\text{Ar}/^{39}\text{Ar}$  age (Dalrymple et al., 1980). The best age constraint for Meiji was a minimum age of 70 Ma based on biostratigraphic data from the overlying sediments (Worsley, 1973). Leg 145 also recovered basalts at Site 887 on the Patton-Murray seamount platform, the northern end of a prominent linear seamount chain in the Gulf of Alaska (Figure II.1). Patton-Murray seamount platform had previously been dredged and radiometrically dated (Dalrymple et al., 1987).

Leg 145 also drilled to basalt in the north-central Pacific near the Chinook Trough (Figure II.1). The Chinook Trough is thought to be a spreading center that was last active during a plate reorganization at approximately 82 Ma (Rea and Dixon, 1983). Based upon site survey geophysical data, drilling was expected to penetrate approximately 150 m of Tertiary and Cretaceous sediments and bottom in Lower(?) Cretaceous oceanic crust.

## DESCRIPTIONS OF THE SAMPLES

Drilling at the two basement holes at Site 883 penetrated 24 m and 38 m of basalt at locations approximately 20 m apart, and recovered a series of fractured and altered basalt pillows and flows (Rea, Basov, Janacek, Palmer-Julson, et al., 1993). Numerous lithologic units were identified aboard ship, but this was based almost entirely upon the presence of glassy margins rather than observable lithologic differences. The majority of the samples contain 10%–15% plagioclase microphenocrysts, with minor amounts of altered olivine microphenocrysts. Seven samples were selected for XRF analyses from a range of depths below seafloor in the two holes. Two of these seven samples were selected for  $^{40}\text{Ar}/^{39}\text{Ar}$  dating. There were no significant macroscopic differences among the samples.

Drilling at Hole 884E penetrated 87 m into basement and recovered basaltic pillows and massive flows (Rea, Basov, Janacek, Palmer-Julson, et al., 1993). Aboard the *Resolution* these were divided into 13 lithologic units based upon the presence of chilled margins or changes in crystallinity. These units fall into three general lithologic groups:

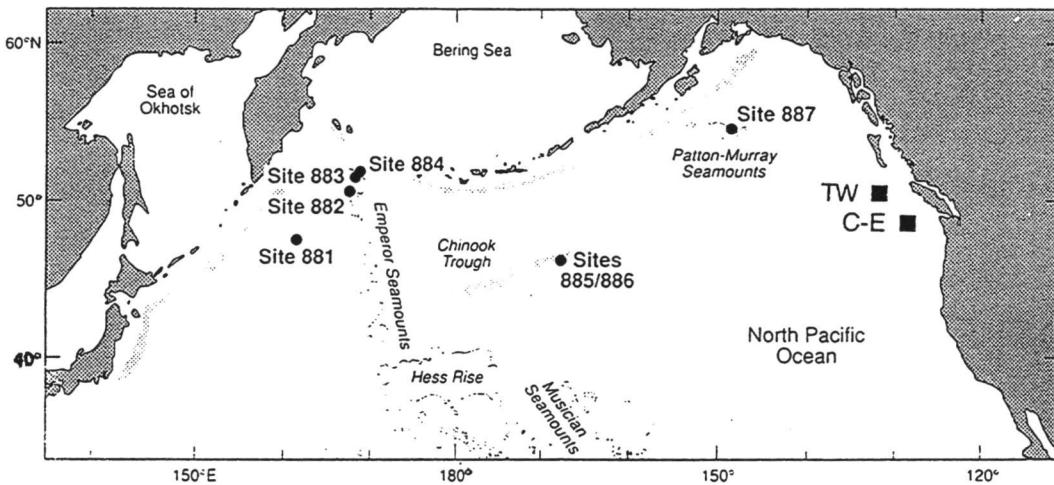


Figure II.1. Index map of the North Pacific Ocean showing the locations of Leg 145 drill sites (modified from Rea, Basov, Janacek, Palmer-Julson, et al., 1993). Locations for Tuzo Wilson seamounts (TW) and Cobb-Eickelberg seamounts (C-E) are shown for comparison to Site 887 (see text).

(1) aphyric, massive (up to 30 m thick) basalt flows (Units 1, 6, and 7); (2) moderately to highly plagioclase-phyric to megaphyric, massive (up to 6.5 m thick) basalt flows (Units 2–5 and 8–10); and (3) highly plagioclase- to plagioclase-olivine-phyric pillow basalts (Units 11–13). Two representative samples from each of these three groups were chosen for XRF analyses, and one sample each from two of the groups was used in  $^{40}\text{Ar}/^{39}\text{Ar}$  incremental heating experiments.

Drilling at Sites 885 and 886 encountered basalt after coring less than one-half of the anticipated 150 m of sediment (Rea, Basov, Janacek, Palmer-Julson, et al., 1993). Approximately 60 cm of angular cobbles of altered, aphyric basalt were recovered at each site. The Site 885 basalt was in slightly larger fragments and appeared less altered, so it was chosen for shore-based XRF and  $^{40}\text{Ar}/^{39}\text{Ar}$  analyses.

Drilling at Site 887 penetrated 87 m beneath the first basalt, and recovered 16 m of highly clinopyroxene-plagioclase-phyric to sparsely plagioclase-phyric basalts ranging from massive flows to cobbles that may be pillow fragments (Rea, Basov, Janacek, Palmer-Julson, et al., 1993). Aboard the *Resolution* the basalts were divided into five

lithologic units, and six representative samples from four of these units were selected for shore-based XRF analyses, and two of these were selected for  $^{40}\text{Ar}/^{39}\text{Ar}$  analyses.

## METHODS

Normally, basalt samples are analyzed in the X-ray fluorescence (XRF) laboratory aboard the *JOIDES Resolution* for major and trace element concentrations, but technical problems and rough seas limited the shipboard analyses to trace elements in samples from Sites 883 and 884 only (Rea, Basov, Janacek, Palmer-Julson, et al., 1993). A subset of those samples, and samples from Sites 885 and 887, were analyzed for major and trace element concentrations in this post-cruise study. The results from the shipboard and shore-based laboratories are within analytical error of each other, so only the more complete shore-based data set is presented here (Table II.1).

After shipboard examination of hand specimens and thin sections, 20 samples of representative diversity were selected for shore-based XRF analyses. Concentrations of 23 major and trace elements were measured at Washington State University on a wavelength-dispersive Rigaku 3370 automatic X-ray fluorescence spectrometer following the procedures of Hooper (1981). Each powdered sample was mixed with lithium tetraborate, fused, ground, and refused. Element concentrations were determined by comparing X-ray intensities from the unknowns with recommended values for eight international standards. Estimated precision and accuracy are generally better than 5% for major elements, and better than 10% for most trace elements, although precision can be less than 20% at concentrations below 50 ppm.

Seven of the samples that were analyzed by XRF were also selected for  $^{40}\text{Ar}/^{39}\text{Ar}$  age determinations (Table II.2). The least altered samples with the coarsest grained groundmass were usually preferred. All samples were crushed to 0.5–1-mm chips, ultrasonically washed in deionized water, and dried in a warm oven. Splits of approximately 1 g of the prepared chips were sealed in evacuated quartz tubes and irradiated in the Oregon State University (OSU) TRIGA reactor, where they received a neutron dose of approximately  $0.7 \times 10^{18} \text{ n/cm}^2$ . The flux gradient and the efficiency of the conversion of  $^{39}\text{K}$  to  $^{39}\text{Ar}$  by neutron capture were monitored with samples of the biotite standard FCT-3 ( $27.7 \pm 0.2 \text{ Ma}$ ; Hurford and Hammerschmidt, 1985). Further details of the sample preparation and irradiation procedures are given in Duncan (1991).

**Table II.1. Whole-rock major and trace element concentrations by XRF.**

Hole	Detroit Seamount										Chinook Trough										Patton-Murray seamount platform									
	883E					883F					884E					885A					887D									
Section	20R-2	20R-3	21R-1	21R-5	21R-6	1R-3	2R-3	3R-1	2R-2	4R-4	6R-3	10R-4	10R-5	10R-6	8X-1	4R-4	7R-3	8R-2	10R-2	12R-1	13R-1									
Interval	1-2	23-26	23-26	108-111	26-30	37-41	129-133	100-104	32-36	23-27	30-33	6-10	83-86	136-140	38-42	47-49	67-70	84-89	68-71	13-18	18-21									
SiO <sub>2</sub>	46.7	46.6	46.7	47.0	46.5	45.4	46.5	45.6	48.8	50.1	49.3	48.5	48.4	49.4	49.4	49.5	47.5	47.1	49.9	49.1	48.8									
Al <sub>2</sub> O <sub>3</sub>	14.1	15.5	14.4	15.2	15.2	16.9	14.7	14.9	15.1	15.8	15.0	19.7	23.5	21.0	14.8	15.0	15.0	15.6	16.4	15.4	14.9									
TiO <sub>2</sub>	2.74	2.11	2.19	2.12	2.26	2.39	2.07	2.15	1.37	1.26	1.53	0.95	0.77	0.97	2.34	2.03	3.68	3.32	1.80	1.95	1.96									
FeO*	13.7	11.4	10.4	10.8	10.8	12.8	11.1	13.7	10.8	9.0	11.1	7.6	5.6	7.0	12.2	10.1	13.2	13.1	9.1	11.2	11.5									
MnO	0.22	0.12	0.15	0.17	0.19	0.18	0.12	0.15	0.18	0.16	0.16	0.11	0.10	0.11	0.20	0.22	0.16	0.16	0.12	0.19	0.19									
CaO	11.4	12.6	12.8	11.7	11.4	12.1	12.7	11.8	11.6	13.2	12.1	13.4	14.3	14.0	11.3	11.9	8.0	8.3	11.9	11.6	11.1									
MgO	6.01	4.70	6.11	6.96	7.09	1.77	5.95	5.13	8.82	6.75	7.11	6.99	4.60	5.02	5.35	6.43	5.66	6.34	5.44	5.25	6.41									
K <sub>2</sub> O	0.39	1.24	1.06	0.63	0.53	1.46	1.09	1.20	0.10	0.61	0.13	0.11	0.35	0.25	0.54	0.52	0.85	0.84	0.53	0.63	0.70									
Na <sub>2</sub> O	3.04	2.99	2.85	3.04	3.07	3.37	2.81	2.86	2.42	2.74	2.84	2.28	2.14	2.32	2.83	3.21	3.69	3.27	3.28	2.85	2.43									
P <sub>2</sub> O <sub>5</sub>	0.32	0.31	0.24	0.23	0.25	0.45	0.23	0.30	0.11	0.09	0.11	0.08	0.06	0.08	0.20	0.30	0.55	0.45	0.19	0.43	0.18									
Total	98.56	97.61	96.87	97.90	97.28	96.88	97.25	97.77	99.37	99.72	99.39	99.72	99.77	100.06	99.13	99.13	98.30	98.38	98.67	98.59	98.09									
Ni	76	63	69	74	61	134	49	79	94	72	85	47	72	42	64	31	45	53	33	31										
Cr	150	158	153	159	151	146	147	302	198	271	246	214	245	196	219	74	85	131	118	120										
Sc	41	44	40	43	41	34	37	49	48	47	35	28	34	45	31	30	32	38	45	44										
V	297	291	325	335	325	288	348	297	313	355	201	165	236	414	257	316	278	248	301	301										
Ba	46	19	26	29	96	44	54	4	0	0	4	0	0	0	161	131	125	13	6	0										
Rb	71	51	4	5	21	53	50	1	14	2	1	7	6	13	7	14	9	12	12	8										
Sr	234	217	213	214	294	215	228	123	113	128	149	160	159	145	427	280	281	208	194	163										
Zr	135	137	132	141	147	133	137	81	67	84	60	50	60	144	115	272	237	118	127	125										
Y	33	35	33	33	36	33	33	31	31	33	21	16	21	43	24	46	38	31	36	37										
Nb	10	12	10	10	11	11	11	4	3	5	2	2	3	7	22	35	30	7	10	9										
Ga	19	26	21	22	21	21	21	15	16	20	16	18	14	25	19	27	29	20	22	17										
Cu	88	128	103	100	100	129	89	140	106	180	112	101	109	52	75	34	39	76	79	72										
Zn	180	103	93	92	135	102	151	74	73	100	59	51	52	120	100	130	118	90	102	97										

Note: Sample 145-883E-20R-2 is an average of 4 glass analyses by electron microprobe at OSU. Oxides are in weight percent; trace elements are in parts per million. FeO\* is total Fe as FeO.

Argon extractions were performed at OSU by incremental heating in a glass extraction line using radio-frequency (RF) induction heating. Samples were held at each heating step for 30 min, and then analyzed with an AEI MS-10S mass spectrometer. Heating steps were set from RF power levels, determined from previous experience to divide total Ar into six approximately equal portions. After correction for background, mass fractionation, and isotopic interferences, the data were reduced to age spectra and  $^{39}\text{Ar}/^{40}\text{Ar}$  vs.  $^{36}\text{Ar}/^{40}\text{Ar}$  isotope correlation plots.

Two different methods were used to calculate plateau ages (Table II.2) from heating steps that formed a contiguous sequence of at least three statistically indistinguishable (at  $1\sigma$ ) step ages. The first method weights each step age by the inverse of its variance to arrive at a weighted mean (Dalrymple et al., 1987). This mean emphasizes the more precisely determined step ages, and is the plateau age shown in the age spectra figures. The second method of calculating a mean weights each step by the % $^{39}\text{Ar}$  released in that step. This method produces more conservative (larger) calculated standard errors than the first method, but otherwise there are no significant differences between the results from the two methods.

Isochron ages (Table II.2) were determined from the  $^{39}\text{Ar}/^{40}\text{Ar}$  vs.  $^{36}\text{Ar}/^{40}\text{Ar}$  correlation plots, which allow independent determination of both the sample age and initial  $^{40}\text{Ar}/^{36}\text{Ar}$  composition (McDougall and Harrison, 1988). Only those steps that had concordant ages in the plateau plots were used for the isochron. The goodness-of-fit parameter SUMS has a  $\chi^2$ -distribution with ( $N - 2$ ) degrees of freedom (York, 1969), with  $N$  being the number of steps used for the isochron regression. Experiments that yield an acceptable goodness-of-fit, a  $^{40}\text{Ar}/^{36}\text{Ar}$  intercept near the atmospheric value (295.5), and relatively concordant isochron and plateau ages are likely to have determined reliable crystallization ages (Lanphere and Dalrymple, 1978).

Apparent Ca/K was calculated for each heating step using the relationship  $\text{Ca}/\text{K} = 1.852 \times ^{37}\text{Ar}/^{39}\text{Ar}$  (Fleck et al., 1977; Walker and McDougall, 1982).

Microprobe analyses were done on a four-spectrometer Cameca SX-50 at OSU using natural mineral phases and basalt glass from the Smithsonian reference collection as standards. Software provided with the microprobe corrected measured concentrations for atomic number, absorption, and fluorescence effects. Glass in Sample 145-883E-20R-2, 1–2 cm, (Table II.1) was analyzed with 15-kV accelerating voltage, 30-nA beam current, and 10-s counting times, except Ti and Al were counted for 20 s. Precision based upon multiple analyses of the Makaopuhi basalt glass is reported in Forsythe and Fisk (1994). Conditions for the plagioclase analyses (Tables II.3 and II.4) were 15-kV

Table II.2.  $^{40}\text{Ar}/^{39}\text{Ar}$  plateau and isochron ages for basalts from ODP Leg 145.

Core, section, interval	<u>Plateau age <math>\pm 1\sigma</math> (Ma)</u>		Isochron age $\pm 1\sigma$ (Ma)	Integrated age (Ma)	$^{39}\text{Ar}$ (% of total)	N	SUMS (N - 2)	$^{40}\text{Ar}/^{36}\text{Ar}$ intercept
	Weighted by $1/\sigma^2$	Weighted by % $^{39}\text{Ar}$						
145-883F								
-1R-3, 37–41 cm	No plateau developed			(50.4)				
-2R-3, 129–133 cm	No plateau developed			(52.6)				
145-884E								
-10R-4, 6–10 cm, pl	No plateau developed							
-10R-4, 6–10 cm, np	$81.2 \pm 1.3$	$80.8 \pm 2.6$	$80.0 \pm 0.9$	(128.1)				
-10R-6, 136–140 cm	No plateau developed			77.8 (47.5)	85.1	5	0.1	$294.6 \pm 4.0$
145-885A								
-8X-1, 38–42 cm	$80.0 \pm 1.0$	$80.6 \pm 1.2$	$79.3 \pm 0.8$	80.6	100.0	5	0.1	$301.0 \pm 3.3$
145-887D								
-4R-4, 47–49 cm	$17.1 \pm 0.3$	$17.0 \pm 0.5$	$16.8 \pm 0.5$	17.0	100.0	6	1.7	$295.4 \pm 1.4$
-7R-3, 67–70 cm	$27.3 \pm 0.3$	$27.4 \pm 0.3$	$27.5 \pm 0.4$	27.4	100.0	5	3.0	$292.7 \pm 2.1$

Note: The pl and np suffixes for Sample 145-884E-10R-4, 6–10 cm, denote plagioclase-megacryst separate and plagioclase-megacryst-free separates, respectively. Integrated ages given in parentheses are unreliable, and are not crystallization ages.

**Table II.3. Representative analyses of minerals in Sample 884E-10R-4, 0-4 cm.**

	Olivine <sup>a</sup>	Clinopyroxene				Rim	Core
					Plagioclase		
SiO <sub>2</sub>	39.60	52.60	49.87	49.29		55.52	49.53
Al <sub>2</sub> O <sub>3</sub>	0.04	2.11	1.85	3.33		27.33	31.66
TiO <sub>2</sub>	0	0.63	1.14	1.64			
FeO*	14.48	8.42	19.02	13.90		0.84	0.52
MnO	0.14	0.21	0.57	0.38			
CaO	0.38	19.89	17.71	18.66		9.94	14.96
MgO	45.32	16.15	9.83	12.65		0.12	0.27
Na <sub>2</sub> O		0.26	0.38	0.46		5.81	2.96
K <sub>2</sub> O						0.08	0.03
NiO	0.16						
Cr <sub>2</sub> O <sub>3</sub>		0.08	0	0.01			
Sum	100.12	100.35	100.37	100.32		99.64	99.93

Note: Concentrations are in weight %, and are by electron microprobe at Oregon State University. FeO\* is total Fe as FeO.

<sup>a</sup> Average of four analyses of a single phenocryst.

accelerating voltage, 30-nA beam current, and 10-s counting times. Conditions for the clinopyroxene and olivine analyses (Tables II.3 and II.4) were 15-kV accelerating voltage, 50-nA beam current, and 10-s counting times, except Ti was counted for 20 s. Na was analyzed first in all procedures, and showed no evidence for loss under these conditions.

## RESULTS

All seven of the Site 883 samples analyzed by XRF are chemically similar to each other (Table II.1), and show no systematic variation with stratigraphic position. Their MgO contents range from 2 to 7 wt% (Figure II.2), although the sample with the lowest MgO also has the lowest SiO<sub>2</sub> (Table II.1), and there is no correlation between MgO content and Ni or Cr content. Incompatible element concentrations increase slightly with decreasing MgO, except that those elements most susceptible to alteration (e.g. K, Rb, Ba) do not show a correlation with MgO. Incompatible element ratios are essentially constant (except for those elements susceptible to alteration). What little variation there is in the Site 883 samples that is not due to alteration can be accounted for by minor amounts of fractional crystallization.

**Table II.4. Representative analyses of minerals in samples from Site 887.****Clinopyroxene**

Sample	887D-4R-4,			887D-10R-2, 68-71 cm			
	49-50 cm	Core	Rim	Core	w/mega	Gm	Gm
Description	Gm						
SiO <sub>2</sub>	47.13	44.51	48.70	46.36	47.01	48.88	52.69
Al <sub>2</sub> O <sub>3</sub>	5.17	7.25	3.64	5.44	6.02	4.97	2.14
TiO <sub>2</sub>	1.95	4.10	1.70	3.21	2.59	1.74	0.58
FeO*	8.35	10.92	13.85	11.23	11.82	8.83	6.14
MnO	0.16	0.15	0.33	0.24	0.21	0.18	0.15
CaO	20.58	20.84	20.48	21.16	19.91	20.96	21.17
MgO	13.86	11.43	10.68	11.52	12.17	13.96	16.84
Na <sub>2</sub> O	0.38	0.43	0.43	0.45	0.42	0.34	0.23
Cr <sub>2</sub> O <sub>3</sub>	0.27	0.02	0	0	0	0.03	0.12
Sum	97.85	99.65	99.81	99.61	100.15	99.89	100.06

**Plagioclase**

Sample	887D-4R-4, 49-50 cm			887D-10R-2, 68-71 cm	
	Rim	Core		Gm	Mega
Description					
SiO <sub>2</sub>	61.46	50.73		50.86	45.01
Al <sub>2</sub> O <sub>3</sub>	23.26	29.91		30.94	35.35
FeO*	0.34	0.58		0.61	0.20
CaO	4.49	13.01		14.03	18.08
MgO	0.02	0.14		0.16	0.17
Na <sub>2</sub> O	8.39	3.93		3.43	1.16
K <sub>2</sub> O	0.81	0.19		0.06	0.04
Sum	98.77	98.49		100.09	100.01

Note: Concentrations are in weight %, and are by electron microprobe at Oregon State University. FeO\* is total Fe as FeO.

Description codes: Gm – groundmass crystal, Core – core of phenocryst, Rim – rim of phenocryst, w/mega –with plagioclase megacryst, Mega – megacryst.

The two samples with the highest MgO contents have one-half of the K<sub>2</sub>O and an order of magnitude lower Rb than the other samples, and may be the least altered samples recovered at the site. Aboard ship the area of the core around these two samples appeared fresher (blacker) than the rest of the core. Samples from deeper in the hole than these two samples were not analyzed on shore, but shipboard trace element analyses suggest that they are similar to samples from the upper part of the section.

The highly altered condition of the samples makes it difficult to determine whether their original igneous compositions were alkalic or tholeiitic. The two samples thought to be the least altered are the lowest in Na<sub>2</sub>O + K<sub>2</sub>O, but still plot above the silica saturation line in SiO<sub>2</sub> vs. Na<sub>2</sub>O + K<sub>2</sub>O space. However, all of the samples may be too altered to be classified using the alkali elements. TiO<sub>2</sub> contents in the samples are

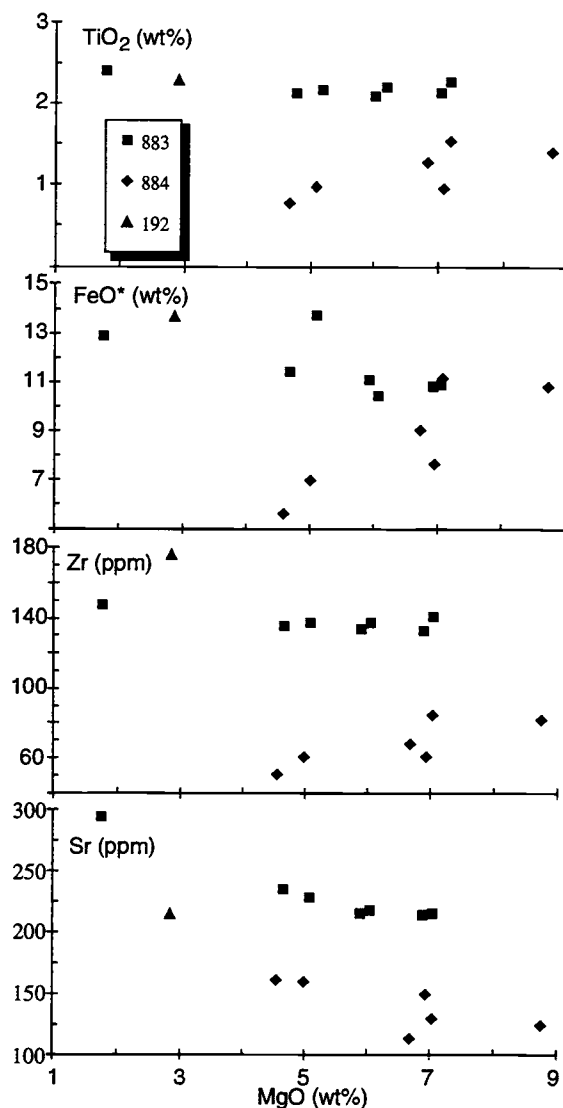


Figure II.2. MgO vs. FeO\*, TiO<sub>2</sub>, Zr, and Sr for samples from Detroit Seamount (Sites 883 and 884) and Meiji seamount (DSDP Site 192).

between 2.1 and 2.4 wt%, which when compared to Hawaiian alkalic and tholeiitic basalts is not diagnostic of either. The same is true for other incompatible elements. Thus the samples may be transitional. The chemistry of the Site 883 basalts is quite similar to that of the DSDP Site 192 (Meiji seamount) basalt, which was tentatively classified based upon mineralogy as an alkali basalt (Stewart et al., 1973), but later analyses of glass and pyroxene in the sample suggested that it may be tholeiitic

(Dalrymple et al., 1980). The composition of the Site 883 basalts is equally as ambiguous.

Many of the pillow margins recovered at Site 883 contained fresh glass. Microprobe analyses of the glass (Table II.1) yielded data similar to the whole-rock XRF analyses, with the exception of K<sub>2</sub>O, which is much lower in the glass. This may represent the true K<sub>2</sub>O content of the Site 883 basalts prior to alteration, in which case the Site 883 basalts are less alkalic than indicated by the whole-rock data, but would still be classified as alkalic basalts based upon SiO<sub>2</sub> vs. total alkalis.

The six samples from Site 884 analyzed by XRF (Table II.1) range from 4.6 to 8.8 wt% MgO (Figure II.2). Their low alkali contents suggest that they are tholeiitic (Table II.1). Four of the samples contained plagioclase megacrysts (Rea, Basov, Janacek, Palmer-Julson, et al., 1993), which explains their higher Al<sub>2</sub>O<sub>3</sub> and CaO contents and consequently lower MgO, TiO<sub>2</sub>, and FeO\* contents. The small chemical differences between the samples that are not due to alteration or the effects of the plagioclase megacrysts can be accounted for by minor amounts of fractional crystallization.

Even when the effects of the plagioclase megacrysts are considered, all of the Site 884 samples have unusually low incompatible trace element concentrations when compared with typical ocean island tholeiites. Their moderate MgO and Ni contents indicate that they are not of exceptionally primitive composition, so their low incompatible element concentrations must be due to large extents of melting, or melting of an unusually depleted source. Tholeiitic basalts with such low incompatible element concentrations (TiO<sub>2</sub> < 1.5, Sr < 200, Zr < 100) have not been reported from the Hawaiian Islands, but do occur at other ocean islands (e.g., Galapagos – Geist et al., 1986; White et al., 1993; Nauru – Castillo et al., 1986; Réunion/Kerguelen – Weis et al., 1992). Site 884 was located deep on the flank of Detroit Seamount, and may represent an early phase of volcanism that is not usually sampled by dredges or exposed on islands.

A few representative microprobe analyses of phenocrysts in Sample 145-884E-10R-4, 0-4 cm, are given in Table II.3. The clinopyroxene compositions are compatible with the tholeiitic nature of the basalts: TiO<sub>2</sub> and Al<sub>2</sub>O<sub>3</sub> contents are higher than in clinopyroxenes from mid-ocean ridge tholeiites, but similar to clinopyroxenes in tholeiites from Suiko Seamount (Clague et al., 1980).

All of the samples from Site 883 are fine grained and have highly altered groundmass; however, two of the coarsest grained and least altered were selected for <sup>40</sup>Ar/<sup>39</sup>Ar dating. Sample 145-883F-1R-3, 37-41 cm, is a highly plagioclase-olivine-

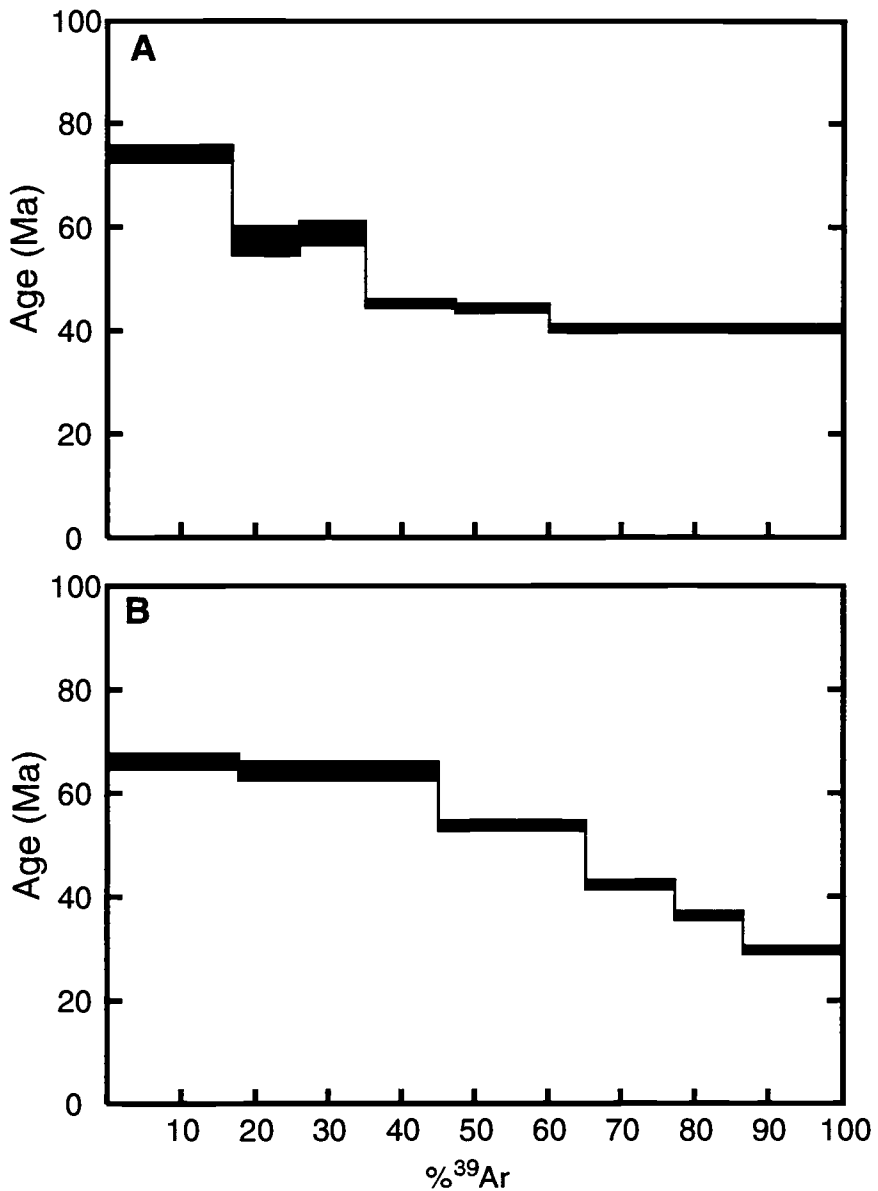


Figure II.3. Apparent age spectrum (plateau) diagrams for: (A) Sample 145-883F-1R-3, 37–41 cm, and (B) Sample 145-883F-2R-3, 129–133 cm. Heights of the black boxes indicate the analytical standard error ( $\pm 1 \sigma$ ) about each calculated step age.

microphyric basalt from a pillow interior. Sample 145-883F-2R-3, 129–133 cm, is a moderately plagioclase-microphyric basalt from a pillow interior. Neither of these samples yielded a concordant plateau age (Figure II.3), and could not be fit with a statistically significant isochron. Both samples show a decrease in apparent age with increasing temperature steps, which is characteristic of samples that have experienced

$^{39}\text{Ar}$  recoil from relatively K-rich to K-poor sites during neutron irradiation. It also appears that these samples have lost radiogenic  $^{40}\text{Ar}$  from low-temperature sites. In this case the only age estimates possible are calculated by recombining the Ar compositions from all temperature steps (Integrated ages 50 to 53 Ma in Table II.2). In view of the likelihood of radiogenic  $^{40}\text{Ar}$  loss, we consider these as minimum age estimates only. The extensive alteration and fine-grained nature of the samples recovered at Site 883 make them poorly suited to  $^{40}\text{Ar}/^{39}\text{Ar}$  analysis, and further dating of samples from this site was not attempted.

Sample 145-884E-10R-4, 6-10 cm, is a highly plagioclase-olivine-clinopyroxene-phyric basalt containing plagioclase megacrysts. This sample was hand-picked into a plagioclase component and a plagioclase-free component and was run as two separate samples. The plagioclase separate did not yield a reliable isochron or concordant plateau age (Figure II.4). The erratic and high apparent ages of most of the heating steps are consistent with excess  $^{40}\text{Ar}$  in the megacrysts due to incomplete equilibration with atmospheric  $^{40}\text{Ar}$  upon eruption. The integrated age of this sample, which does not represent a true crystallization age, is 128.1 Ma (Table II.2). The plagioclase-free component of this same sample, however, yielded a good plateau age and isochron (Figure II.5). The calculated plateau age is  $81.2 \pm 1.3$  Ma, and the calculated isochron age is  $80.0 \pm 0.9$  Ma (Table II.2), which are concordant. Isotopic data for the five steps that define the plateau produced an excellent isochron fit, with an initial  $^{40}\text{Ar}/^{36}\text{Ar}$  of atmospheric composition. Hence, we conclude that the tholeiitic portion of Detroit Seamount was constructed at 81 Ma. The phases outgassing during the first five temperature steps have similar Ca/K ratios (Figure II.5C), appropriate to fine-grained matrix. The highest temperature step, which yielded a younger age than the plateau, reflecting radiogenic  $^{40}\text{Ar}$  loss, produced a Ca/K appropriate to plagioclase (200–800; Table II.3).

Sample 145-884E-10R-6, 136-140 cm, is a highly plagioclase-phyric basalt from a pillow interior. This sample did not yield a reliable isochron or concordant plateau age (Figure II.6), and appears to have lost radiogenic  $^{40}\text{Ar}$  during alteration. The small age plateau at approximately 80 Ma may be fortuitous in its similarity to the crystallization age of Sample 145-884E-10R-4, 6-10 cm, or it may represent the crystallization age.

One of the aphyric basalt cobbles from Site 885 (Sample 145-885A-8X-1, 38-42 cm) was selected for XRF analysis (Table II.1). The basalt has 5.4 wt% MgO (Figure II.7) and 49.4 wt% SiO<sub>2</sub>. It plots as a subalkaline basalt, but the alkali and alkali earth

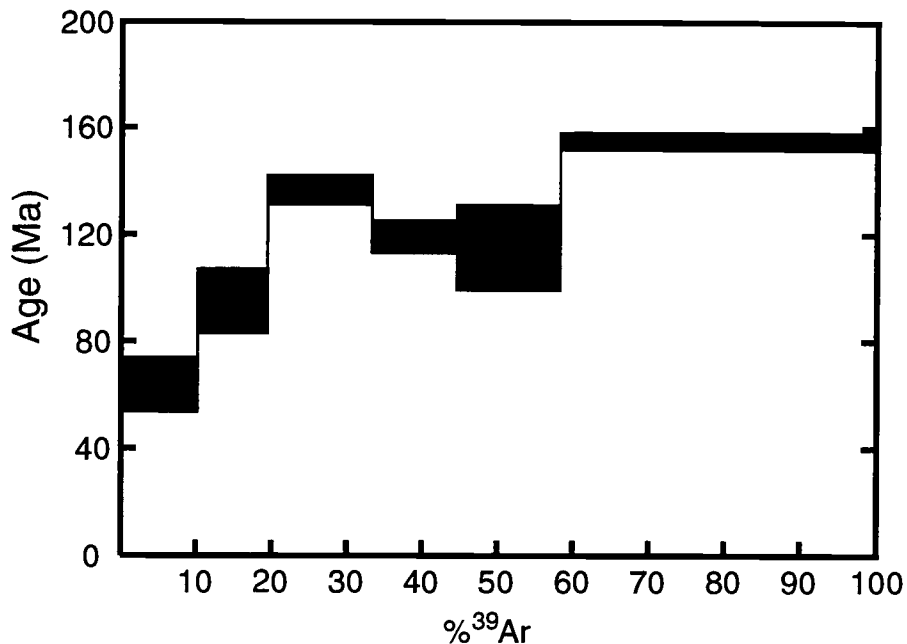
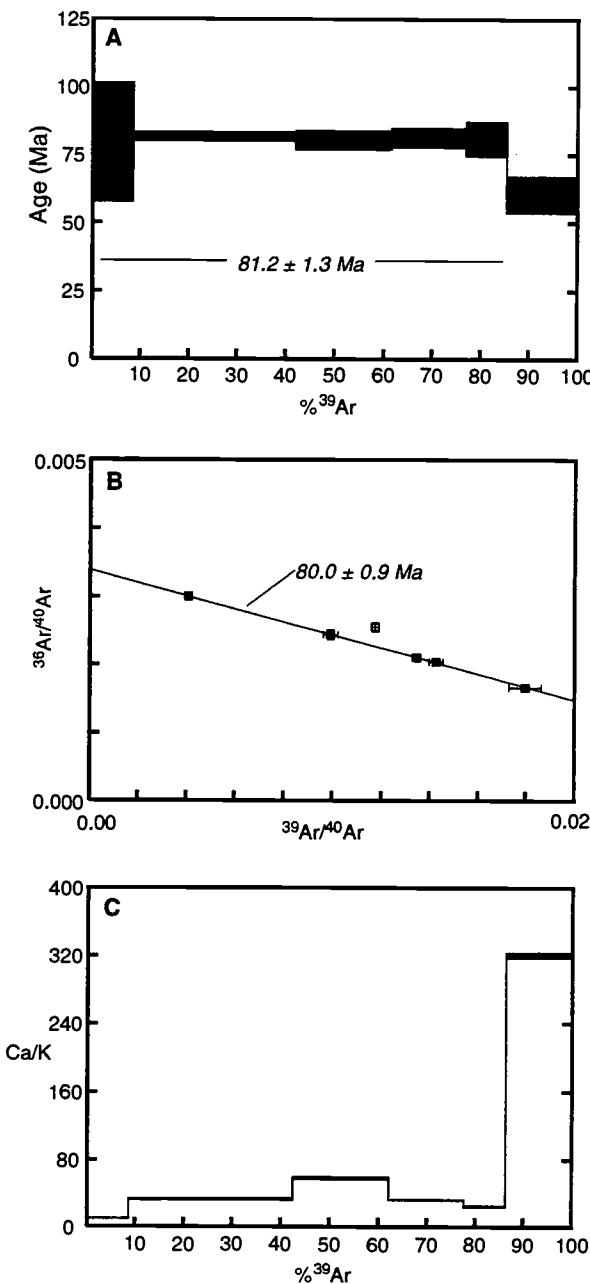


Figure II.4. Apparent age spectrum (plateau) diagram for Sample 145-884E-10R-4, 6–10 cm (plagioclase separate). Details as in Figure II.3.

element concentrations in this sample are suspect because of alteration. High Y (and therefore low Zr/Y and Nb/Y) is consistent with it being a mid-ocean ridge tholeiite.

The same aphyric basalt cobble that was selected for XRF was also sampled for  $^{40}\text{Ar}/^{39}\text{Ar}$  age dating. The sample yielded a plateau age of  $80.0 \pm 1.0$  Ma, and an isochron age of  $79.3 \pm 0.8$  Ma (Figure II.8 and Table II.2). The isochron age is statistically significant, and the  $^{40}\text{Ar}/^{36}\text{Ar}$  intercept is only slightly above the atmospheric value. Hence, we conclude that 80 Ma is a reliable crystallization age for this basalt. This age is younger than the Early(?) Cretaceous age of seafloor in the area predicted from analysis of marine magnetic anomalies (Rea and Dixon, 1983), but is consistent with the observation that the basalt was encountered after drilling only 66 m of sediment instead of the 150 m of sediment expected from interpretation of seismic reflections records. Also, drilling did not penetrate the Lower Cretaceous carbonates that are thought to underlie all of the North Pacific (Rea, Basov, Janacek, Palmer-Julson, et al., 1993). The high stratigraphic position and young age of the basalt therefore suggest that it is not true basement, but represents a volcanic rejuvenation of the area associated with the Late Cretaceous plate reorganization at approximately 82 Ma (Rea and Dixon,



**Figure II.5.** Radiometric dating results for Sample 145-884E-10R-4, 6–10 cm, (plagioclase-free). A. Apparent age spectrum (plateau) diagram. B.  $^{39}\text{Ar}/^{40}\text{Ar}$  vs.  $^{36}\text{Ar}/^{40}\text{Ar}$  isochron diagram with a point for each heating step shown in A. C. Apparent Ca/K release diagram. Heights of the black boxes in the gas release plots (A and C) indicate the analytical standard error ( $\pm 1 \sigma$ ) about each calculated step age or Ca/K. A plateau age (Table II.2) was determined from the weighted mean of contiguous, concordant gas increment steps. The isochron age was determined from the best-fitting line to collinear gas increment compositions (filled squares), after York (1969). The Ca/K compositions reflect the minerals outgassing as a function of temperature.

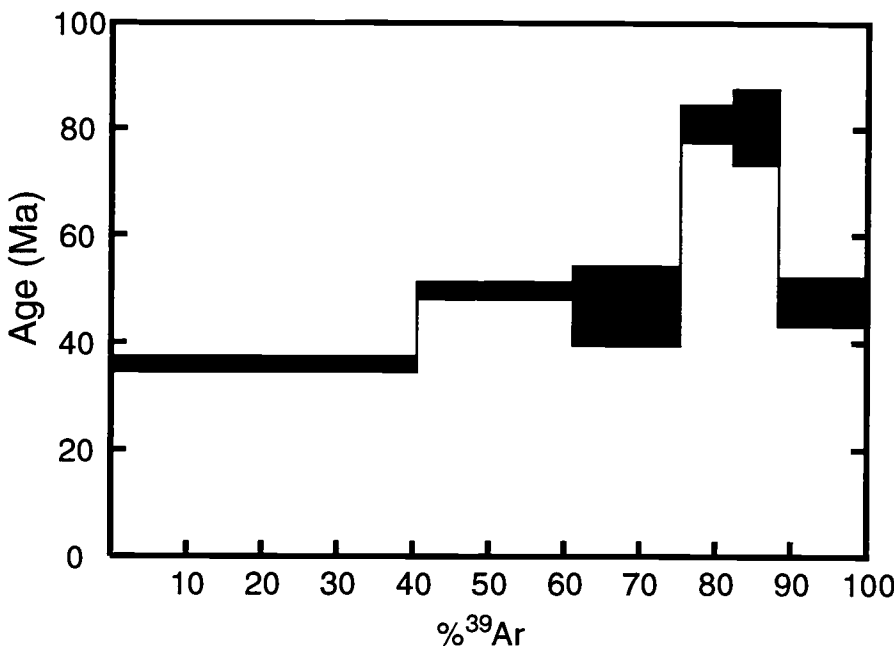


Figure II.6. Apparent age spectrum (plateau) diagram for Sample 145-884E-10R-6, 136–140 cm. Details as in Figure II.3.

1983; Rea, Basov, Janacek, Palmer-Julson, et al., 1993). Volcanism associated with the Chinook Trough spreading center apparently affected a wider area of the north central Pacific than was previously thought.

Six representative basalts from a range of depths in Hole 887D were chosen for XRF analysis. Their narrow ranges in MgO and SiO<sub>2</sub> contents (5.2 to 6.4 wt% and 47.1 to 49.5 wt%, respectively; Table II.1 and Figure II.7) contrast with their much wider relative ranges of many other elements (Table II.1). Nb contents vary by a factor of 5 (7 to 35 ppm), whereas most other incompatible elements vary by a factor of 2 or so (e.g., Sr: 163–427 ppm; Zr: 115–272 ppm; Y: 24–46 ppm). With the exception of Ba, alteration does not appear to be controlling these variations. Nor can simple fractional crystallization explain these variations.

Representative electron microprobe analyses of clinopyroxene and plagioclase in the Site 887 basalts are given in Table II.4. The high TiO<sub>2</sub> and Al<sub>2</sub>O<sub>3</sub> in clinopyroxene in Sample 145-887D-7R-3, 67–70 cm, reflects the strongly alkalic character of the middle group of basalts. Clinopyroxene in Sample 145-887D-10R-2, 68–71 cm, from the lower group of basalts is much lower in TiO<sub>2</sub> and Al<sub>2</sub>O<sub>3</sub>, with the exception of a

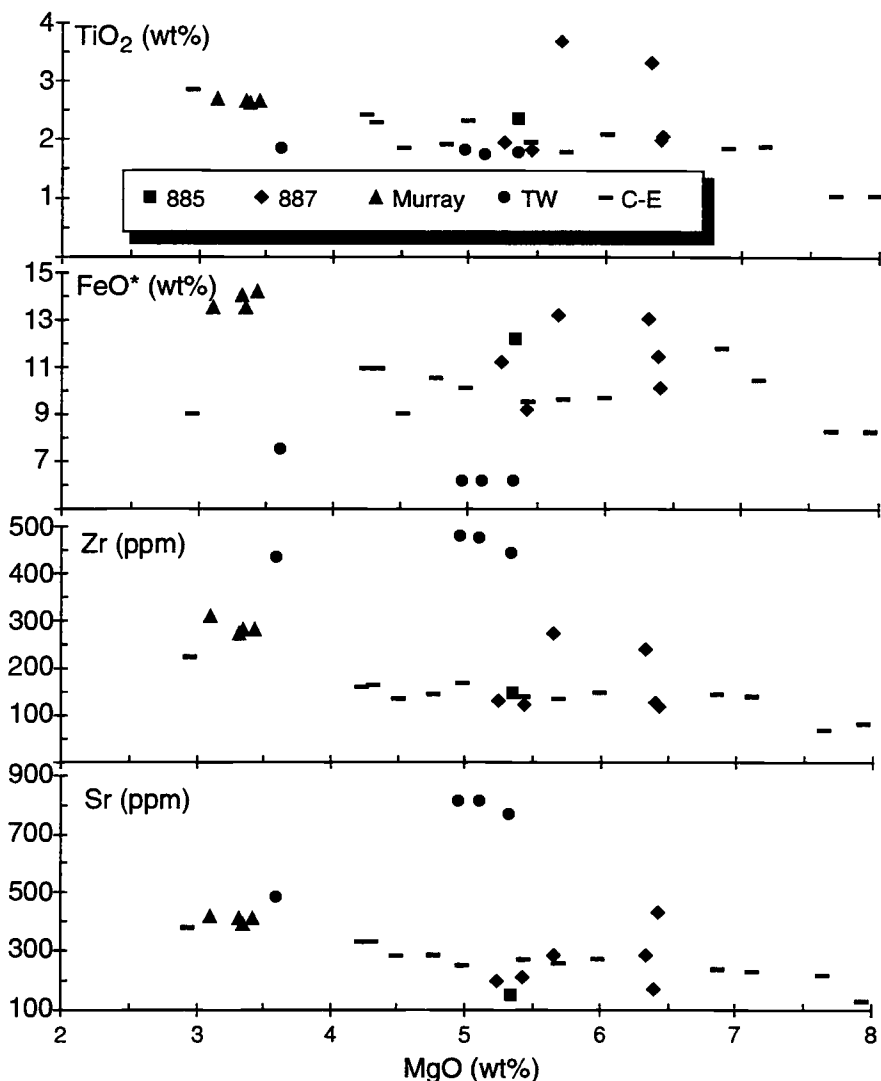


Figure II.7.  $\text{MgO}$  vs.  $\text{FeO}^*$ ,  $\text{TiO}_2$ ,  $\text{Zr}$ , and  $\text{Sr}$  for samples from Chinook Trough (Site 885) and Patton-Murray seamount platform (Site 887). Shown for comparison are data from other seamounts in the northeast Pacific: Murray = Murray seamount (data from Dalrymple et al., 1987), TW = Tuzo Wilson seamounts (data from Allan et al., 1993), and C-E = Cobb-Eickelberg seamounts (data from Desonie and Duncan, 1990). Murray seamount is 40 km from Site 887. Locations of Cobb-Eickelberg and Tuzo Wilson seamounts are shown in Figure II.1.

clinopyroxene that is in a glomerocryst with a plagioclase megacryst. Plagioclase analyses from that same sample show the large contrast between the megacrysts, which are An<sub>90</sub>, and groundmass phenocrysts of plagioclase (Table II.4).

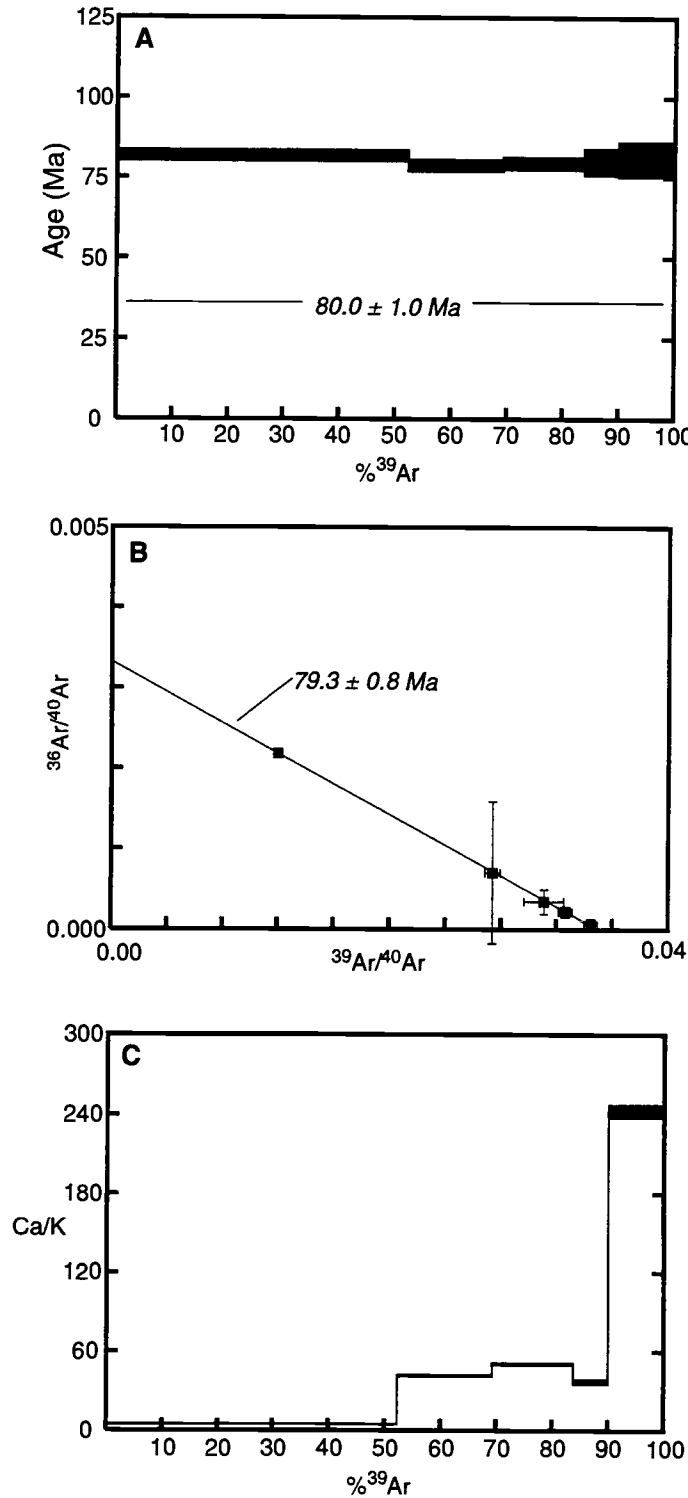


Figure II.8. Radiometric dating results for Sample 145-885A-8X-1, 38–42 cm. A. Apparent age spectrum (plateau) diagram. B.  ${}^{39}\text{Ar}/{}^{40}\text{Ar}$  vs.  ${}^{36}\text{Ar}/{}^{40}\text{Ar}$  isochron diagram. C. Apparent Ca/K release diagram. Details as in Figure II.5.

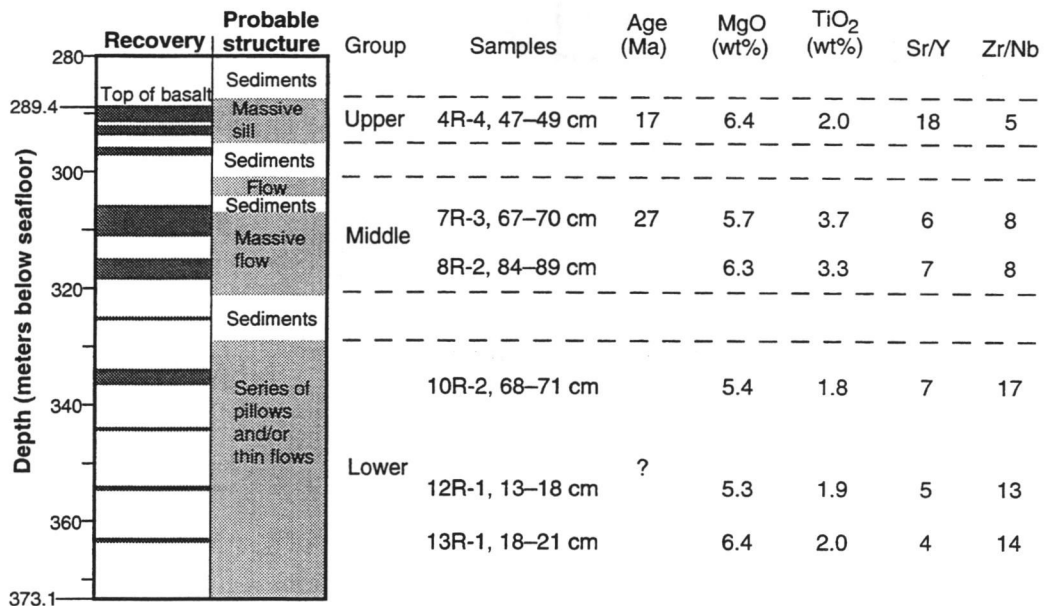


Figure II.9. Stratigraphy for the basement portion of Hole 887D interpreted from downhole logging data and core recovery data (Rea, Basov, Janacek, Palmer-Julson, et al., 1993). Radiometric ages for the middle and upper groups of basalts are shown. Some geochemical characteristics of all three basalt groups are also shown.

Two samples were selected from Site 887 for  $^{40}\text{Ar}/^{39}\text{Ar}$  age determinations. Sample 145-887D-4R-4, 47-49 cm, is a highly plagioclase-clinopyroxene-phyric basalt from a flow interior at 291.01 meters below sea floor (mbsf) (Figure II.9). The sample yielded a good age plateau and isochron (Figure II.10). The calculated plateau age (using all heating steps) is  $17.1 \pm 0.3$  Ma, and the calculated isochron age is concordant at  $16.8 \pm 0.5$  Ma (Table II.2). The isochron fit is statistically significant, and the  $^{40}\text{Ar}/^{36}\text{Ar}$  intercept is atmospheric composition (Table II.2).

Sample 145-887D-7R-3, 67-70 cm, is a highly clinopyroxene-plagioclase-phyric basalt from a flow interior at 309.33 mbsf (Figure II.9). The sample yielded a good age plateau and isochron (Figure II.11). The weighted mean plateau age is  $27.3 \pm 0.3$  Ma, and the calculated isochron age is concordant at  $27.5 \pm 0.4$  Ma (Table II.2). The excellent fits of the isochrons and the initial  $^{40}\text{Ar}/^{36}\text{Ar}$  of atmospheric composition in both Site 887 samples (Table II.2) lead us to conclude that these represent crystallization ages. The age of the lower basalt is within analytical error of the  $27.6 \pm 0.2$  Ma

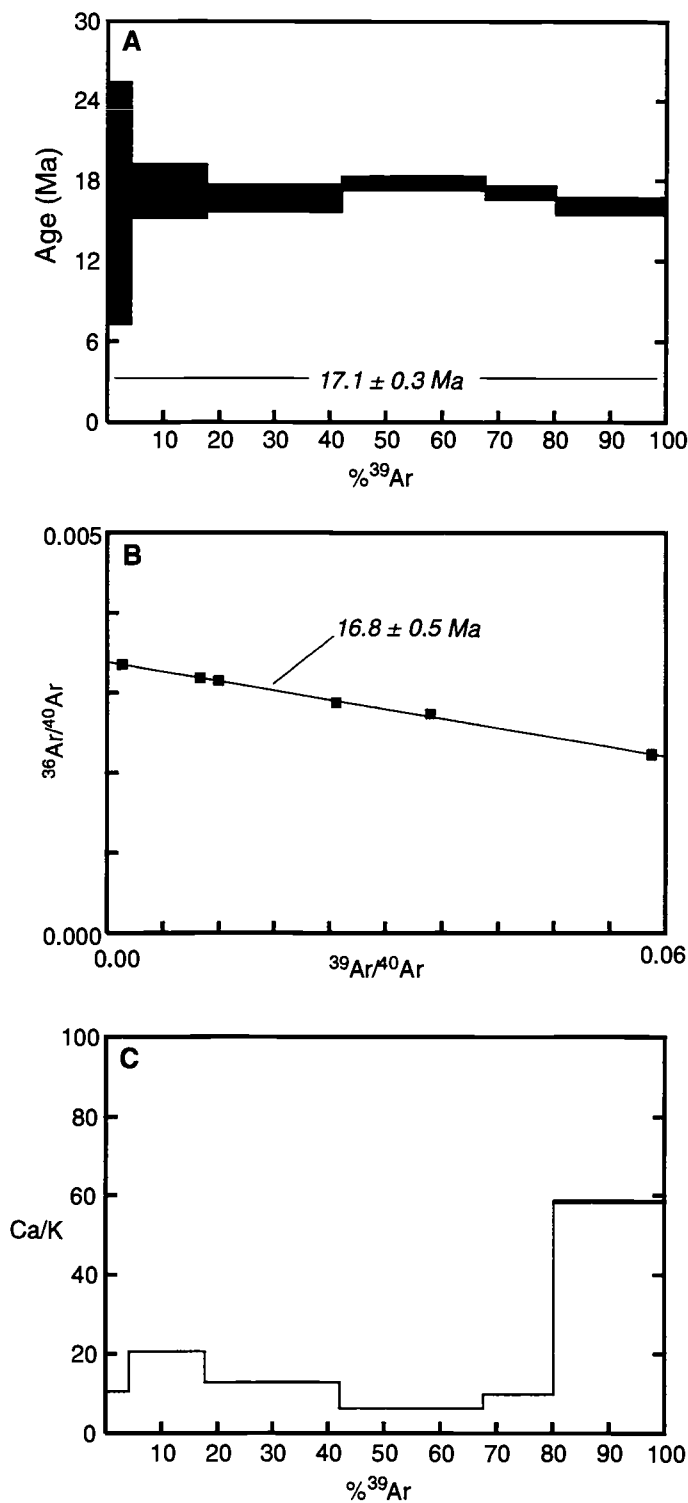


Figure II.10. Radiometric dating results for Sample 145-887D-4R-4, 47–39 cm. A. Apparent age spectrum (plateau) diagram. B. <sup>39</sup>Ar/⁴⁰Ar vs. <sup>36</sup>Ar/⁴⁰Ar isochron diagram. C. Apparent Ca/K release diagram. Details as in Figure II.5.

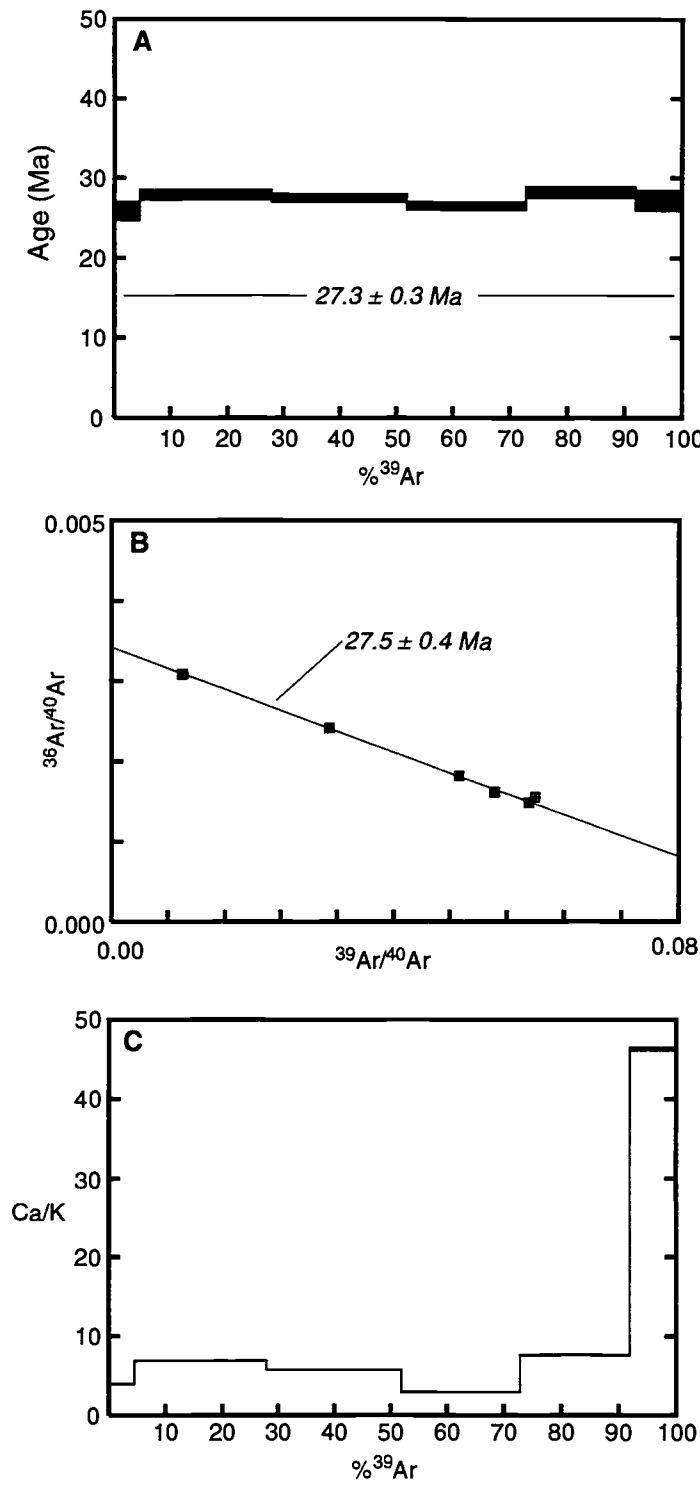


Figure II.11. Radiometric dating results for Sample 145-887D-7R-3, 67–70 cm. A. Apparent age spectrum (plateau) diagram. B. <sup>39</sup>Ar/⁴⁰Ar vs. <sup>36</sup>Ar/⁴⁰Ar isochron diagram. C. Apparent Ca/K release diagram. Details as in Figure II.5.

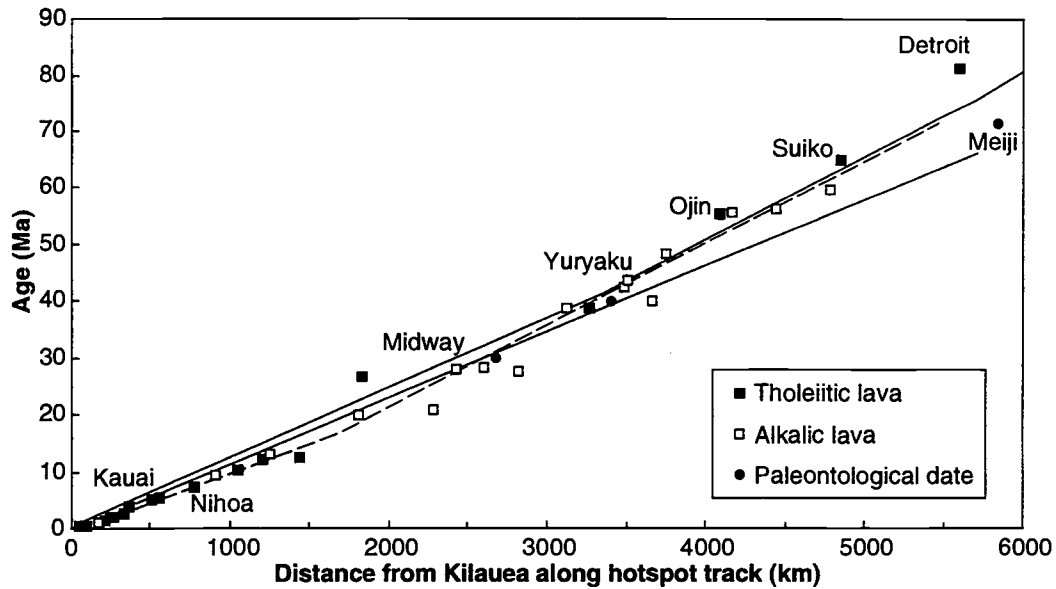


Figure II.12. Distance (measured along seamount chain) from Kilauea vs. age for islands and seamounts in the Hawaiian-Emperor chain (modified from Clague and Dalrymple, 1987). Solid line is a least-squares cubic fit to all of the data, regardless of stage of volcano-building. Dashed line is a two-segment fit. Dotted line is a four-stage rotation sequence (from Duncan and Clague, 1985) for the Pacific Plate over hotspots, best fit to radiometric age determinations of Pacific island and seamount lineaments. "Detroit" data point is from this study.

$^{40}\text{Ar}/^{39}\text{Ar}$  age reported by Dalrymple et al. (1987) for basalt dredged from Murray Seamount, 40 km from Site 887.

## DISCUSSION

When the 81 Ma age of Detroit Seamount and its distance from the island of Hawaii (measured along the seamount chain) are compared to data for other volcanoes in the Hawaiian-Emperor volcanic chain (Clague and Dalrymple, 1987), the Detroit Seamount sample appears to be too old (Figure II.12). Extrapolation of distance vs. age data from the < 65 Ma Hawaiian-Emperor seamounts (Suiko and younger) predicts that Detroit Seamount should be 65 to 75 m.y. old. A similar result is obtained from a model for Pacific plate motion in the hotspot reference frame based on a best fit to radiometric ages of Pacific island and seamount lineaments (Duncan and Clague, 1985). Part of this age

discrepancy could be explained if the Detroit Seamount sample is from early in the history of the volcano, as its tholeiitic composition suggests. But typical estimates of the lifespan of a Hawaiian volcano are less than 2 m.y., unless an alkalic rejuvenated stage occurs and extends the lifespan of the volcano to as much as 4 m.y. (Clague and Dalrymple, 1987). So even if the Detroit Seamount tholeiite is from early in the history of the volcano, it appears that previous plate motion models overestimate the velocity of the Pacific plate relative to the Hawaiian hotspot prior to approximately 65 Ma. The velocity of the Pacific plate must have increased sometime between when Detroit Seamount formed at 81 Ma and when Suiko Seamount formed at 65 Ma. Paleomagnetic (Sager and Pringle, 1988) and geochronological (Duncan and Clague, 1985) data from other Pacific seamount chains also suggest at least one change in Pacific plate motion between 81 and 65 Ma.

The 17 Ma age of the uppermost Site 887 basalt has interesting implications for its mode of emplacement. The extraordinarily complete paleomagnetic record of the sediments at Site 887 is continuous down to the top of Chron 5eN (18.3 Ma) at 272 mbsf (Rea, Basov, Janacek, Palmer-Julson, et al., 1993), which is still 19 m above the basalt. The sedimentation rate in that part of the section (5 m/m.y.) suggests that those 19 m represent another 3–4 m.y. of time. Thus the uppermost basalt would be expected to be approximately 21–22 m.y. old if it were erupted onto the seafloor. Paleontological evidence also suggests that the sediments directly overlying the basalt are Early Miocene in age (Rea, Basov, Janacek, Palmer-Julson, et al., 1993). Apparently the uppermost basalt is a sill that intruded sediments that were 4–5 m.y. old at the time. The resistivity and bulk density logs show that this sill is 6–7 m thick (Figure II.9), 4 m of which was recovered (Rea, Basov, Janacek, Palmer-Julson, et al., 1993). Such a massive flow should not have had any trouble intruding the soft sediments. Unfortunately, the contact between the sill and the overlying sediments was not recovered, so its nature could not be determined.

A small amount of sediment recovered between the uppermost basalt and the middle group of basalts (Figure II.9) contained Oligocene to Early Miocene radiolarians, an Oligocene calcareous nannofossil assemblage, and late Oligocene benthic foraminifers (Rea, Basov, Janacek, Palmer-Julson, et al., 1993). These ages fit between the 17 and 27 Ma ages of the basalts above and below the recovered sediment.

The 10-m.y. age difference between the two dated Site 887 samples is unusual, but is not unprecedented in a single seamount platform (Rurutu, Austral Islands, Duncan and McDougall, 1976; Kodiak-Bowie seamount chain, Chapman et al., 1987;

Christmas Island, T. Falloon et al., unpublished data, 1994). Our knowledge of the lifespan of ocean island volcanoes and seamount platforms may be biased by the fact that nearly all of the samples from these locations are taken from the volcanic summits that can be dredged or can be sampled where they project above sea level.

The whole-rock geochemistry of the Site 887 samples supports the complex history of the seamount platform suggested by the age data. The samples can be divided into three groups (Figure II.9) an alkalic to transitional group represented by Sample 145-887D-4R-4, 47–49 cm, and characterized by high Sr/Y and low Zr/Nb; a strongly alkalic group represented by Samples 145-887D-7R-3, 67–70 cm, and 145-887D-8R-2, 84–89, and characterized by high TiO<sub>2</sub> and low Sr/Y and Zr/Nb; and a tholeiitic to transitional group represented by Samples 145-887D-10R-2, 68–71 cm, 145-887D-12R-1, 13–18 cm, and 145-887D-13R-1, 18–21 cm, and characterized by low Sr/Y and high Zr/Nb. These three groups also occur in stratigraphic order (Figure II.9), with the alkalic to transitional group at the top (dated at 17 Ma), the strongly alkalic group in the middle (dated at 27 Ma), and the tholeiitic to transitional group at the bottom (undated). The volcanic stratigraphy of the hole can be assembled from the geochemical data, the recovered cores, and the downhole logging data (Rea, Basov, Janacek, Palmer-Julson, et al., 1993). Resistivity and bulk density logs and hole diameter data from the caliper tool show an upper massive sill, two massive flows in the middle, and a lower series of thin flows or pillows (Figure II.9). These three flow groups coincide with the geochemical groups, and can be shown on the logs to be separated by several meters of sediments.

Although Site 887 is the only place where one of the northeast Pacific seamounts has been drilled, several of these seamounts have been dredged. Dalrymple et al. (1987) reported analyses of samples from the Gulf of Alaska seamounts, including four samples dredged from Murray seamount, 40 km from Site 887. The Murray samples are more evolved than anything recovered at Site 887 (Figure II.7), but the Sr/Y (6–7) and Zr/Nb (7–10) of the dredged samples are similar to the middle group of basalts recovered at Site 887. Dalrymple et al. (1987) obtained a radiometric age of 27 Ma for a Murray sample, which matches with the age of the middle group of basalts (Figure II.9). Samples dredged from the Tuzo Wilson seamounts (Figure II.1; Allan et al., 1993) have much higher trace element concentrations at a given MgO content, and are compositionally distinct from the Site 887 basalts (Figure II.7).

The Cobb-Eickelberg seamount chain (Figure II.1) extends northwestward from the Juan de Fuca Ridge, and formed at the Cobb hotspot from 9 Ma to the present (Desonie

and Duncan, 1990). The Patton-Murray seamount platform lies along the northwestward extension of the Cobb-Eickelberg trend in the direction of Pacific plate motion, and could also have formed above the Cobb hotspot (Duncan and Clague, 1985). However, backtracking of Patton-Murray seamounts to 27 Ma using the Pacific plate motion models of Duncan and Clague (1985) and Pollitz (1988) places them 150–250 km west of the Cobb hotspot. For the Patton-Murray seamounts to be related to the Cobb hotspot, the 27 Ma basalts would have to represent a volcanic rejuvenescence of the seamounts. The higher alkali and  $\text{TiO}_2$  contents of the middle and upper groups of Site 887 basalts and the basalts dredged from Murray seamount (Dalrymple et al., 1987) are consistent with their eruption during a low-degree-partial-melt, rejuvenescent phase of volcanism downstream from the Cobb hotspot. Late-stage volcanic phases are a common feature of other hotspot lineaments (e.g., Hawaiian, Society, and Réunion hotspots).

The lower group of basalts from Site 887 is chemically indistinguishable from the Cobb-Eickelberg basalts (Figure II.7). Trace element ratios such as  $\text{Sr}/\text{Y}$  and  $\text{Zr}/\text{Nb}$  are identical for the two locations. If the Patton-Murray seamounts can be linked to the Cobb hotspot by compositional and geometrical arguments, the discontinuity of the volcanic lineament requires an unusually variable plume flux. Desonie and Duncan (1990) argued that the MORB-like isotopic ratios of the Cobb-Eickelberg basalts could be the result of a weak, intermittent, thermal plume that melts the depleted upper mantle. This model may also apply to the Patton-Murray seamounts, but isotopic data are necessary to determine if the Patton-Murray basalts are indeed MORB-like.

## CONCLUSIONS

Detroit Seamount was volcanically active approximately 81 m.y. ago. Basalts there have tholeiitic (Site 884) and transitional (Site 883) compositions. The position of the Pacific plate above the Hawaiian hotspot is now constrained back to 81 Ma, approximately 15 m.y. earlier than previous data allowed. Previous plate-motion models, based on other seamount chains and extrapolation from younger parts of the Hawaiian-Emperor chain, suggested an age for Detroit Seamount of approximately 65 to 75 Ma. Either the 81 Ma sample is from very early in the history of a volcano that remained active for at least 6 m.y., or the velocity of the Pacific plate relative to the Hawaiian hotspot increased sometime between 81 and 65 Ma.

Chinook Trough was volcanically active approximately 80 m.y. ago, and erupted basalt similar to mid-ocean ridge tholeiites. Drilling at Site 885/886 encountered these Upper Cretaceous basalts, perhaps as a sill, and did not penetrate to underlying Lower Cretaceous seafloor.

Patton-Murray seamount platform was constructed over a period of at least 10 m.y. (from at least 27 Ma to 17 Ma). These dates are from two compositionally distinct volcanic phases in the upper half of the recovered section, and probably underestimate the volcanic lifespan of this seamount platform. Basalts from the lower part of the recovered section are compositionally indistinguishable from basalts from the Cobb-Eickelberg seamounts. If the Patton-Murray seamounts can be linked to the Cobb hotspot by compositional and geometrical arguments, an unusual (thermal?) mantle plume with variable flux and depleted chemistry is required.

#### ACKNOWLEDGMENTS

We are grateful to Roger Nielsen and Lew Hogan for facilitating the microprobe analyses and Ar analyses, respectively. Brian Hausback and an anonymous reviewer provided helpful reviews of the original manuscript. This work was supported by a grant from JOI-USSAC.

## **Chapter 3**

### **Isotopic Characteristics of Cretaceous Volcanism at the Hawaiian Hotspot**

Randall A. Keller, Martin R. Fisk, and William M. White

## ABSTRACT

Tholeiitic basalts from the next-to-oldest seamount in the Hawaiian-Emperor seamount chain (81 Ma Detroit at 51°N) have:  $^{87}\text{Sr}/^{86}\text{Sr}$ ,  $^{207}\text{Pb}/^{204}\text{Pb}$ , and  $^{208}\text{Pb}/^{204}\text{Pb}$  lower than anything previously reported from the Hawaiian hotspot;  $^{143}\text{Nd}/^{144}\text{Nd}$  similar to the majority of Hawaiian tholeiites; and  $^{206}\text{Pb}/^{204}\text{Pb}$  lower than any Hawaiian tholeiite except those from Lanai and Koolau (which in contrast have high  $^{87}\text{Sr}/^{86}\text{Sr}$ ). The isotopic shifts between 81 Ma and the present are too large to have been accomplished by radioactive decay in the mantle plume or its source. We propose that the Hawaiian plume melted or entrained a larger proportion of depleted upper mantle during the Late Cretaceous compared to the Tertiary. This was probably due to the proximity of the plume to an active spreading center during the Late Cretaceous.

## INTRODUCTION

A hotspot is a persistent point of volcanism that creates a linear chain of volcanic islands and seamounts as a lithospheric plate passes over it (Duncan and Clague, 1985). The spatial fixity and geochemical characteristics (White, 1985; Weaver, 1991) of hotspot volcanism suggest that they are caused by mantle plumes originating below the depleted, convecting upper mantle; either at the 650 km discontinuity (Ringwood and Irfune, 1988) or at the core-mantle boundary (Davies, 1988).

Mantle plumes are important in the chemical and thermal evolution of the earth (Ringwood, 1990; Sleep, 1990; White, 1993), yet we have a very limited understanding of how they evolve chemically, and to what extent interaction with the asthenosphere and lithosphere affects the volcanism they produce. This may be at least partly because only four hotspot tracks (Louisville, Kerguelen, Réunion, and Hawaiian) are long enough and have been sampled in sufficient detail to study the chemical evolution of the mantle plumes (Weis et al., 1992). Louisville hotspot chemistry appears to have been relatively constant (Cheng et al., 1987), although there are significant sampling gaps. Kerguelen and Réunion hotspot tracks cross spreading centers that may have disturbed their plume signatures, but these two hotspots appear to have evolved away from originally MORB-like characteristics, toward higher Nb/Y and lower  $^{143}\text{Nd}/^{144}\text{Nd}$  (Fisk et al., 1989; White et al., 1990; Weis et al., 1992). The only previously published

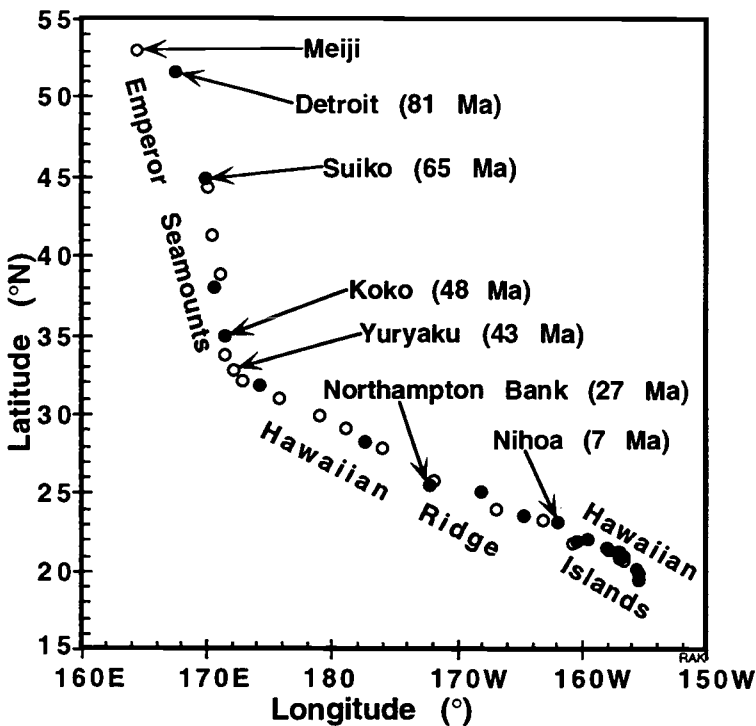


Figure III.1. Location of samples from the Hawaiian-Emperor island/seamount chain that have been dated. Additional locations have been sampled, but not dated. Seamounts mentioned in the text are labeled with names and ages (except the age of Meiji is unknown). Age data are from compilation by Clague and Dalrymple (1987), except Detroit age is from Keller et al. (1995). Locations from which tholeiites have been reported are shown by filled circles. Locations where no tholeiites were reported, or the identification of the tholeiites is in doubt, are shown by open circles.

study of the long-term evolution of the Hawaiian hotspot covered only the last 65 m.y., and used only Sr isotopes (Lanphere et al., 1980). We present here new Sr-Nd-Pb isotopic data for basalts from the three oldest Emperor seamounts that have been sampled (>81 Ma Meiji, 81 Ma Detroit, and 64.7 Ma Suiko). Our study focused on Detroit seamount platform, but we included single samples from Suiko and Meiji for correlation to the other data sets (Lanphere et al., 1980; and see below).

The Hawaiian hotspot is by far the most productive mantle plume on earth (Sleep, 1990). Over the past 81+ million years (Keller et al., 1995) it has produced the age-progressive Hawaiian-Emperor chain of volcanic islands and seamounts, extending for 5800 km from the present location of volcanic activity on the island of Hawaii, to the northernmost Emperor seamount (Meiji) at 53°N (Figure III.1). There are over 100

volcanic edifices along the Hawaiian-Emperor chain, and more than 30 of these (in addition to the Hawaiian Islands) have been sampled by dredge and drill (see compilation in Clague and Dalrymple, 1987). It is only recently, however, that Detroit seamount platform (the next-to-northernmost Emperor seamount) was sampled. A dredge haul recovered rocks from the alkalic rejuvenated stage of volcanism (Lonsdale et al., 1993), and Leg 145 of the Ocean Drilling Program (ODP) recovered tholeiitic basalts (Rea et al., 1993; Keller et al., 1993, 1995). The dredged samples are highly altered, and have not been analyzed for isotopes.

It is especially important for our study that tholeiites were recovered by ODP. On the Hawaiian Islands, shield-building tholeiites tend to have less MORB-like isotopic ratios than do the post-shield alkalic lavas. This has been interpreted as being a result of less lithospheric contribution to the tholeiitic lavas (Chen and Frey, 1985), which, if correct, means that tholeiites are more suitable for studying the plume signature.

The long-term chemical evolution of the Hawaiian hotspot, as measured by Sr isotopes, shows an interesting age progression (Figure III.2; Lanphere et al., 1980). The mean  $^{87}\text{Sr}/^{86}\text{Sr}$  in tholeiitic basalts is fairly constant and high (0.7037) along the Hawaiian Islands/Ridge between Kilauea volcano on Hawaii and Yuryaku Seamount (Figure III.1) at the Hawaiian-Emperor bend (43 Ma); but  $^{87}\text{Sr}/^{86}\text{Sr}$  then decreases steadily northward along the Emperor seamounts to Suiko Guyot (0.7032), which was the oldest seamount analyzed (64.7 Ma; Dalrymple et al., 1980). Note that this trend was only evident in the tholeiitic basalts (Lanphere et al., 1980).

The northward decrease in  $^{87}\text{Sr}/^{86}\text{Sr}$  along the Emperor seamount chain may be related to the decrease in the age difference between each seamount and its underlying crust, or to the decrease in distance between the hotspot and the nearest spreading center (Lanphere et al., 1980). A more recent, detailed Sr and Nd isotopic study of Hawaiian Ridge seamounts as old as 26.6 Ma (Northampton Bank, Figure III.1) also found no systematic variation with time in that part of the Hawaiian-Emperor chain (Basu and Faggart, 1994). Sr, Nd, and Pb isotopic data from Meiji Guyot have been presented (Tatsumoto, 1994), but are not yet published. Isotopic data also exist for nine seamounts from 7 Ma Nihoa to 65 Ma Suiko (Figure III.1), but are published only as two figures in an abstract (Unruh et al., 1987).

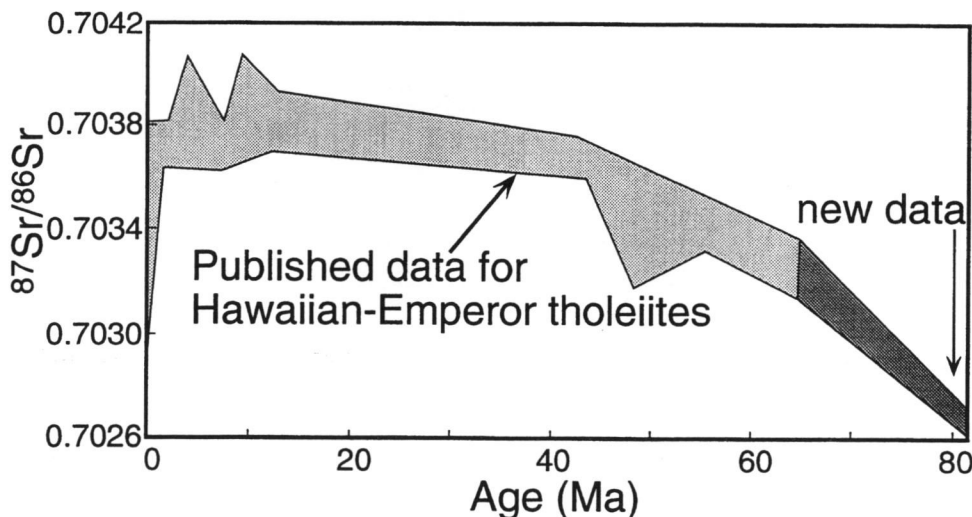


Figure III.2. Plot of sample age vs.  $^{87}\text{Sr}/^{86}\text{Sr}$  for tholeiitic basalts from the Hawaiian-Emperor island/seamount chain (modified from Lanphere et al., 1980). Previously published data went only as far back as 65 Ma (Suiko). Our new data from Detroit seamount platform extend the trend back to 81 Ma.

## SAMPLES AND DATA

ODP Leg 145 recovered basalts at two locations (Sites 883 and 884) on the Detroit seamount platform (Rea et al., 1993) near 51°N. Moderately-to-highly-altered basalt pillows and flows recovered at Site 883 are too altered to use the alkaline elements to determine if they are tholeiitic, but their  $\text{TiO}_2$  contents are between 2.1 and 2.4 wt% (at 45.4–47.0 wt.%  $\text{SiO}_2$ ; Keller et al., 1995), a range compatible with both the alkalic and tholeiitic stages of volcanism. Other incompatible elements are equally ambiguous, and thus the basalts may be transitional. Similar ambiguity was found in the DSDP Site 192 (Meiji Guyot) basalt, which was tentatively classified based upon mineralogy as an alkali basalt (Stewart et al., 1973), but later analyses of glass and pyroxene in the sample suggested that it may be tholeiitic (Dalrymple et al., 1980). We include new data for the Site 883 basalts because they are isotopically similar to the Site 884 basalts, but since we are not certain that they are tholeiitic, we do not base our arguments upon them.

Drilling at Site 884 on the flank of Detroit seamount platform recovered massive flows and pillows of aphyric-to-plagioclase megaphyric tholeiitic basalts. The Site 884 basalts have low concentrations of alkalis,  $\text{TiO}_2$ , and other incompatible elements at

moderate MgO (4.6–8.8 wt.%) and Ni (47–94 ppm), and are unambiguously tholeiitic (Keller et al., 1995). Small chemical differences between the samples are due to alteration, the presence of plagioclase megacrysts, or minor amounts of fractional crystallization. All of the Site 884 samples have unusually low incompatible trace element concentrations ( $\text{TiO}_2 < 1.5$ ,  $\text{Sr} < 200$ ,  $\text{Zr} < 100$ ) when compared with other ocean island tholeiites, even when the effects of the plagioclase megacrysts are considered. Such low incompatible element concentrations are unprecedented in the Hawaiian-Emperor chain, but have been reported on other ocean islands (e.g., Galápagos – Geist et al., 1986; White et al., 1993; Nauru – Castillo et al., 1986; Réunion/Kerguelen – Weis et al., 1992). The Site 884 basalts may be from a phase of tholeiitic volcanism early in the life of the volcano that is only rarely sampled by dredges or exposed on islands.

The Site 883 basalts did not yield a reliable  $^{40}\text{Ar}$ - $^{39}\text{Ar}$  crystallization age, but a basalt from Site 884 yielded a  $^{40}\text{Ar}$ - $^{39}\text{Ar}$  age of  $81.2 \pm 1.3$  Ma (Keller et al., 1995). We take this to be the age of Detroit Seamount, although the dated sample is a tholeiite from the flank of the seamount, so it may be from early in the history of the volcano (Keller et al., 1995). This is the oldest reliable radiometric age determination for an Emperor seamount (Meiji did not yield a reliable  $^{40}\text{Ar}$ - $^{39}\text{Ar}$  date; Dalrymple et al., 1980), and adds 16 million years to the period of dated activity of the Hawaiian hotspot (Keller et al., 1995).

A tholeiitic basalt from DSDP Site 433 on Suiko Guyot (64.7 Ma, Dalrymple et al., 1980), and a basalt of uncertain (possibly tholeiitic) composition (Dalrymple et al., 1980) from DSDP Site 192 on Meiji Guyot were included in our sample set for comparison to other studies (Lanphere et al., 1980; Stille et al., 1987; Tatsumoto, 1994).

All of the samples analyzed here are moderately to highly altered basalts that required repeated leaching in hot HCl to remove secondary minerals and isolate the primary isotopic ratios. Measured isotopic ratios are given in Table III.1, along with age-corrected (initial) ratios calculated from values for Rb/Sr, Sm/Nd, U/Pb, and Th/Pb obtained by ID-TIMS and ICP-MS. The ages of the Site 433 (Suiko) and Site 884 (Detroit) samples are known from  $^{40}\text{Ar}$ - $^{39}\text{Ar}$  dating (Dalrymple et al., 1980; Keller et al., 1995). For age correction purposes, the Site 883 samples are assumed to be 1 m.y. younger than the Site 884 samples because Site 883 was slightly higher up on the Detroit seamount platform than Site 884, and the Site 883 samples appear to be of transitional composition. The Meiji (Site 192) sample is estimated to be 85 m.y. old for

**Table III.1. Measured and initial isotopic ratios and trace element ratios.**

<b>Seamount</b>	<b>Suiko</b>	<b>Detroit</b>				<b>Meiji</b>
<b>Sample</b>	433-31-1	883-1-3	883-2-3	884-6-3	884-10-4	192-6-2
<b>Age (Ma)</b>	64.7	80?	80?	81	81	85?
<b>Measured ratios</b>						
<b><math>^{87}\text{Sr}/^{86}\text{Sr}</math></b>	0.703297	0.702884	0.702864	0.702768	0.702652	0.703079
<b><math>^{143}\text{Nd}/^{144}\text{Nd}</math></b>	0.513068	0.513081	0.513100	0.513184	0.513152	0.513072
<b><math>^{206}\text{Pb}/^{204}\text{Pb}</math></b>	18.609	18.355	18.500	18.175	18.058	18.750
<b><math>^{207}\text{Pb}/^{204}\text{Pb}</math></b>	15.463	15.443	15.452	15.419	15.410	15.453
<b><math>^{208}\text{Pb}/^{204}\text{Pb}</math></b>	38.136	37.856	37.809	37.680	37.582	38.036
<b>Rb/Sr</b>	0.015	0.024	0.024	0.012	0.010	0.031
<b>Sm/Nd</b>	0.278	0.285	0.285	0.349	0.350	0.280
<b>Th/Pb</b>	0.833	0.941	0.938	0.321	0.312	0.812
<b>U/Pb</b>	0.300	0.470	0.438	0.143	0.156	0.500
<b>Initial ratios</b>						
<b><math>^{87}\text{Sr}/^{86}\text{Sr}</math></b>	0.703257	0.702808	0.702788	0.702730	0.702620	0.702972
<b><math>^{143}\text{Nd}/^{144}\text{Nd}</math></b>	0.512994	0.512987	0.513006	0.513068	0.513035	0.512974
<b><math>^{206}\text{Pb}/^{204}\text{Pb}</math></b>	18.394	17.938	18.113	18.047	17.918	18.279
<b><math>^{207}\text{Pb}/^{204}\text{Pb}</math></b>	15.453	15.423	15.434	15.413	15.403	15.431
<b><math>^{208}\text{Pb}/^{204}\text{Pb}</math></b>	37.945	37.589	37.543	37.588	37.492	37.791

All isotopic ratios were measured at Cornell University using procedures described in White et al. (1990). All samples were repeatedly leached in hot HCl prior to digestion, and all isotopic ratios were corrected for fractionation. Sr and Pb isotopic ratios are referenced to standards NBS987 and NBS981, respectively. The average  $^{143}\text{Nd}/^{144}\text{Nd}$  for the La Jolla Nd standard measured at the time of these analyses (via Ames Nd) was  $0.511876 \pm 14$ . Two-sigma standard errors based upon numerous analyses of standards during the time of the unknown runs are:  $^{87}\text{Sr}/^{86}\text{Sr} \pm 0.000014$ ,  $^{143}\text{Nd}/^{144}\text{Nd} \pm 0.000016$ ,  $^{206}\text{Pb}/^{204}\text{Pb} \pm 0.010$ ,  $^{207}\text{Pb}/^{204}\text{Pb} \pm 0.011$ , and  $^{208}\text{Pb}/^{204}\text{Pb} \pm 0.030$ . Within-run standard errors due to machine precision are smaller than these between-run errors. Trace element concentrations were measured by TIMS-ID of leached samples (Pb, Th, and U) and ICP-MS of unleached samples (Rb, Sr, Nd, and Sm).

age correction purposes. Errors in the estimated ages of the Meiji and Site 883 samples of several million years or less are inconsequential to our story.

Initial  $^{87}\text{Sr}/^{86}\text{Sr}$ ,  $^{207}\text{Pb}/^{204}\text{Pb}$ , and  $^{208}\text{Pb}/^{204}\text{Pb}$  values (Table III.1) in the Detroit tholeiites (Site 884) are lower than anything previously reported from the Hawaiian-Emperor chain (Figure III.3).  $^{143}\text{Nd}/^{144}\text{Nd}$  and  $^{206}\text{Pb}/^{204}\text{Pb}$  values for the Site 884 tholeiites overlap the Hawaiian field. Age corrections to the isotopic data for these tholeiites are small (Table III.1), and even the measured ratios are distinct from the

Hawaiian data. The Site 883 Detroit (transitional?) basalts have isotopic ratios similar to, but not quite as depleted as, the Site 884 tholeiites.

The Meiji sample has isotopic ratios (Table III.1) within the range of tholeiites from the Hawaiian Islands, except its  $^{87}\text{Sr}/^{86}\text{Sr}$  and  $^{207}\text{Pb}/^{204}\text{Pb}$  are lower (Figure III.3). Its  $^{87}\text{Sr}/^{86}\text{Sr}$ ,  $^{206}\text{Pb}/^{204}\text{Pb}$ , and  $^{208}\text{Pb}/^{204}\text{Pb}$  values are higher than the Detroit samples, but lower than the Suiko sample. On the other hand, Meiji and Detroit have similar  $^{143}\text{Nd}/^{144}\text{Nd}$  and  $^{207}\text{Pb}/^{204}\text{Pb}$  values.

The Suiko sample has the highest Sr and Pb isotopic ratios measured in this study, and  $^{143}\text{Nd}/^{144}\text{Nd}$  similar to Meiji (Table III.1). Suiko isotopic ratios are within the range of published values for tholeiites from the Hawaiian Islands/Ridge (although its  $^{87}\text{Sr}/^{86}\text{Sr}$  is slightly lower than the lowest published  $^{87}\text{Sr}/^{86}\text{Sr}$  for Hawaiian tholeiites that also have Nd and Pb data available; Figure III.3). Our  $^{87}\text{Sr}/^{86}\text{Sr}$  value for the Suiko sample is within analytical error of the Suiko tholeiite analyses in Lanphere et al. (1980) and Unruh et al. (1987).

The uniqueness of the Cretaceous Emperor seamount isotopic data is most obvious on the  $^{206}\text{Pb}/^{204}\text{Pb}$  vs.  $^{87}\text{Sr}/^{86}\text{Sr}$  plot (Figure III.3a). The Detroit data plot close to the MORB field, well away from the Hawaiian Islands/Ridge field. The Meiji and Suiko data are displaced from the highly depleted values of the Detroit field, toward the high  $^{206}\text{Pb}/^{204}\text{Pb}$  - low  $^{87}\text{Sr}/^{86}\text{Sr}$  end of the Hawaiian Islands/Ridge field. This displacement could be interpreted as mixing between a depleted reservoir with the isotopic characteristics of MORB, and the low- $^{87}\text{Sr}/^{86}\text{Sr}$  component of the Hawaiian Islands/Ridge field. The positive slope of our Meiji-Detroit-Suiko data in Figure III.3a is distinct from the negative slope of the array formed by tholeiites from the 0 to 48 Ma part of the Hawaiian-Emperor chain.

## DISCUSSION AND INTERPRETATION

The Sr and Pb isotopic ratios of the Detroit tholeiites are the lowest ever reported from the Hawaiian-Emperor seamounts, and must have a higher proportion of a long-term depleted component than any other known product of the Hawaiian hotspot. The question is: Was this depleted component a feature of the mantle plume itself, or was it a result of greater interaction between the mantle plume and the depleted upper mantle during the Late Cretaceous? We present three possible models for how the plume could have changed (Models 1, 2, and 3), and three possible models for how the plume's

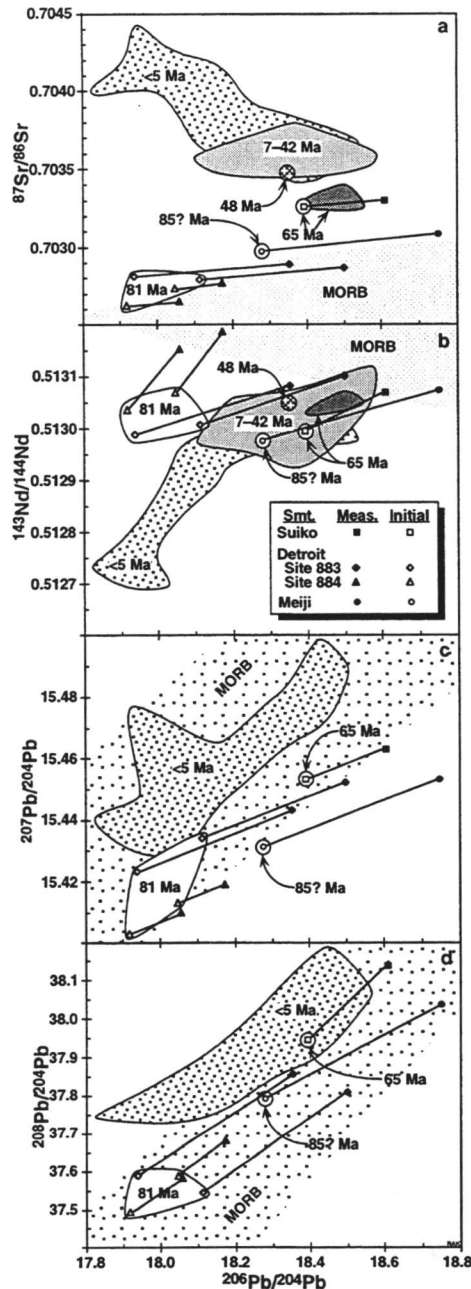


Figure III.3.  $^{206}\text{Pb}/^{204}\text{Pb}$  versus other isotopic ratios for tholeiitic basalts from the Hawaiian Islands (<5 Ma field), the Hawaiian Ridge (7–42 Ma field), Koko Guyot (48 Ma), Suiko Guyot (65 Ma), Detroit Guyot (81 Ma), and Meiji Guyot (~85? Ma). For Suiko, Detroit, and Meiji, filled symbols are measured ratios and open symbols are age-corrected (initial) ratios (Table III.1). Only data from tholeiites are shown, with the possible exception of the Meiji and the Site 883 Detroit samples. Hawaiian Islands and MORB fields from various sources. Hawaiian Ridge and Koko and Suiko data in plots a and b are age-corrected (Unruh et al., 1987).

surroundings could have changed (Models 4, 5, and 6). The models are not mutually exclusive, so acceptance of any one of these models does not exclude contributions from any of the other models.

Our models will not attempt to account for the high  $^{87}\text{Sr}/^{86}\text{Sr}$ -low  $^{206}\text{Pb}/^{204}\text{Pb}$  Hawaiian Islands data (Figure III.3a) because this component has been found at only two volcanoes (Lanai and Koolau). We are more concerned with explaining the differences between our data and data from the rest of the Hawaiian-Emperor seamounts and the majority of the Hawaiian Islands.

(1) *Isotopic ratios in the plume changed due to radioactive decay.* Radioactive decay in the plume and its source region will increase the Sr and Pb isotopic ratios (Class et al., 1993), but by only a small amount compared to the isotopic differences between the Detroit tholeiites and the Hawaiian Ridge/Islands. We do not know the Rb/Sr, Th/Pb, and U/Pb values in the plume, but we do know that all of these ratios are higher in a partial melt than in the source that produced that melt, so we can use ratios in the rocks (Table III.1) as maximum possible ratios in the plume. Based upon this assumption, the amount the plume has changed due to radioactive decay is no greater than the isotopic age corrections that we made in Table III.1 (for Site 884 tholeiites: 0.00003  $^{87}\text{Sr}/^{86}\text{Sr}$  units; 0.13  $^{206}\text{Pb}/^{204}\text{Pb}$  units; 0.006  $^{207}\text{Pb}/^{204}\text{Pb}$  units; and 0.09  $^{208}\text{Pb}/^{204}\text{Pb}$  units). Compare these values to the differences between the Site 884 tholeiites and the low- $^{87}\text{Sr}/^{86}\text{Sr}$  end of the Hawaiian Ridge/Islands field (~0.0009  $^{87}\text{Sr}/^{86}\text{Sr}$ ; ~0.5  $^{206}\text{Pb}/^{204}\text{Pb}$  units; ~0.09  $^{207}\text{Pb}/^{204}\text{Pb}$  units; and 0.6  $^{208}\text{Pb}/^{204}\text{Pb}$  units).

Using the inverse approach, the trace element ratios required to account for the differences between the Site 884 tholeiites and the Hawaiian Ridge/Islands data (i.e., Rb/Sr=0.278, U/Pb=0.558-2.11, Th/Pb=2.09) are 4 to 28 times the ratios in the tholeiites (Table III.1), and 1 to 2 orders of magnitude higher than the maximum likely ratios found in plumes (Weaver, 1991). Thus, although the plume has undoubtedly evolved isotopically, this explains only a small fraction of the observed differences between the Cretaceous volcanism and the more recent products of the plume. Also, this model predicts that the oldest sample (from Meiji) should have lower Sr and Pb ratios than Detroit, which it does not (Figure III.3).

(2) *The isotopic characteristics of the source region of the plume changed.* The region of the mantle where the Hawaiian plume acquires its isotopic signature has probably not been homogeneous and static over the course of the past 81+ million years. Isotopically diverse packages of mantle material may be randomly swept into this region. If a package of depleted mantle was swept into the plume source region during the Late

Cretaceous, that would explain the more-depleted composition of the Detroit samples. This model cannot be tested, but it could be reasonable in the absence of any other explanation of the isotopic data.

(3) *A physical change in the plume caused a change in the amount of upper mantle entrainment.* Lower plume buoyancy flux results in more entrainment (Hauri et al., 1994), so anything that leads to lower buoyancy flux, such as lower mass flux or lower temperature contrast, would cause more upper mantle entrainment. The depleted isotopic values of the Detroit and Meiji samples could thus be explained if there was less contrast between the Hawaiian plume and the depleted upper mantle during the Cretaceous. Although there have been variations in plume flux over the life of the Hawaiian hotspot, there is no evidence for a significant change in plume flux between the time of Detroit and Suiko (Clague and Dalrymple, 1987), when almost all of the isotopic change occurred (Figure III.3).

A variation of this model is based upon explanations of the chemical evolution of the Réunion and Kerguelen hotspots. Both of those hotspot tracks begin at flood basalts that have been interpreted to be the initial bursts of volcanism caused by the heads of new mantle plumes (Richards et al., 1989). Laboratory tank experiments suggest that a plume head entrains more of its surroundings than does an established plume conduit (Richards et al., 1989). So the MORB-like compositions found early in the life of Réunion and Kerguelen hotspots have been interpreted to be due to larger amounts of entrainment of depleted upper mantle by the heads of those two mantle plumes (Fisk et al., 1989; White et al., 1990; Weis et al., 1992). This model has two problems: subsequent numerical models suggest that the melting zone of plume heads entrain less rather than more upper mantle (Farnetani and Richards, 1995); and it is not known if this model can be applied to the Hawaiian plume because the old end of the Hawaiian hotspot track ends at a subduction zone, so the existence of older seamounts or a plume-head-associated flood basalt is speculative.

(4) *A nearby spreading center caused greater entrainment of upper mantle into the plume during the Late Cretaceous.* In the few locations where a spreading ridge is close to a hotspot (Bouvet, Galápagos, Iceland) the isotopic characteristics of the hotspot volcanism extend toward MORB-like values (Hauri et al., 1994). Most plate reconstructions place an active spreading center close to the position of the Hawaiian hotspot at ~80 Ma (Mammerickx and Sherman, 1988; Hart, 1994). Proximity to the spreading center could have had a variety of implications for nearby Hawaiian hotspot volcanism. The spreading ridge could have created a higher temperature and lower

viscosity and density regime in the upper mantle at ~81 Ma, conditions that lead to more entrainment (Hauri et al., 1994). Hotter upper mantle temperatures close to the spreading center also could have allowed greater degrees of melting of the upper mantle (Weis et al., 1992), and thus more entrainment. The nearby spreading center also could have caused more vigorous upper mantle convection and a mechanical stirring effect that increased entrainment.

(5) *The isotopic composition of the upper mantle entrained by the plume was more depleted in the Cretaceous.* Upper mantle recently passed over by a spreading center has been partially melted and wrung of any pods of enriched material, and will have an especially depleted bulk composition. If this enriched material is then replenished via long-term/low-intensity metasomatism, upper mantle beneath 90 million year old crust (such as the present Hawaiian Islands) will have less depleted bulk composition than upper mantle beneath young crust.

(6) *The amount and effects of lithospheric interaction with the plume changed.* Some workers propose that the lithosphere is an important component of the isotopic signature of most basalts from the Hawaiian Islands (e.g., Stille et al., 1986), although others claim that only the alkalic rocks contain a lithospheric component (e.g., Chen and Frey, 1985). If the lithosphere is an important component in the tholeiites, then radioactive decay within the lithosphere would increase the radiogenic isotopes in the hotspot volcanism over time. This change would be less than the age corrections in Table III.1, however, because typical MORB values of Rb/Sr, Th/Pb, and U/Pb are lower than those ratios in the Site 884 tholeiites (Table III.1). Seawater alteration of the crust could increase the isotopic change in Sr, but should not affect the Pb isotopic ratios.

The thickness of the lithosphere could also determine how much it contributes to hotspot volcanism. If the depth range of melting in the plume is fairly constant, an area of very young (thin) lithosphere will have less lithosphere and more asthenosphere in that melting zone. If the upwelling mantle plume begins to melt when it reaches a depth of say, approximately 100 km, and continues to produce melt until it reaches a depth of approximately 10–30 km, under very young crust most or all of that melting column will be asthenosphere, while under old crust a large portion of that melting column will be in the lithosphere. Hotspot volcanism on old crust would then contain more of a lithospheric component than hotspot volcanism on young crust.

## CONCLUSIONS

Basalts from the two oldest seamounts ( $\geq 81$  Ma) in the Hawaiian-Emperor chain are isotopically more depleted than any other products of the Hawaiian hotspot. Radioactive decay within the plume can explain only a small amount of the observed isotopic change since 81 Ma. More important is that an active spreading center was very close to the Hawaiian hotspot at  $\sim 80$  Ma, and somehow caused the mantle plume to entrain large amounts of depleted upper mantle. Late Cretaceous plate reconstructions of the area are not well-constrained, but would fit the isotopic data best if the spreading ridge was approaching the hotspot at the time of Meiji Guyot ( $\sim 85$ ? Ma), was closest to the hotspot at the time of the Detroit seamount platform (81 Ma), had moved far away by the time of Suiko (65 Ma), and has remained even farther away since then. The exact physical or chemical process by which a spreading center could change the chemistry of nearby hotspot volcanism remains to be determined, but it is especially impressive that the process(es) was(were) powerful enough to overwhelm the chemical characteristics of the most productive mantle plume on Earth.

## ACKNOWLEDGMENTS

We thank M. Cheatham for assistance with the TIMS analyses, A. Ungerer for assistance with the ICP-MS analyses, and A. Basu for a pre-publication copies of his Hawaiian Ridge isotope plots. This work was supported by a JOI/USSAC Ocean Drilling Fellowship.

## **Chapter 4**

### **Sixteen Million Years of Volcanism on the Patton-Murray Seamount Platform, Gulf of Alaska**

Randall A. Keller, Martin R. Fisk, Robert A. Duncan, and William M. White

## ABSTRACT

Drilling at Ocean Drilling Program Hole 887D recovered basalts from 16 m.y. of periodic volcanism on the Patton-Murray seamount platform at the old (NW) end of the Cobb hotspot track in the Gulf of Alaska. Tholeiitic basalts recovered 329 m below the seafloor erupted when the seamount platform was above the Cobb hotspot at 33 Ma, and are chemically and isotopically similar to basalts from the rest of the Cobb hotspot track (i.e., the Cobb-Eickelberg seamounts) and the Juan de Fuca Ridge. A 27 Ma massive alkalic basalt flow recovered 8 m higher in the hole represents the alkalic capping-phase of volcanism, and is similar in age and composition to basalts dredged nearby from Murray Guyot. A 17 Ma massive tholeiitic basalt sill recovered 5 m higher in the section is chemically and isotopically distinct from the other basalts, and erupted too long after the seamount platform moved away from the hotspot to have been related to the initial hotspot activity. However, this youngest phase of volcanism could have been associated with minor extension along a zone of weakness created when the plate passed over the hotspot.

## INTRODUCTION

The seafloor in the northeast Pacific is peppered with discontinuous volcanic lineaments roughly aligned with the direction of absolute motion of the Pacific plate (Morgan, 1972). These lineaments are broadly age-progressive (younging to the southeast), although there are some out-of-sequence ages, and many edifices are of unknown age. Linear chains of age-progressive seamounts elsewhere in the ocean basins have been attributed to stationary, sub-lithospheric hotspots that create volcanic tracks on a lithospheric plate as it passes over a focus of upper mantle melting (Wilson, 1963). Such a hotspot origin has been suggested for the NE Pacific seamounts, although there are some discrepancies between the known history of Pacific plate motion and the trends of the seamount chains (Silver et al., 1974; Dalrymple et al., 1987). Also, many of the seamount chains are not continuous enough nor have been surveyed in enough detail to be unambiguously attributed to a particular hotspot. Basalts from the NE Pacific seamounts are also unusual in that they lack the enriched Sr and Pb isotopic signatures of most hotspots (Hegner and Tatsumoto, 1989). The discontinuous nature and anomalous isotopic compositions of the NE Pacific seamounts could be

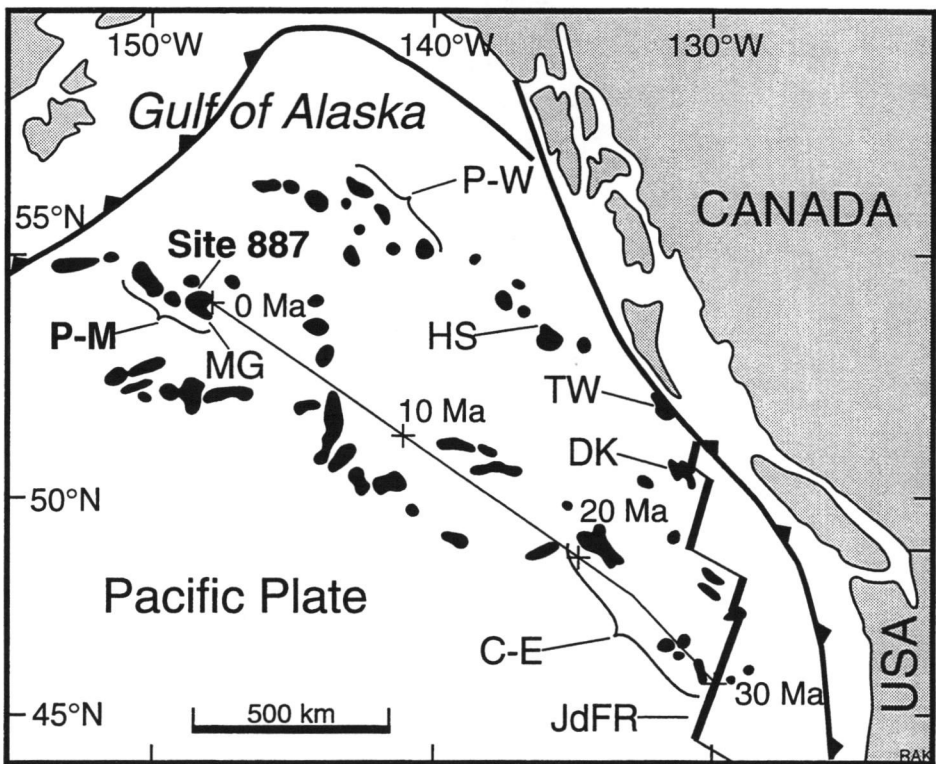


Figure IV.1. Locations of seamounts and spreading ridges in the northeast Pacific/Gulf of Alaska region (after Karsten and Delaney, 1989). Seamounts are black blobs. Spreading ridges, transform faults, and trenches are thick black lines. Volcanic systems mentioned in the text are labeled: C-E = Cobb-Eickelberg seamounts, DK = Dellwood Knolls, HS = Hodgkins Seamount, JdFR = Juan de Fuca Ridge spreading center, MG = Murray Guyot, P-M = Patton-Murray seamounts, P-W = Pratt-Welker seamounts, and TW = Tuzo Wilson seamounts. The location of ODP Site 887 on Patton-Murray seamount platform is shown. The Cobb hotspot is presently centered under the JdFR at the SE end of the Cobb-Eickelberg chain. The position of the Patton-Murray seamount platform relative to the Cobb hotspot over the last 30 m.y. is shown by the thin line with tick marks at 10 m.y. increments (based upon plate models of Gripp and Gordon, 1990 for 0–5 Ma; Pollitz, 1988 for 0–9 Ma; and Duncan and Clague, 1985 for 0–30 Ma).

explained if hotspots in this area are caused by weak, thermally-buoyant rather than compositionally-buoyant mantle plumes (Desonie and Duncan, 1990).

The Patton-Murray seamount platform is built on 40 m.y. old crust at 54°N in the Gulf of Alaska (Figure IV.1), and has been attributed to the Cobb hotspot (Duncan and Clague, 1985). However, backtracking the motion of the Pacific Plate to the time of alkalic basalt volcanism at Murray Guyot (27.6 Ma; Dalrymple et al., 1987) leaves the

Patton-Murray platform approximately 200 km west of the Cobb hotspot (Desonie and Duncan, 1990). So for the bulk of the Patton-Murray platform to have been created at the Cobb hotspot, it would have to be a few million years older than 27.6 Ma.

In September 1992, Hole 887D (Site 887 in Figure IV.1) of Ocean Drilling Program (ODP) Leg 145 penetrated 373 m of sediments and basalts at the eastern end of the Patton-Murray seamount platform near the northern foot of Murray Guyot (Rea et al., 1993). We have already presented the results of x-ray fluorescence analyses and two  $^{40}\text{Ar}/^{39}\text{Ar}$  ages of the basalts (Keller et al., 1995; Chapter 2). Here we present new trace element and rare earth element data, Sr-Nd-Pb isotopic data, and an additional  $^{40}\text{Ar}/^{39}\text{Ar}$  age for the Hole 887D basalts (Table IV.1). We interpret these data in light of the history of volcanism on the seamount platform, and its relationship to other seamounts in the northeast Pacific.

## SAMPLES AND DATA

Drilling in ODP Hole 887D encountered basalt at 289 m below the seafloor (Figure IV.2). Another 84 m of drilling recovered 16 m of basalt from a series of pillows and flows interbedded with sediments (Keller et al., 1995). The basalts can be divided into three groups (lower, middle, and upper) based upon their chemical compositions (Table IV.1; Figure IV.2) and the lithostratigraphy of the hole (as seen by downhole logging tools). The lower group is a series of pillows or thin flows of vesicular, sparsely plagioclase-phyric basalts. Many of the recovered fragments in this group have glass margins. On top of the lower group are approximately 8 m of sedimentary material, none of which was recovered (Rea et al., 1993). Atop the sediments is a pair of massive flows of plagioclase-clinopyroxene-phyric basalts that are the 'middle group'. Above this are another 5 m of sediments, of which a small chunk was recovered (Rea et al., 1993). On top of these sediments is a single 6–7 m-thick sill of clinopyroxene-plagioclase-phyric basalt that is the 'upper group'. All of the basalts are somewhat altered, with the degree of alteration generally increasing downward in the hole.

We previously dated whole-rock samples from the upper and middle groups by  $^{40}\text{Ar}-^{39}\text{Ar}$  incremental heating (Figure IV.2; Keller et al., 1995). Samples from the lower group initially appeared to be too fine-grained and altered to date, but we have since been able to obtain a reliable  $^{40}\text{Ar}-^{39}\text{Ar}$  plateau age of  $33.0 \pm 1.3$  Ma from sample 10R-2 (Figures IV.2 and IV.3). Sample 7R-3 from the middle group yielded a reliable  $^{40}\text{Ar}-$

**Table IV.1. Trace element and isotopic data for the Hole 887D basalts.**

Group Sample	Upper 4R-4	Middle		Lower	
		7R-3	8R-2	10R-2	13R-1
Rb	6.8	12.5	10.9	11.4	8.4
Sr	414	278	265	204	160
Y	22	46	39	33	36
Zr	100	298	259	125	132
Nb	22.3	35.2	29.7	7.7	8.0
Cs	0.05	0.09	0.04	0.95	0.18
Ba	192	155	138	43	32
La	12.6	22.4	18.8	6.5	6.5
Ce	27.3	52.9	44.8	17.3	17.8
Pr	3.87	7.56	6.48	2.80	2.92
Nd	16.4	32.7	28.1	13.4	14.3
Sm	4.32	8.62	7.25	3.97	4.39
Eu	1.48	2.51	2.28	1.32	1.52
Gd	4.63	8.99	7.71	4.82	5.31
Tb	0.71	1.42	1.23	0.83	0.94
Dy	4.15	8.19	7.06	5.08	5.78
Ho	0.78	1.59	1.34	1.11	1.21
Er	2.05	4.33	3.71	3.14	3.51
Tm	0.29	0.63	0.55	0.47	0.53
Yb	1.78	3.75	3.34	2.91	3.29
Lu	0.25	0.57	0.50	0.45	0.49
Hf	2.58	6.89	6.00	2.96	3.12
Ta	1.34	2.40	1.84	0.82	1.15
Pb	0.99	1.04	2.13	1.46	0.82
Th	1.15	2.05	1.78	0.46	0.48
U	0.99	0.83	0.60	1.01	0.18
Measured isotopic ratios					
$^{87}\text{Sr}/^{86}\text{Sr}$	0.702570	0.702735			0.702508
$^{143}\text{Nd}/^{144}\text{Nd}$	0.513216	0.513098			0.513220
$^{206}\text{Pb}/^{204}\text{Pb}$	19.130	19.406			18.636
$^{207}\text{Pb}/^{204}\text{Pb}$	15.563	15.534			15.458
$^{208}\text{Pb}/^{204}\text{Pb}$	38.416	38.542			38.031
Initial isotopic ratios (age-corrected)					
$^{87}\text{Sr}/^{86}\text{Sr}$	0.702559	0.702686			0.702439
$^{143}\text{Nd}/^{144}\text{Nd}$	0.513198	0.513068			0.513178
$^{206}\text{Pb}/^{204}\text{Pb}$	18.942	19.166			18.556
$^{207}\text{Pb}/^{204}\text{Pb}$	15.554	15.523			15.454
$^{208}\text{Pb}/^{204}\text{Pb}$	38.346	38.352			37.963

See Figure IV.2 for full sample numbers. Age-correction for 13R-1 used the 10R-2 age of 33 Ma. Trace element concentrations were measured by ICP-MS at OSU, and were referenced to USGS rock standards BCR-1, BHVO-1, BIR-1, and W-1. Isotopic ratios were measured at Cornell University using procedures described in White et al. (1990). Isotopic samples were leached repeatedly in hot HCl, and all ratios were corrected for fractionation. Sr and Pb isotopic ratios were referenced to standards NBS987 and NBS981, respectively. The average  $^{143}\text{Nd}/^{144}\text{Nd}$  for the La Jolla Nd standard measured at the time of these analyses (via Ames Nd) was  $0.511870 \pm 14$ . Two-sigma standard errors based upon numerous analyses of standards during the time of the unknown runs are:  $^{87}\text{Sr}/^{86}\text{Sr} \pm 0.000014$ ,  $^{143}\text{Nd}/^{144}\text{Nd} \pm 0.000016$ ,  $^{206}\text{Pb}/^{204}\text{Pb} \pm 0.010$ ,  $^{207}\text{Pb}/^{204}\text{Pb} \pm 0.011$ , and  $^{208}\text{Pb}/^{204}\text{Pb} \pm 0.030$ . Within-run standard errors due to machine precision are smaller than these between-run errors.

Probable structure	Group	Samples	Age (Ma)	MgO (wt%)	TiO <sub>2</sub> (wt%)	Sr/Y	Zr/Nb	La <sub>N</sub> /Yb <sub>N</sub>	<sup>87</sup> Sr/ <sup>86</sup> Sr <sub>j</sub>	<sup>206</sup> Pb/ <sup>204</sup> Pb <sub>j</sub>
Sediments										
Massive sill	Upper	4R-4	17.1	6.4	2.0	18	5	4.7	0.70256	18.94
Sediments										
Flow Sediments										
Massive flow	Middle	7R-3	27.3	5.7	3.7	6	8	4.0	0.70269	19.17
		8R-2		6.3	3.3	7	8	3.7		
Sediments										
Series of pillows and/or thin flows		10R-2	33.0	5.4	1.8	7	17	1.5		
Lower		12R-1		5.3	1.9	5	13			
		13R-1		6.4	2.0	4	14	1.3	0.70244	18.56

Figure IV.2. Stratigraphy and geochemical characteristics of the basement portion of Hole 887D (modified from Keller et al., 1995). Stratigraphy was constructed from downhole logging data and core recovery data (Rea et al., 1993). <sup>40</sup>Ar-<sup>39</sup>Ar ages and major element data are from Keller et al. (1995) and Figure IV.3. Rare earth elements and isotopic data are from Table IV.1. La/Yb is normalized to chondrites. Isotopic ratios are age-corrected. Full sample numbers are 145-887D-: 4R-4, 47-49 cm; 7R-3, 67-70 cm; 8R-2, 84-89 cm; 10R-2, 68-71 cm; 12R-1, 13-18 cm; and 13R-1, 18-21 cm.

<sup>39</sup>Ar plateau age of 27.3±0.3 Ma. This age is within analytical error of the 27.6±0.2 Ma <sup>40</sup>Ar-<sup>39</sup>Ar age reported for a basalt dredged from the south side of Murray Guyot approximately 50 km from Site 887 (Dalrymple et al., 1987). Sample 4R-4 from the upper group yielded a reliable <sup>40</sup>Ar-<sup>39</sup>Ar plateau age of 17.1±0.3 Ma. Paleomagnetic, paleontological, and sedimentological data (Rea et al., 1993) suggest that the sediments bounding the upper group are approximately 21–22 m.y. old, so the upper group is actually a sill that intruded sediments that were 4–5 m.y. old at the time (Keller et al., 1995).

Major element and trace element data obtained by x-ray fluorescence were published in the Leg 145 post-cruise Scientific Results volume (Keller et al., 1995), and are only briefly reviewed here. The Hole 887D samples are moderately evolved (MgO: 5.3–6.4

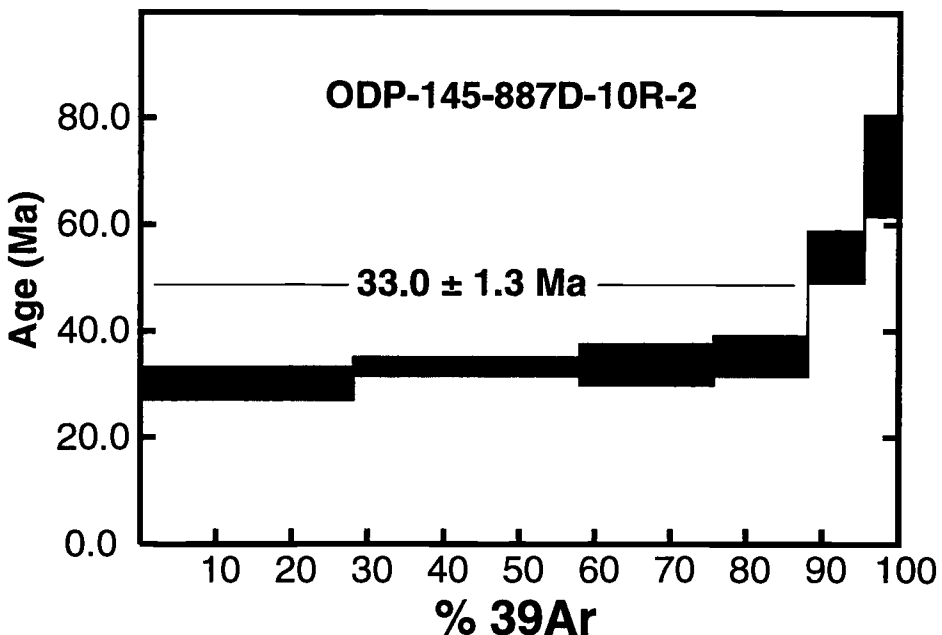


Figure IV.3. Sample 10R-2 dating results

wt.%), tholeiitic (lower and upper groups) and alkalic (middle group) basalts. The lower and upper groups have similar major element concentrations ( $\text{SiO}_2$ : 48.8–49.9;  $\text{TiO}_2$ : 1.8–2.0;  $\text{FeO}^*$ : 9.1–11.5;  $\text{CaO}$ : 11.1–11.9) that are distinct from the major element concentrations of the middle group ( $\text{SiO}_2$ : 47.1–47.6;  $\text{TiO}_2$ : 3.3–3.7;  $\text{FeO}^*$ : 13.0–13.2;  $\text{CaO}$ : 8.0–8.3). The high  $\text{TiO}_2$  and  $\text{Na}_2\text{O}+\text{K}_2\text{O}$  of the middle group indicates alkalic affinities, while the lower and upper groups have concentrations of alkalis,  $\text{TiO}_2$ , and other incompatible elements similar to tholeiitic to transitional basalts. However, the similarities between the upper and lower groups are limited to the major elements; the upper group has distinctly higher  $\text{Sr}$ ,  $\text{Nb}$ , and light rare earth element concentrations, and lower  $\text{Y}$  and heavy rare earth element concentrations (Table IV.1). The middle group has incompatible trace element concentrations significantly higher than the other two groups (with the exception of elements readily mobilized by alteration), but  $\text{La}_{\text{N}}/\text{Yb}_{\text{N}}$  similar to the upper group (Figure IV.2).

The three groups are easily distinguished by their  $\text{Sr}/\text{Y}$  and  $\text{Zr}/\text{Nb}$  (Figure IV.4). The lower group has the lowest  $\text{Sr}/\text{Y}$  and the highest  $\text{Zr}/\text{Nb}$ , and overlaps the data fields of the Cobb-Eickelberg seamounts and the Juan de Fuca Ridge (C-E and JdFR in Figures IV.1 and IV.4). The middle group has slightly higher  $\text{Sr}/\text{Y}$  and slightly lower  $\text{Zr}/\text{Nb}$ ,

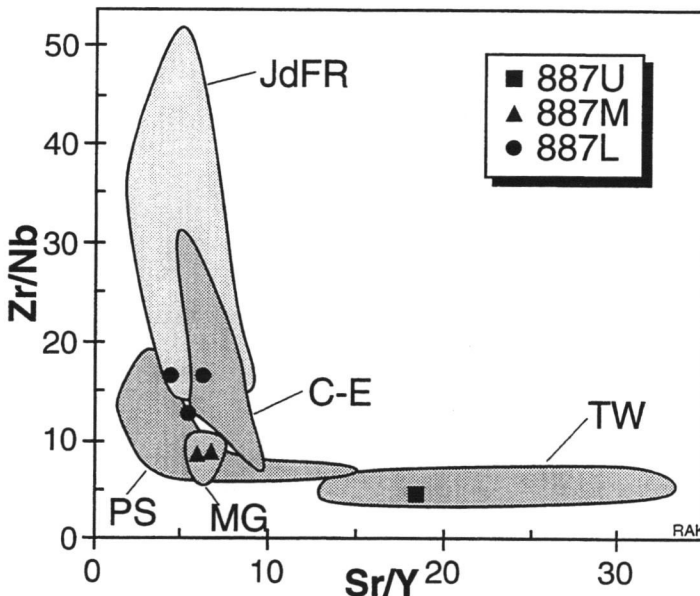


Figure IV.4. Sr/Y vs. Zr/Nb for the Hole 887D samples compared to other data from the northeast Pacific. Field labels are: C-E = Cobb-Eickelberg seamounts (Desonie and Duncan, 1990), JdFR = Juan de Fuca Ridge spreading center (including Axial Seamount) (Rhodes et al., 1990), MG = Murray Guyot (Dalrymple et al., 1987), PS = Patton Seamount (Dalrymple et al., 1987), TW = Tuzo Wilson seamounts (Allan et al., 1993), and 887L/M/U = Site 887 lower/middle/upper groups.

and falls exactly on the published data field for Murray Guyot. The upper group has distinctly higher Sr/Y and lower Zr/Nb, and is similar to published data for the Tuzo Wilson seamounts.

Our major and trace element data indicate that each group is fairly homogeneous, so we are confident that a single isotopic analysis from each group is sufficiently representative. The isotopic data emphasize the uniqueness of each basalt group (Table IV.1). The lower group has the least radiogenic Sr and Pb isotopic ratios, and plots within or just outside the JdFR data fields (Figure IV.5). The middle group has the most radiogenic Sr and Pb isotopic ratios (except  $^{207}\text{Pb}/^{204}\text{Pb}$ ) and the least radiogenic Nd isotopic ratios, and plots at the more-radiogenic-Pb end of the NE Pacific seamounts (NEPS) data field. The upper group is between the other two groups in  $^{87}\text{Sr}/^{86}\text{Sr}$ ,  $^{206}\text{Pb}/^{204}\text{Pb}$ , and  $^{208}\text{Pb}/^{204}\text{Pb}$ , and falls in the middle of the NEPS field in those ratios. Its  $^{143}\text{Nd}/^{144}\text{Nd}$  and  $^{207}\text{Pb}/^{204}\text{Pb}$ , however, are the highest of the three groups, and in these two isotopic ratios it plots at the high end of the NEPS field.

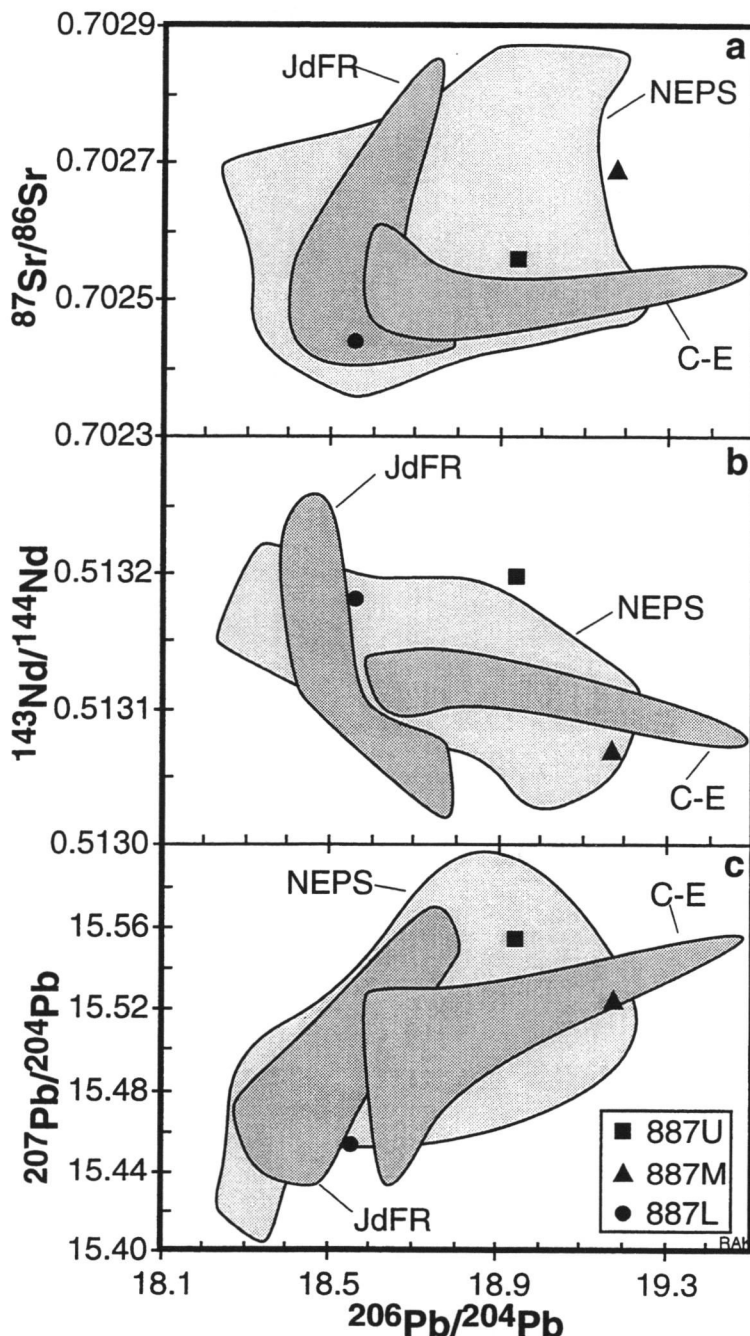


Figure IV.5.  $^{206}\text{Pb}/^{204}\text{Pb}$  vs. other isotopic ratios for the Site 887 samples compared to other data from the northeast Pacific. Field labels are: C-E = Cobb-Eickelberg seamounts (Desonie and Duncan, 1990); JdFR = Juan de Fuca Ridge spreading center (Hegner and Tatsumoto, 1987); NEPS = Northeast Pacific seamounts [including Tuzo Wilson (Allan et al., 1993), Pratt-Welker (Church and Tatsumoto, 1975; Cousens, 1988; and Hegner and Tatsumoto, 1989), and Dellwood, Explorer, Heckle, and Union (Hegner and Tatsumoto, 1989)]; and 887L/M/U = Site 887 lower/middle/upper groups. Site 887 data are age-corrected.

## DISCUSSION

Although ODP Hole 887D penetrated only 84 m after striking the first basalt, it sampled a long period of volcanism on the Patton-Murray seamount platform. The lower group of basalt is 33 m.y. old, and is isotopically and chemically similar to the recent products of the Cobb hotspot (Cobb-Eickelberg seamounts; Desonie and Duncan, 1990) and the Juan de Fuca Ridge (Figures IV.4 and IV.5). Plate motion models (Duncan and Clague, 1985) place the Patton-Murray platform above the Cobb hotspot between 33 and 30 Ma (Figure IV.1). We therefore conclude that the lower group erupted when the seamount platform was above the Cobb hotspot. The bulk of the seamount platform was probably created at this time, but this phase of volcanism is covered by later volcanism and sediments, and was not sampled by dredging.

It is also interesting to note that the lower group is isotopically more similar to the Juan de Fuca Ridge than to the Cobb-Eickelberg seamounts (Figure IV.5). Although the differences are small, and it is dangerous to draw too many conclusions from a single analysis of the lower group, the isotopic composition of the Cobb hotspot seems to have become slightly more enriched over the last 20–30 m.y. Similar (though larger) shifts toward more enriched isotopic values have been reported from the Kerguelen, Réunion, and Hawaiian hotspots (White et al., 1990; Weis et al., 1992; Keller et al., 1994). In the case of the Cobb hotspot, the shift is especially impressive because the hotspot is actually closer to a spreading ridge now than it was 33 m.y. ago. The Patton-Murray platform erupted onto crust  $\geq$ 7 m.y. old, while the Cobb-Eickelberg seamounts erupted onto crust <3 m.y. old (Desonie and Duncan, 1990).

At 27.3 Ma, the alkalic basalts of the middle group erupted after the seamount platform had moved approximately 200 km west of the Cobb hotspot. Alkalic basalts are typical of late-stage rejuvenescent volcanism downstream of hotspots (Macdonald and Katsura, 1964; Clague and Dalrymple, 1987). This middle group has the same age and chemistry as the alkalic basalts dredged from the opposite side of Murray Guyot and dated at 27.6 Ma (Dalrymple et al., 1987), which shows that alkalic volcanism was widespread on Murray Guyot at that time. The 8 m of sediments between the lower and middle groups represent approximately 6 m.y. of time (assuming that the middle group of basalts flowed onto the seafloor rather than intruded the sediments). Unfortunately, none of those sediments were recovered.

From 27.3 Ma to 17.1 Ma there was a hiatus in volcanism at Site 887. During this time sedimentation continued as the seamount platform moved further northwestward

away from the hotspot. At 17.1 Ma, a very-late phase of volcanism (the upper group of basalt) occurred that is chemically and isotopically distinct from the two earlier phases. This phase had not previously been sampled during dredging of the Patton-Murray seamounts (Dalrymple et al., 1987), and is chemically distinct from anything previously reported from the NE Pacific (although it happens to have Sr/Y and Zr/Nb similar to some of the Tuzo Wilson seamounts basalts).

Possibly similar to the very-late rejuvenescence on Patton-Murray is the report of a 11.5 m.y. difference (14.3 Ma vs. 2.8 Ma) in ages of dredged samples from Hodgkins Seamount (HS in Figure IV.1; Turner et al., 1980). Although it is possible that these conventional K-Ar ages were disturbed by loss of Ar during alteration, the authors considered them to be reliable because they obtained similar results from both whole rock samples and plagioclase separates.

This phenomenon of very-late phase rejuvenescence is not unique to the NE Pacific, and may have a separate cause unrelated to hotspot volcanism. Alkalic capping lavas on Detroit Guyot (NW Pacific) are interpreted, based upon typical subsidence rates, to have erupted into a shallow submarine environment approximately 60 m.y. ago (Lonsdale et al., 1993), which is approximately 20 m.y. after the bulk of the Detroit seamount platform erupted (Keller et al., 1995), and was after the seamount platform had moved more than 1000 km from the Hawaiian hotspot (Lonsdale et al., 1993). On Christmas Island (NE Indian Ocean), episodic volcanism over the course of 37 m.y. (40 Ma, 34 Ma, and 3 Ma) has ocean-island-basalt-type chemistry (Falloon et al., in prep). The initial two volcanic phases may have been caused by hotspot activity or a global reorganization of spreading ridges, but the most recent phase of volcanism is likely due to passage of the island over the flexural bulge outboard of the Java Trench, or to extension caused by the general state of tension in that area of the Australian Plate (Cloetingh and Wortel, 1985).

Another possible mechanism for intraplate volcanism unrelated to hotspots was elicited by recent work on the bathymetric ridges and troughs that cause the 'crossgrain' gravity lineations in the central South Pacific. Along the axis of the larger troughs are linear volcanic ridges elongate in the direction of present absolute plate motion (Sandwell et al., 1995). However, a hotspot origin for the ridges is ruled out by the fact that the ridges do not match the plate motion prior to 24 Ma, and basalts dredged from the ridges show no systematic age progressions. Sandwell et al. (1995) proposed that diffuse extension of the Pacific Plate caused by trench pull can cause extension and volcanism where the plate is weakest. In the central South Pacific, the plate is weakest

where it is youngest. In the Gulf of Alaska, the plate would be weakest where it had previously passed over a hotspot. Thus, very-late stage volcanism unrelated to a hotspot can occur on a seamount platform that was originally created by a hotspot. This model not only suggests that the 17 Ma upper basalt at Hole 887D is unrelated to any hotspot, but also that additional, even more recent, volcanism could have occurred on the Patton-Murray platform, or on any other NE Pacific seamount for that matter.

## CONCLUSION

Basalts recovered from ODP Hole 887D on Patton-Murray seamount platform record 16 m.y. of intermittent volcanism during and after the time the seamount platform was above the Cobb hotspot. Basalts from the deepest portion of the hole erupted at 33 Ma while the seamount platform was above the hotspot, and are chemically and isotopically similar to basalts from the Cobb-Eickelberg seamounts and the Juan de Fuca Ridge. A 27 Ma alkalic basalt flow recovered higher in the hole is similar to basalts dredged from other seamounts in the northeast Pacific, and may be the alkalic rejuvenescent volcanism typical of many hotspots. A 17 Ma basalt sill recovered at the top of the basalt section is chemically and isotopically distinct from the other basalts in the hole, and erupted well after the seamount platform had moved away from the hotspot. We attribute the youngest basalt to minor extension at a pre-existing weakness in the plate. The isotopic ratios of the 33 Ma lower basalt are even more depleted than the 0–9 Ma products of the Cobb hotspot, despite the fact that the hotspot was closer to a spreading ridge at 0–9 Ma. It appears that this hotspot, like several others, has become more enriched with time.

## ACKNOWLEDGMENTS

We thank M. Cheatham for assistance with the TIMS analyses, A. Ungerer for assistance with the ICP-MS analyses, and C. Sinton for dating sample 10R-2. This work was supported by a JOI/USSAC Ocean Drilling Fellowship.

## Chapter 5

### An Isotopic Profile Across the Northern Antarctic Peninsula: Relationships Between Subduction History and Geochemical Components

Randall A. Keller, Martin R. Fisk, John L. Smellie, Jorge A. Strelin,  
William M. White, Ian L. Millar, and Lawrence A. Lawver

## ABSTRACT

On the northern Antarctic Peninsula, Tertiary to Recent volcanism at distances ranging from 100 to 360 km from the South Shetland Trench allows us to determine how large a region of the mantle is influenced by a single subduction zone. Sediments on the subducting plate have high  $^{87}\text{Sr}/^{86}\text{Sr}$ , low  $^{143}\text{Nd}/^{144}\text{Nd}$ , and moderate  $^{206}\text{Pb}/^{204}\text{Pb}$ . This subducted sediment component is most evident in the Tertiary basalts from the South Shetland Islands Arc (100–125 km from the trench), which have elevated  $^{87}\text{Sr}/^{86}\text{Sr}$  and Ba/Nb values. Isotopic compositions of the Quaternary volcanic rocks in the Bransfield Strait backarc basin (125–150 km from the trench) show less of the subducted component, and these rocks have low to moderate Ba/Nb. Isotopic data from the Upper Miocene to Recent basalts of the James Ross Island Volcanic Group in the far backarc (300–360 km from the trench) show even less of the subducted component, and these rocks have low Ba/Nb. Isotopic data from all three areas can be described by mixing of the subducted component with different amounts of a depleted mantle component plus a high  $^{206}\text{Pb}/^{204}\text{Pb}$ -low  $^{87}\text{Sr}/^{86}\text{Sr}$  (St. Helena-like) mantle component. This latter component is seen in Cenozoic volcanism throughout West Antarctica, but is diluted by recently subducted Pb to various extents in different areas, depending upon the Mesozoic-Cenozoic subduction history of each area.

## INTRODUCTION AND BACKGROUND

Subduction of oceanic crust is the only significant flux of material from the surface to the deep interior of the earth, and is important for the mass balance of the mantle and the chemical history of the earth. Numerous chemical characteristics of volcanic rocks in arcs and backarcs (e.g., Saunders and Tarney, 1984; White and Patchett, 1984), as well as global-scale chemical and isotopic variation of the mantle (e.g., Hofmann and White, 1982; White, 1985; Zindler and Hart, 1986; Ringwood, 1990) have been attributed to contamination of the mantle by subducted lithosphere. But the exact process by which this contamination occurs, and how widespread it can be in a single subduction zone, are still being determined (Stern et al., 1990; Woodhead and Johnson, 1993).

The northern Antarctic Peninsula is an extinct Mesozoic-Cenozoic magmatic arc recently modified by extension and its related volcanic activity. At the South Shetland Trench, a piece of the Antarctic Plate is subducting toward the southeast beneath the

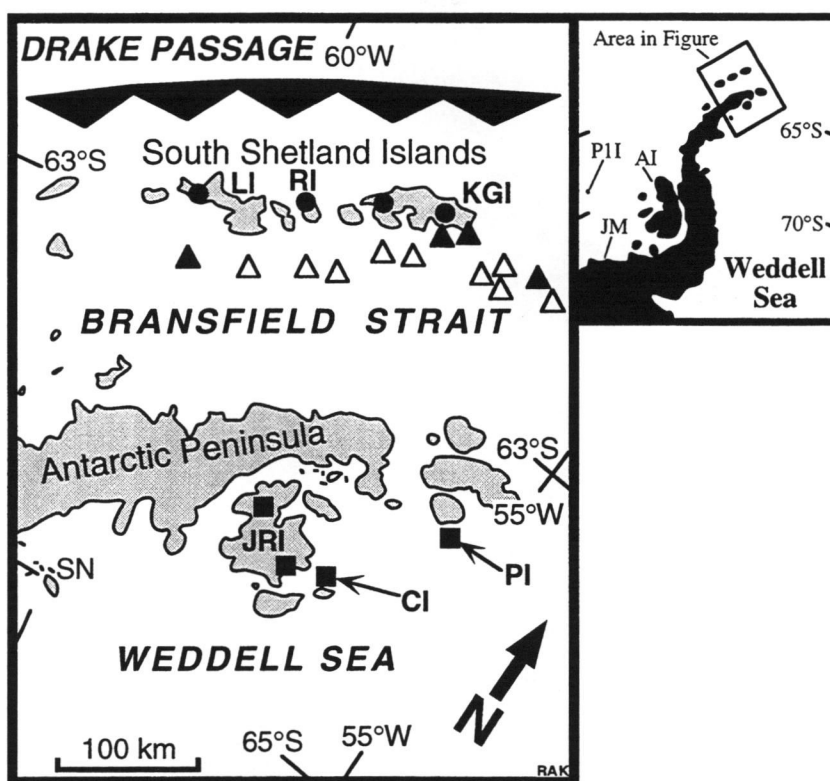


Figure V.1. Map of the northern Antarctic Peninsula showing locations of volcanism discussed in this study. Inset shows some other locations of late Tertiary-Quaternary volcanism on and around the Antarctic Peninsula: AI = Alexander Island, JM = Jones Mountains, PII = Peter I Island. Filled circles on the South Shetland Islands show locations of the Cretaceous-Tertiary arc samples. Triangles show locations of <0.3 m.y. old volcanic rocks in Bransfield Strait. Filled triangles are subaerial, unfilled triangles are submarine. Square symbols show the locations of Late Miocene and younger alkalic basalts of the James Ross Island Volcanic Group used in this study. CI = Cockburn Island, JRI = James Ross Island, KGI = King George Island, LI = Livingston Island, PI = Paulet Island, RI = Robert Island, SN = Seal Nunataks. The approximate location of the South Shetland Trench is shown by a chain of large triangles with their peaks pointing to the overriding plate.

South Shetland microplate (Figure V.1), deforming sediments in the trench (Maldonado et al., 1994) and causing earthquakes beneath the South Shetland Islands (Pelayo and Wiens, 1989; SEAN, 1993). Overlying this subducting slab are three distinct types of Tertiary and Quaternary volcanism at different distances from the trench (Figure V.2): the extinct Cretaceous-Tertiary South Shetland Islands arc at 100–125 km distance; the active, Quaternary Bransfield Strait backarc at 125–150 km; and the Late Miocene-

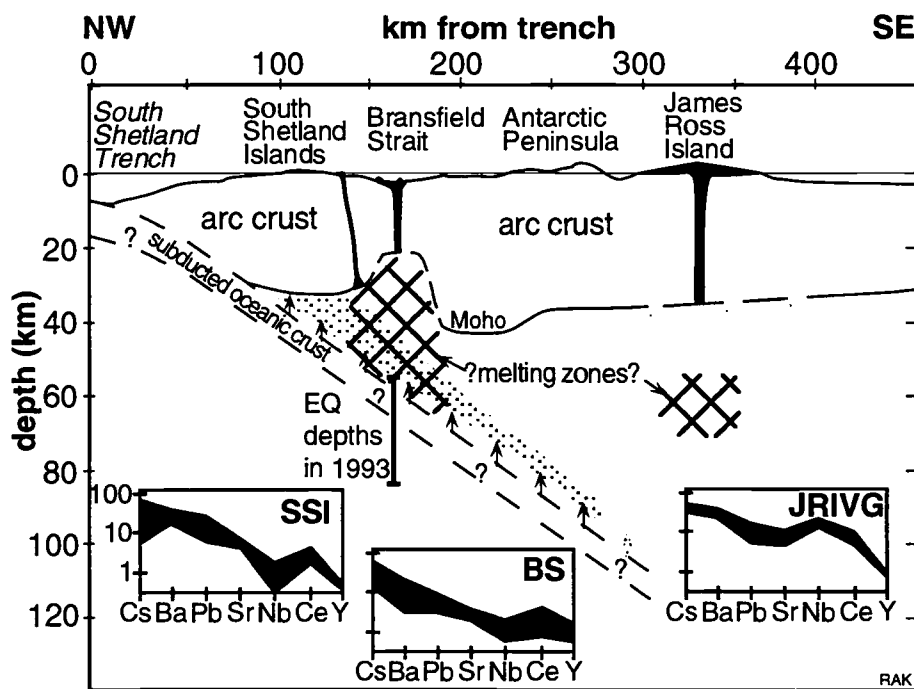


Figure V.2. Generalized crustal and upper mantle cross-section of the northern Antarctic Peninsula. The dip of the subducting slab is poorly constrained, but is shown as 20°, as suggested by earthquakes (Pelayo and Wiens, 1989; Seismic Event Alert Network, 1993) and seismic refraction data (Grad et al., 1993). Tertiary-Quaternary volcanic rocks are found from 100 to 360 km from the South Shetland Trench at the South Shetland Islands, Bransfield Strait, and James Ross Island. Trace element characteristics of the volcanism in each area are shown on NMORB-normalized spider diagrams (NMORB values from Sun and McDonough, 1989).

Recent James Ross Island Volcanic Group (JРИVG) extreme backarc at 300–360 km. We have shown previously that the major and trace element data document a decrease in subduction zone signature with increasing distance from the trench (Keller et al., 1993; Lawver et al., 1995). Here we present new data that identify the isotopic characteristics of the subducted component on the northern Antarctic Peninsula, and show that the subduction-related geochemical signature appears even in the JРИVG at 360 km from the trench.

Closest to the trench (100–125 km) is the Cretaceous to Early Miocene South Shetland Islands volcanic arc (Figure V.1). Most of the arc is calc-alkaline basalts and basaltic andesites with slight tholeiitic affinities (Smellie et al., 1984). The Tertiary

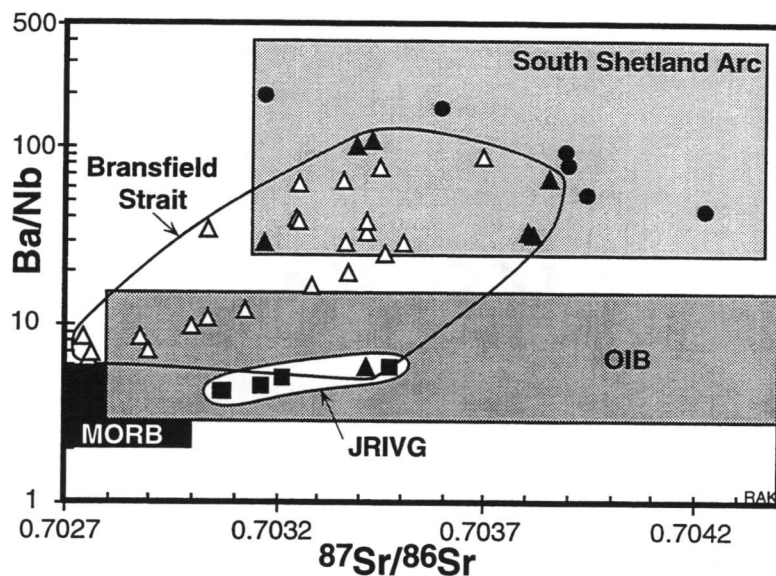


Figure V.3.  $^{87}\text{Sr}/^{86}\text{Sr}$  vs. Ba/Nb for northern Antarctic Peninsula basalts. Symbols as in Figure A. Fields are shown for the South Shetland Arc (data points are from Table V.1 and Keller et al., 1992; remainder of field from references given in text), Bransfield Strait islands and seamounts (Table V.2 and Keller et al., 1992), and James Ross Island Volcanic Group (JРИVG; Table V.3). Figure concept and MORB and OIB fields from Stern et al. (1990).

basalts of the arc are enriched in the large-ion lithophile elements (especially Ba), but depleted in Nb, which gives them the high Ba/Nb (Figure V.3) typical of arc volcanism (e.g., Pearce and Parkinson, 1993). Sr isotopic ratios mostly range from 0.7033 to 0.7043 (Smellie et al., 1984; Barbieri et al., 1989; Jin et al., 1991; Keller et al., 1992). The only previously published Sr-Nd-Pb isotopic data from the arc are from a 24 m.y. old basalt from King George Island (Keller et al., 1992). For this study, we analyzed an additional sample from King George Island as well as samples from Robert Island and Livingston Island (Figure V.1 and Table V.1). The arc samples have the highest  $^{87}\text{Sr}/^{86}\text{Sr}$  and lowest  $^{143}\text{Nd}/^{144}\text{Nd}$ ,  $^{206}\text{Pb}/^{204}\text{Pb}$ , and  $^{208}\text{Pb}/^{204}\text{Pb}$  of any of the northern Antarctic Peninsula volcanism (Figure V.4). Although our isotopic data are only of a reconnaissance nature, they represent a range of ages and locations on the South Shetland Islands, and are sufficient for comparing the arc to Bransfield Strait and James Ross Island.

Bransfield Strait (BS) is a Quaternary marginal basin with numerous locations of recent (<0.3 Ma; see Lawver et al., 1995 for a review) volcanism on seamounts and

**Table V.1. Isotopic Data for Basalts From the South Shetland Island Arc**

Sample	KGI.LH1	KGI.615.1	RI.842.9	LI.864.4	LI.845.9	LI.862.4
<b>Measured ratios</b>						
$^{87}\text{Sr}/^{86}\text{Sr}$	0.703593	0.703186 (0.703229)	0.703966 (0.704226)	0.704281 (0.704226)	(0.703928)	(0.704003)
$^{143}\text{Nd}/^{144}\text{Nd}$	0.512955	0.513030 (0.513004)	0.512814 (0.512822)	(0.512822)	(0.512864)	(0.512797)
$^{206}\text{Pb}/^{204}\text{Pb}$	18.754	18.532	18.616	18.617	18.585	18.891
$^{207}\text{Pb}/^{204}\text{Pb}$	15.603	15.567	15.581	15.581	15.587	15.619
$^{208}\text{Pb}/^{204}\text{Pb}$	38.539	38.196	38.312	38.353	38.313	38.726
Age (Ma)	24	51	82	95	109	123
<b>Age-corrected (initial) ratios</b>						
$^{87}\text{Sr}/^{86}\text{Sr}$	0.703585	0.703173	0.703944	0.704227	0.703902	0.703896
$^{143}\text{Nd}/^{144}\text{Nd}$		0.512986	0.512737	0.512718	0.512741	0.512665
$^{206}\text{Pb}/^{204}\text{Pb}$		18.446	18.543	18.544	18.564	18.636
$^{207}\text{Pb}/^{204}\text{Pb}$		15.563	15.578	15.577	15.586	15.607
$^{208}\text{Pb}/^{204}\text{Pb}$		38.092	38.224	38.262	38.291	38.404

Sample locations: KGI=King George Island; LI=Livingston Island; RI=Robert Island. Isotopic ratios were measured at Cornell University (except those in parentheses were measured at NERC-BAS) using procedures described in White et al. (1990). All samples were leached repeatedly in hot HCl prior to digestion, and all isotopic ratios were corrected for fractionation. Sr and Pb isotopic ratios were referenced to standards NBS987 and NBS981, respectively. The average  $^{143}\text{Nd}/^{144}\text{Nd}$  for the La Jolla Nd standard measured at the time of these analyses was  $0.511856 \pm 15$ . Two-sigma standard errors based upon numerous analyses of standards during the time of the unknown runs are:  $^{87}\text{Sr}/^{86}\text{Sr} \pm 0.000012$ ,  $^{143}\text{Nd}/^{144}\text{Nd} \pm 0.000015$ ,  $^{206}\text{Pb}/^{204}\text{Pb} \pm 0.005$ ,  $^{207}\text{Pb}/^{204}\text{Pb} \pm 0.007$ , and  $^{208}\text{Pb}/^{204}\text{Pb} \pm 0.017$ . Within-run standard errors due to machine precision are smaller than these between-run errors. Upgraded collector cups account for the better precision of these data and the Bransfield Strait data (Table V.2) compared to the JRIVG data (Table V.3). ICP-MS trace element data (Chapter 6) were used for age corrections. Nd-Sm-Pb-Th-U concentrations in sample KGI.LH1 have not been measured. Ages are K-Ar dates, except the KGI.LH1 age is a  $^{40}\text{Ar}/^{39}\text{Ar}$  incremental-heating date.

islands 125 to 150 km from the South Shetland Trench (Figure V.1) (Keller et al., 1992; 1994). These rocks are mainly subalkaline olivine basalts and basaltic andesites, although Penguin Island has slightly alkalic basalts and Deception Island includes a complete basalt-to-trachydacite evolutionary suite. The seamount samples are moderately enriched in the large-ion lithophile elements (LILE), and have slight negative Nb anomalies (Figure V.2). The subaerial samples are more variable, and generally LILE enriched, but range from strongly depleted to slightly enriched in Nb relative to mid-ocean ridge basalt (MORB). Pb isotopic ratios have narrow ranges compared to Sr

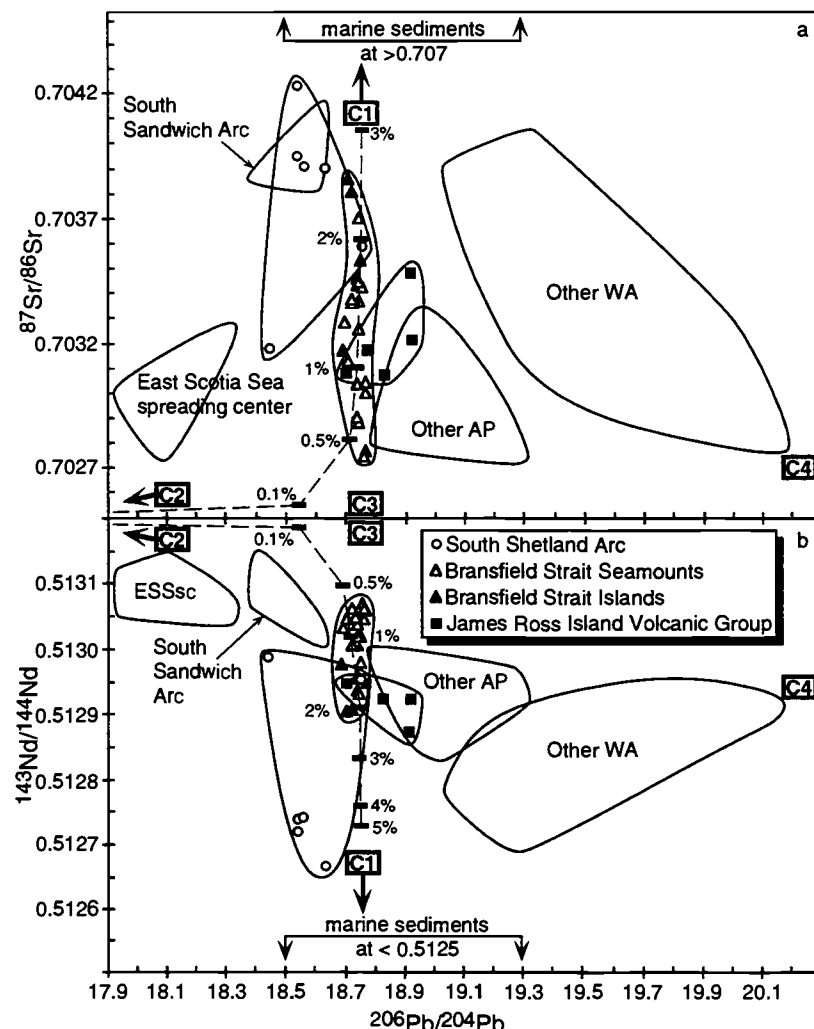


Figure V.4.  $^{206}\text{Pb}/^{204}\text{Pb}$  vs. other isotopic ratios for northern Antarctic Peninsula basalts. Symbols and data sources as in Figure V.3. "Other AP" data fields are samples from other locations on the Antarctic Peninsula at Alexander Island and Seal Nunataks (Figure V.1) (Hole et al., 1993). "Other WA" data fields are samples from elsewhere in West Antarctica (Peter I Island and Jones Mountains - Hart et al., 1995; McMurdo Volcanic Group - Rocholl et al., 1995). South Sandwich Islands data from Hawkesworth et al. (1977), Cohen and O'Nions (1982), and Barreiro (1983). East Scotia Sea Spreading Center data from Cohen and O'Nions (1982). Marine sediments fields from data in O'Nions et al. (1978), Sun (1980), Barreiro (1983), White et al. (1985), and Ben Othman et al. (1989). Approximate compositions of the isotopic mixing components C1–C4 (Table V.5) are shown. Dashed lines with tick marks labeled with percentages are mixing lines between depleted mantle (C2) with  $^{87}\text{Sr}/^{86}\text{Sr}$  :  $^{143}\text{Nd}/^{144}\text{Nd}$  :  $^{206}\text{Pb}/^{204}\text{Pb}$  values of 20 : 0.7025 : 1.1 : 0.5132 : 0.043 : 17.6 and the labeled percentages of a high-Pb, low-Sr/Pb sediment component (special type of C1) with values of 200 : 0.709 : 30 : 0.5124 : 200 : 18.75. A mixing line between depleted mantle with higher  $^{206}\text{Pb}/^{204}\text{Pb}$  (C3) and sediment with more typical composition (Table V.4) would have similar form at sediment percentages >0.5%.

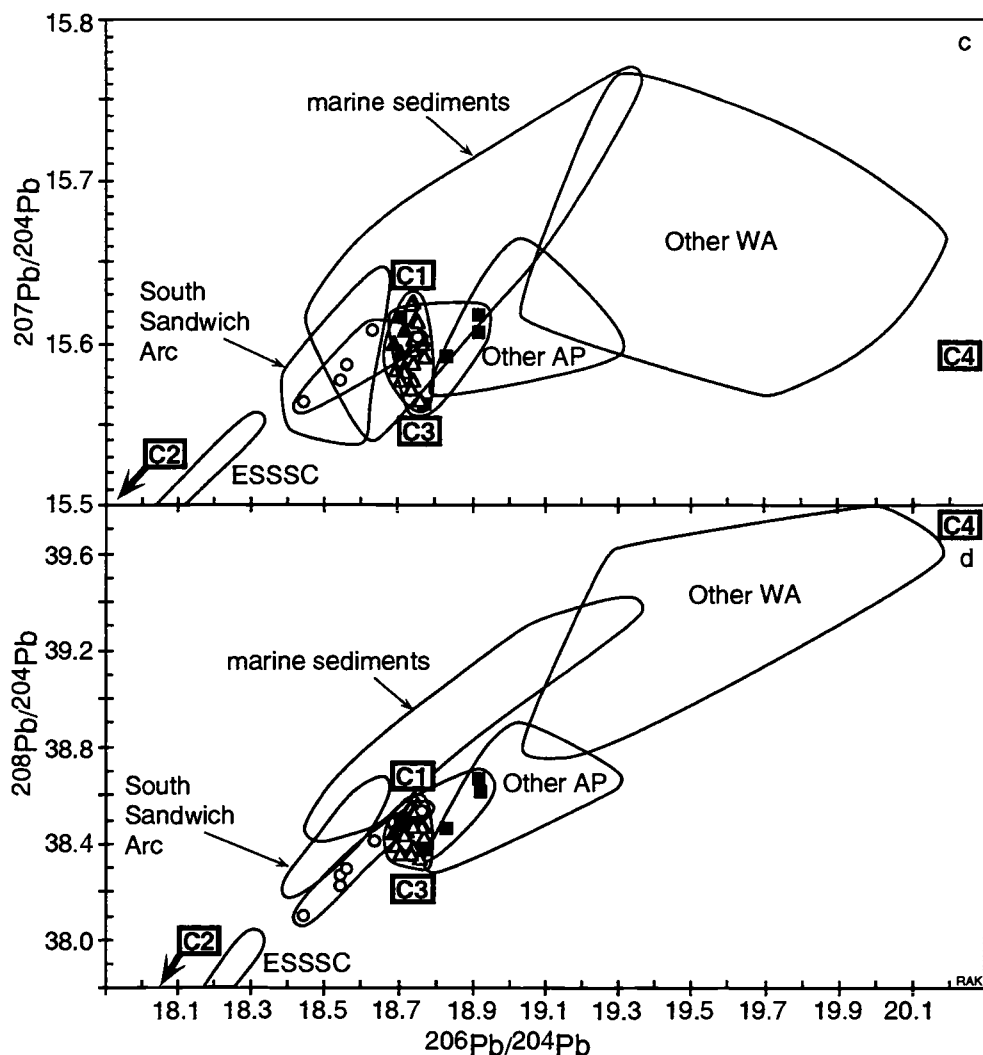


Figure V.4. (continued)

and Nd isotopic ratios (Table V.2, Figure V.4, and Keller et al., 1992). Although there is considerable overlap, the submarine samples extend to lower  $^{87}\text{Sr}/^{86}\text{Sr}$ ,  $^{207}\text{Pb}/^{204}\text{Pb}$ , and  $^{208}\text{Pb}/^{204}\text{Pb}$  values, and higher  $^{143}\text{Nd}/^{144}\text{Nd}$  and  $^{206}\text{Pb}/^{204}\text{Pb}$  values than the subaerial samples. The BS data range to lower  $^{87}\text{Sr}/^{86}\text{Sr}$  and higher  $^{143}\text{Nd}/^{144}\text{Nd}$  than the arc, but the arc ranges to lower  $^{206}\text{Pb}/^{204}\text{Pb}$  and  $^{208}\text{Pb}/^{204}\text{Pb}$  than BS. Although the youngest arc sample has Sr, Nd, and Pb isotopic ratios nearly identical to some of the BS samples, Keller et al. (1992) showed that the range in the BS isotopic data could not be modeled by assimilation of arc crust without using unreasonably high Sr concentrations for the assimilant.

**Table V.2. Isotopic Data for Samples Dredged From Bransfield Strait**

Sample	$^{87}\text{Sr}/^{86}\text{Sr}$	$^{143}\text{Nd}/^{144}\text{Nd}$	$^{206}\text{Pb}/^{204}\text{Pb}$	$^{207}\text{Pb}/^{204}\text{Pb}$	$^{208}\text{Pb}/^{204}\text{Pb}$
BSD1A	0.702760	0.513079	-	-	-
BSD1F	0.702765	0.513058	18.771	15.592	38.426
BSD2G	0.702743	0.513068	18.763	15.564	38.332
BSD2N	0.702878	0.513036	18.744	15.577	38.382
BSD3C	0.703039	0.513044	18.766	15.600	38.480
BSD4D	0.702997	0.513061	18.769	15.602	38.473
BSD6D	0.703448	0.512936	18.746	15.595	38.520
BSD7A	0.703360	0.513005	18.724	15.585	38.455
BSD8F	0.703256	0.513018	18.744	15.587	38.473
BSD10A	0.703698	0.512930	18.748	15.602	38.533
BSDR144.1	0.702897	0.513048	18.740	15.571	38.356
BSDR144.4	0.703372	0.513061	18.723	15.582	38.431
BSDR145.3	0.703285	0.513031	18.696	15.584	38.387
BSDR156.4	0.703125	0.513046	18.710	15.577	38.353

See Keller et al. (1994) for dredge locations. Technique and precision details are given in Table V.1. All samples are thought to be <0.3 m.y. old.

Mildly alkalic olivine basalts of the James Ross Island Volcanic Group (JRIVG; Nelson, 1966) erupted onto Jurassic backarc basin crust (MacDonald et al., 1988) 300–360 km from the South Shetland Trench (Figure V.1) beginning at approximately 7 Ma (Smellie et al., 1988; Sykes, 1988; Lawver et al., 1995), and continuing to Recent times (Strelin et al., 1993). These basalts are geochemically similar to alkalic ocean-island basalts and continental-rift basalts in their high total alkalies,  $\text{Al}_2\text{O}_3$ , and Nb, and low LILE/Nb (Figure V.2) (Lawver et al., 1995). Sr isotopic ratios (Table V.3) are near the middle of the range of BS values, and  $^{207}\text{Pb}/^{204}\text{Pb}$  and  $^{208}\text{Pb}/^{204}\text{Pb}$  have ranges similar to Bransfield Strait, but the JRIVG ranges to lower  $^{143}\text{Nd}/^{144}\text{Nd}$  and higher  $^{206}\text{Pb}/^{204}\text{Pb}$  than does BS (Figure V.4).

## DISCUSSION

Our objectives are to find a parameter that measures the amount of subducted component in the volcanism at various distances from the South Shetland Trench, and to determine whether or not that parameter decreases with increasing distance from the trench. A good candidate for this parameter is Ba/Nb: arc volcanism often has high Ba/Nb (Hickey et al., 1986) due to both high Ba and low Nb. Ba/Nb in samples from

**Table V.3. Isotopic Data for Basalts From the James Ross Island Volcanic Group**

Sample	JRI114	JRI117	JRI208	CK3	PA1	$2\sigma$ error
$^{87}\text{Sr}/^{86}\text{Sr}$	0.703214	0.703076	0.703071	0.703477	0.703167	$\pm 14$
$^{143}\text{Nd}/^{144}\text{Nd}$	0.512922	0.512947	0.512921	0.512870	0.512945	$\pm 16$
$^{206}\text{Pb}/^{204}\text{Pb}$	18.923	18.707	18.832	18.921	18.773	$\pm 10$
$^{207}\text{Pb}/^{204}\text{Pb}$	15.606	15.615	15.592	15.617	15.562	$\pm 11$
$^{208}\text{Pb}/^{204}\text{Pb}$	38.611	38.493	38.456	38.668	38.367	$\pm 30$

JRI = James Ross Island, CK = Cockburn Island, and PA = Paulet Island. Isotopic ratios were measured at Cornell University as described in Table V.1. All samples are <7 m.y. old. The average  $^{143}\text{Nd}/^{144}\text{Nd}$  for the La Jolla Nd standard measured at the time of these analyses (via Ames Nd) was  $0.511870 \pm 14$ . The 2 sigma standard errors given are for the last two decimal places and are based upon numerous analyses of standards during the time of the unknown runs. Whole-rock analyses of these samples are given in Lawver et al. (1995).

the South Shetland Arc ranges from 25 to 400, while BS samples range from 6 to 110, and JRIVG samples range from 4 to 6 (Figure V.3). JRIVG Ba/Nb values are comparable to MORB and ocean island basalt (Figure V.3), and therefore appear to lack the arc component. So if high Ba/Nb can be taken as characteristic of subduction-zone volcanism, then this characteristic decreases from high in the arc to nonexistent in the JRIVG.

Because of the strong affect that  $\text{H}_2\text{O}$  has on Nb partition coefficients (Tatsumi et al., 1986; Ionov and Hofmann, 1995), and the likelihood of a wide range of  $\text{pH}_2\text{O}$  conditions in melts at 100 to 360 km from a trench, the variation in Ba/Nb values of the northern Antarctic Peninsula basalts may reflect differences in melting conditions as well as source differences. We are interested here only in source differences, so we will avoid the problem of variant melting conditions by using radiogenic isotopic ratios, which are unaffected by melt-fractionation processes.

Sediments usually have high concentrations of Sr and Pb compared to uncontaminated mantle (Table V.4), so the geochemical contribution of subducted sediments to arc volcanism should be especially easy to recognize in Sr and Pb isotopes if the sediment has isotopic ratios that are measurably different from those of uncontaminated mantle. The contrast is amplified if the Sr and Pb in the sediments are further concentrated into a fluid phase by dehydration/melting reactions in the subducting slab (e.g., Woodhead, 1989; Stolper and Newman, 1994). Most sediments

**Table V.4. Comparison of depleted mantle, sediment, arc, Bransfield Strait, and JРИVG**

	Depleted mantle	S. Atlantic sediment	Pacific sediment	So. Shetland Arc basalt	Bransfield Strait seamounts	JРИVG basalt
Reference	a	b	c	d	e	f
Sr ppm	16.9	173	218	225–990	174–380	360–1290
Nd ppm	1.1	9.4	50	9.6–19.5	5.0–23.0	17–73
Pb ppm	0.043	13.4	55.7	2.2–8.1	0.8–3.1	2.0–5.6
$^{87}\text{Sr}/^{86}\text{Sr}$	0.7026	0.7089	0.7092	0.7032–0.7043	0.7027–0.7037	0.7029–0.7036
$^{143}\text{Nd}/^{144}\text{Nd}$	0.51319	0.51250	0.51243	0.51267–0.51301	0.51293–0.51308	0.51278–0.51295
$^{206}\text{Pb}/^{204}\text{Pb}$	18.25	18.63	18.71	18.45–18.75	18.70–18.77	18.71–18.92

References: a = Wood et al., 1979; b = average from Ben Othman et al., 1989; c = average from Elderfield et al., 1981; d = Table V.1 and references in text; e = Table V.2, Keller et al. (1992), and Chapter 6; f = Table V.3, Keller et al. (1992), Hole et al. (1993), and Keller et al., unpub. data.

Note: Nd and Pb isotopic data for the arc are extremely rare, and may not represent the full natural range of the arc.

have high  $^{87}\text{Sr}/^{86}\text{Sr}$  and low  $^{143}\text{Nd}/^{144}\text{Nd}$ , and  $^{206}\text{Pb}/^{204}\text{Pb}$  between 18.5 and 19.3 (Figure V.4). Sediments from the South Atlantic (Ben Othman et al., 1989) and Pacific (Elderfield et al., 1981) oceans tend to have  $^{206}\text{Pb}/^{204}\text{Pb}$  near the lower end of this range (Table V.4). So if this is the appropriate subducted component on the northern Antarctic Peninsula, we would expect the arc volcanism to have the highest  $^{87}\text{Sr}/^{86}\text{Sr}$ , lowest  $^{143}\text{Nd}/^{144}\text{Nd}$ , and  $^{206}\text{Pb}/^{204}\text{Pb}$  no higher than about 18.8. This is in fact the case: all but two of the arc samples have Sr and Nd isotopic ratios more enriched than any BS sample, and only the youngest arc sample has  $^{206}\text{Pb}/^{204}\text{Pb} > 18.7$  (Figure V.4). The lower  $^{87}\text{Sr}/^{86}\text{Sr}$  and higher  $^{143}\text{Nd}/^{144}\text{Nd}$  of the BS and JРИVG samples suggest that they contain less of the subducted component than do the South Shetland Arc samples. Note that the narrow range of  $^{206}\text{Pb}/^{204}\text{Pb}$  in the BS samples is not significantly different from the youngest arc sample, but the JРИVG  $^{206}\text{Pb}/^{204}\text{Pb}$  data extend away from the arc and BS to higher values.

In addition to the high  $^{87}\text{Sr}/^{86}\text{Sr}$ -low  $^{143}\text{Nd}/^{144}\text{Nd}$  subducted sediment component (C1), three other isotopic components are required to explain the northern Antarctic Peninsula isotopic data (Table V.5): (C2) a low- $^{206}\text{Pb}/^{204}\text{Pb}$ -and- $^{208}\text{Pb}/^{204}\text{Pb}$  depleted mantle component seen only in the South Shetland Arc samples, (C3) a moderate- $^{206}\text{Pb}/^{204}\text{Pb}$ -and- $^{208}\text{Pb}/^{204}\text{Pb}$  depleted mantle component best seen in the BS seamounts, and (C4) an undepleted mantle component seen only in the high- $^{206}\text{Pb}/^{204}\text{Pb}$  JРИVG samples (Figure V.4).

**Table V.5. Isotopic Characteristics and Possible Identities of Mixing Components**

Component	$\frac{87}{86}Sr$	$\frac{143}{144}Nd$	$\frac{206}{204}Pb$	$\frac{207\&208}{204}Pb$	Strongest in:
C1) Subducted sed	high	low	low	low	So. Shetland Arc
C2) Depleted mantle	low	high	low	low	pre-24 Ma Arc
C3) Depleted mantle	low	high	moderate	low	BS seamounts
C4) Undepleted mantle	low	moderate	high	high	JRIVG

The subducted component (C1) has high  $^{87}Sr/^{86}Sr$  and low  $^{143}Nd/^{144}Nd$ , and moderate  $^{206}Pb/^{204}Pb$ , and is most apparent in samples from the South Shetland Island Arc, and to a lesser extent in some of the subaerial Bransfield Strait samples. Locations highest in this isotopic component have high Ba and low Nb, which is also typical of arc volcanism. The isotopic characteristics of this component are similar to marine sediment (Table V.4 and Figure V.4), and to the enriched mantle component (EMII) of Zindler and Hart (1986), which is thought to have been formed by ancient subducted sediments. Although we refer to this component as sediment, it is more likely a fluid phase produced by sediment dehydration (e.g., Stolper and Newman, 1994). Continental crust can also have these isotopic characteristics, but it has been shown that the BS isotopic data cannot be modeled by crustal assimilation (Keller et al., 1992). Also, it is difficult to imagine why the amount of crustal assimilation would fortuitously decrease with increasing distance from the trench.

The low- $^{206}Pb/^{204}Pb$  depleted isotopic component (C2) is present only in the arc samples older than 24 Ma. There is no evidence for this component in the youngest arc sample (KGI.LH1), nor in the BS and JRIVG samples. This component also has depleted Sr and Nd isotopic ratios, and appears to be similar to the depleted MORB-like component seen in the East Scotia Sea backarc spreading center (Figure V.4).

The moderate- $^{206}Pb/^{204}Pb$  depleted isotopic component (C3) is most evident in the BS seamount samples, but is also important in the low- $^{87}Sr/^{86}Sr$  JRIVG samples. It has low  $^{87}Sr/^{86}Sr$ , high  $^{143}Nd/^{144}Nd$ , and low concentrations of incompatible trace elements, but Pb isotopic ratios similar to the subducted component (C1) (Table V.5 and Figure V.4). In situ depletion of the mantle by repeated melting during backarc rifting could explain the low trace element concentrations, but not the depleted isotopic ratios. The Sr and Nd isotopic ratios of this component are similar to depleted upper mantle such as that tapped by the East Scotia Sea spreading center and mid-ocean ridges

(ESSsc; Figure V.4), but its Pb isotopic ratios are higher than those of the ESSsc. Its Pb isotopic ratios are within the high end of the MORB range, however, so this is probably upper mantle that has upwelled into the rift zone beneath BS. It is possible to eliminate the need for this component and reproduce the wide range of  $^{87}\text{Sr}/^{86}\text{Sr}$  at constant  $^{206}\text{Pb}/^{204}\text{Pb}$  of the BS samples by mixing of components C1 and C2, but a special type of subducted sediment is then required. If the sediment component has very high Pb concentration ( $\geq 200$  ppm) and low Sr/Pb ( $\leq 1$ ), then as little as 0.5% sediment will give the mixture the Pb isotopic ratios of the sediment without noticeable affect on the  $^{87}\text{Sr}/^{86}\text{Sr}$ . Larger amounts of sediment in the mixture will have no further affect on the Pb isotopes, and will only serve to increase the  $^{87}\text{Sr}/^{86}\text{Sr}$ . The only type of sediment that we could find that matches these Sr and Pb characteristics is Mn nodules (e.g., Ben Othman et al., 1989). If the subducted component (C1) is actually a fluid phase, some unique condition of this subduction zone may have made the fluid unusually enriched in Pb, but such an enrichment phenomenon is speculative.

The undepleted component (C4) is most evident in the JRIVG, and has high  $^{206}\text{Pb}/^{204}\text{Pb}$  and  $^{208}\text{Pb}/^{204}\text{Pb}$ , and similar  $^{87}\text{Sr}/^{86}\text{Sr}$  but lower  $^{143}\text{Nd}/^{144}\text{Nd}$  compared to the depleted components (C1 and C2). The Sr and Nd isotopic ratios of this component are similar to the St. Helena (White, 1985) or HIMU (Zindler and Hart, 1986) mantle components, but St. Helena has  $^{206}\text{Pb}/^{204}\text{Pb} > 20.5$ , and JRIVG  $^{206}\text{Pb}/^{204}\text{Pb}$  never exceeds 19.0. The long history of subduction beneath the northern Antarctic Peninsula may have introduced enough sediment with low  $^{206}\text{Pb}/^{204}\text{Pb}$  to have overwhelmed the St. Helena/HIMU Pb isotopic signature there.

Elsewhere in West Antarctica, Cenozoic volcanism of the West Antarctic Rift System has Sr and Nd isotopic ratios similar to HIMU, but to various degrees lacks the high  $^{206}\text{Pb}/^{204}\text{Pb}$  signature of HIMU (Futa and LeMasurier, 1983; Hole et al., 1993; Hart et al., 1995). We suggest that the Pb isotopic characteristics of all of the Tertiary-Recent volcanism of West Antarctica, including our samples from the northern Antarctic Peninsula, are functions of the amount of subducted Pb in their sources. In areas of the Pacific margin of West Antarctica where subduction ceased during the Mesozoic, the high Pb isotopes of HIMU are mostly intact ('Other WA' fields in Figure V.4). Alkalic basalts found midway up the Antarctic Peninsula (Figure V.1; and 'Other AP' fields in Figure V.4) on Alexander Island (<8 Ma; 70°S; Hole et al., 1993), where subduction continued into the Paleogene, and at Seal Nunataks (<4 Ma; 65°S), where subduction ceased at least 4 m.y. ago, show less of the HIMU Pb signature than the West Antarctic Rift samples, but more of the HIMU signature and less of the subducted component

than the northern Antarctic Peninsula samples, including JRIVG. Subduction continues today on the northernmost Antarctic Peninsula, and even the basalts 360 km from the trench on James Ross Island have had almost all of their HIMU Pb signature overwhelmed by Pb in recently subducted sediments. Volcanism in Bransfield Strait and the South Shetland Arc is closer to the active trench, and has Pb isotopic ratios completely dominated by subducted sediments. Subducted sediments can profoundly affect Pb isotopes in the mantle, while having lesser affects on Sr and Nd isotopes and trace element concentrations, because Sr and Nd concentrations are only one order of magnitude higher in sediments than in depleted mantle, while Pb concentrations can be 2–3 orders of magnitude higher in sediment than in depleted mantle (Table V.4).

## CONCLUSIONS

On the northern Antarctic Peninsula the best indicators of a subduction component are high Ba/Nb and  $^{87}\text{Sr}/^{86}\text{Sr}$ , and to a lesser extent low  $^{206}\text{Pb}/^{204}\text{Pb}$ . These factors are most obvious in the South Shetland Arc volcanism, less obvious in Bransfield Strait backarc volcanism, and subtle to nonexistent in the JRIVG extreme backarc volcanism. The isotopic characteristics of the South Shetland Arc can be accounted for by mixtures of 1–4% subducted sediments (C1) and depleted mantle similar to that beneath the nearby East Scotia Sea spreading center (C2). Bransfield Strait isotopic characteristics can be accounted for by mixtures of a moderate- $^{206}\text{Pb}/^{204}\text{Pb}$  depleted mantle (C3) and 0.5–2.5% subducted sediments (C1), or possibly mixtures of low- $^{206}\text{Pb}/^{204}\text{Pb}$  depleted mantle (C2) and 0.5–2% subducted sediments with extremely high Pb concentrations (special variety of C1). JRIVG isotopic characteristics can be accounted for by mixtures of moderate- $^{206}\text{Pb}/^{204}\text{Pb}$  depleted mantle (C3), subducted sediments (C1), and a HIMU-like undepleted mantle (C4). The JRIVG samples contain less subducted component (C1) than the arc or BS, but without knowledge of the Sr-Nd-Pb concentrations of the HIMU-like component (C4), we cannot construct mixing models.

Alkalic basalts (<8 m.y. old) found on the Antarctic Peninsula to the south of our study area, where subduction has ceased, contain still less of the subducted component and more of the HIMU-like component, while isotopic compositions of Upper Miocene to Recent alkalic basalts from elsewhere in West Antarctica are dominated by the HIMU-like component.

In the absence of knowledge of the Pb isotopic composition of the West Antarctic mantle from other isotopic studies, there would be little or no evidence for subduction-contamination of the source of the JRVG at 300–360 km from the trench. Since the mantle was not significantly contaminated by the subducted slab at 360 km from the trench, the mass flux to the upper mantle must be extremely limited here: the slab can still make a significant chemical contribution to deeper parts of the mantle.

#### ACKNOWLEDGMENTS

We are grateful to S. Porebski and E. Godoy for providing the Cockburn Island and Paulet Island samples (respectively), and to M. Cheatham for assisting with the isotopic analyses. Fieldwork on James Ross Island was supported by the Instituto Antártico Argentino and an Oregon State University Research grant to MRF. Dredging in Bransfield Strait was supported by NSF grant DPP90-19247 to LAL. Analytical work was supported by NSF grants DPP88-17126 and DPP93-17307 to MRF.

## **Chapter 6**

**Geochemistry of Backarc Basin Volcanism in Bransfield Strait, Antarctica:  
Subducted Contributions and Along-Axis Variations**

**Randall A. Keller, Martin R. Fisk, John L. Smellie,  
Jorge A. Strelin, and Lawrence A. Lawver**

## ABSTRACT

Bransfield Strait is a Quaternary, ensialic backarc basin at the transition from rifting to drifting (spreading). Previous work on four islands and two juxtaposed seamounts in the strait found calc-alkaline-like basalt-to-rhyodacite on one island, mildly alkalic basalt on another island, basaltic andesite similar to island-arc tholeiite on another island, and tholeiitic basalts and basaltic andesites with slightly elevated LILE concentrations and depleted HFSE concentrations on the seamounts. We have recovered fresh volcanic rocks from eight additional submarine features distributed along the rift, including portions of a discontinuous neovolcanic ridge similar to the nascent spreading centers seen in some other backarc basins. Smaller edifices near the northeast end of the rift yielded basalts with the most arc-like compositions (e.g., high LILE/HFSE and  $^{87}\text{Sr}/^{86}\text{Sr}$ ). The most MORB-like basalts are from a large, caldera-topped seamount and a 30 km-long axial neovolcanic ridge toward the southwest end of the rift, but these two features also yielded andesite and rhyolite, respectively. The most depleted basalts have major and trace element concentrations indistinguishable from MORB except for slightly higher Cs and Pb concentrations. Pb isotopic ratios cover narrow ranges (e.g., 18.69–18.77) compared to the ranges of Sr and Nd isotopic ratios (0.7027–0.7038 and 0.51293–0.51306), and do not extend to the depleted Pb isotopic ratios found in other backarc basins. Either the low- $^{87}\text{Sr}/^{86}\text{Sr}$  depleted mantle beneath Bransfield Strait has higher than normal Pb isotopic ratios, or the subducted sediment component beneath Bransfield Strait has such high Pb concentration that it dominates the Pb isotopic composition of the Bransfield Strait mantle without affecting the Sr and Nd isotopic compositions.

## INTRODUCTION

Recent studies of the backarc basins (BABs) in the western Pacific produced significant advances in our understanding of how these basins form. A generalized model is now emerging wherein BABs form by rifting of arc crust into a series of subbasins that are then taken over by a propagating seafloor spreading center (Tamaki et al., 1992; Hawkins, 1995). Testing this model on BABs in continental and oceanic settings with various subduction zone dynamics can provide significant insight into what factors control and influence how backarc basins form. However, little is known

about how BABs form in continental crust, perhaps because ensialic BABs are so rare. We chose to study the volcanism in Bransfield Strait (BS) because it is the type example of an ensialic BAB: the recent subduction history in this area is extraordinarily well-understood (Maldonado et al., 1994), and it is the only active ensialic BAB that is opening without a large strike-slip component.

The composition of BAB basalts (BABBs) can range from very similar to basalts created by melting of the depleted upper mantle (MORB-like), to very similar to basalts created by the interaction of subducted lithosphere with the mantle wedge (arc-like) (e.g., Saunders and Tarney, 1984). Although MORB-like basalt can occur very early in the history of a BAB, and dominates in more mature BABs, arc-like volcanism can occur at any time (Taylor and Karner, 1983; Hochstaedter et al., 1990; Keller et al., 1992). Whether the dominance of MORB-like basalts later in the development of a BAB is accomplished by preferential melting and removal of enriched portions of the mantle during the early stages of rifting, or by an increasing influx of depleted mantle as the BAB develops, is still debatable (Hawkins, 1995). Critical to this debate is how the magmatic system makes the transition from arc-like to MORB-like volcanism. An excellent place to study this transition is in a backarc rift that is just at the transition from rifting to spreading and MORB-like volcanism. BS is at this transition, which is the second reason that we chose to study BS volcanism.

On the northern tip of the Antarctic Peninsula, a piece of the Antarctic Plate is subducting to the southeast into the South Shetland Trench (Figure VI.1) (Barker, 1982; Maldonado et al., 1994). The Antarctic Peninsula magmatic arc created by this subduction was most recently active in the Early Miocene on what are now the South Shetland Islands (Smellie et al., 1984). Behind the South Shetland Islands Arc, backarc rifting in BS caused Quaternary volcanism ranging from basaltic andesite similar to island arc tholeiite, to tholeiite similar to MORB, to a single volcano with a basalt-to-trachydacite evolutionary suite. Two volcanoes on the northern margin of the strait (Melville Peak and Penguin Island; Figure VI.2) and two volcanoes near the rift axis (Bridgeman Island and Deception Island) are above the sea surface, and have been studied in detail (Weaver et al., 1979; Birkenmajer, 1980; Birkenmajer and Keller, 1990; Birkenmajer, 1992; Keller et al., 1992; Smellie et al., 1992). However, most of the volcanism in the rift is submerged, and occurs at isolated seamounts and along a discontinuous axial neovolcanic ridge roughly aligned with Deception and Bridgeman islands (Fisk, 1990; Keller and Fisk, 1992; Keller et al., 1992; Lawver et al., 1995). This axial ridge is difficult to see in Figure VI.2, but is obvious in the full-coverage

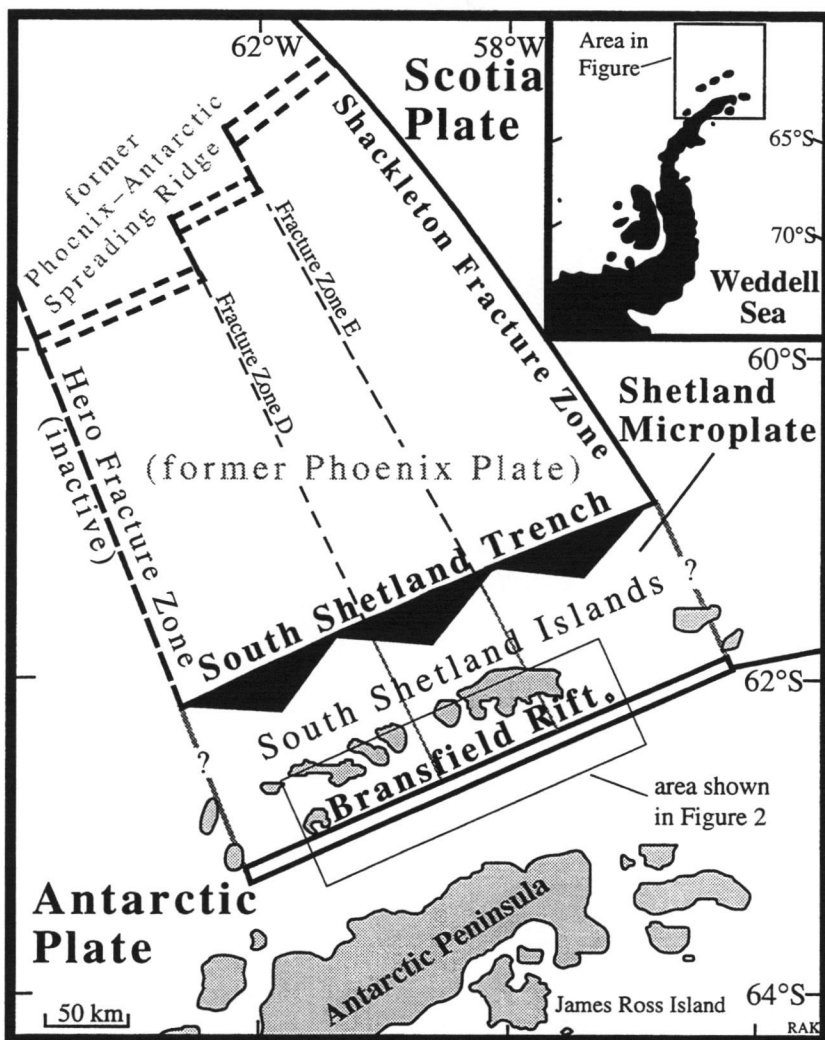


Figure VI.1. Generalized tectonic map of the northern Antarctic Peninsula (area shown in inset). The South Shetland Trench (shown by black triangles pointing to the overriding plate), Bransfield Rift, and Shackleton Fracture Zone are still active, but the Phoenix-Antarctic Ridge ceased spreading approximately 4 m.y. ago (Maldonado et al., 1994). The rectangle in Bransfield Rift shows the area covered by the bathymetric map in Figure VI.2.

multibeam map of Gracia et al. (in press). The axial ridge is similar to the nascent seafloor spreading center in the Mariana Trough (Hawkins et al., 1990), suggesting that BS has progressed beyond the rifting stage into the earliest stages of seafloor spreading (Gracia et al., in press).

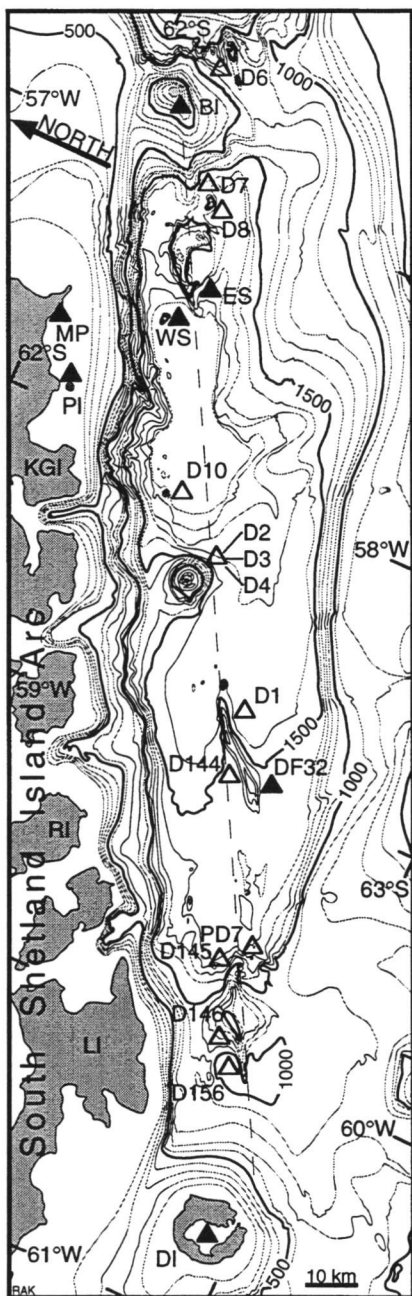


Figure VI.2. Bathymetric map of the Bransfield Rift axis (modified from Klepeis and Lawver, 1994). Sampled locations of Quaternary volcanism are shown by triangles (filled triangles where data are published - Keller and Fisk, 1992, Keller et al., 1992; unfilled triangles where data are new). Location abbreviations: BI = Bridgeman Island, DI = Deception Island, ES = Eastern Seamount, KGI = King George Island, LI = Livingston Island, MP = Melville Peak, PI = Penguin Island, RI = Robert Island, WS = Western Seamount. BI, DI, MP, and PI are subaerial volcanoes. DF32 and PD7 are piston-cored samples DF86.32 and PD89.4.7, respectively. Other samples are dredged samples.

Prior to this work only two neighboring seamounts had been dredged in BS (dredges D292, D297, D300, D309, and D310 in Figure VI.2; Keller and Fisk, 1989). These rocks were compositionally transitional between island arc basalts and mid-ocean ridge basalts (MORB), and thus similar to some BABBs (Fisk, 1990; Keller and Fisk, 1992). The only other submarine basalts available from BS were a few chunks of fresh glass inadvertently recovered by piston-cores at 62.7°S, 59.0°W (DF86.32: Anderson et al., 1987) and 62.8°S, 59.5°W (PD89.4.7: Lawver, unpub.). Partial geochemical analysis of sample DF86.32 showed that it had less of an island arc geochemical signature and more of a MORB signature than did the dredged samples (Keller et al. 1992). A thorough sampling of the submarine volcanism was necessary to determine the amount of along-axis variation in this young ensialic marginal basin. A bathymetric map produced by compilation of single-beam and multibeam data (Klepeis and Lawver, 1994), part of which is shown in Figure VI.2, revealed at least a dozen features that could be volcanic, and could be easily dredged with a few days of shiptime. A more recent, full-coverage multibeam bathymetric map (Gracia et al., in press) provided a more detailed picture of the features, and made clear the highly lineated nature of the discontinuous axial ridge between Deception and Bridgeman islands.

## SAMPLE LOCATIONS AND DESCRIPTIONS

In February-March 1993, cruise NBP93-1 of the RVIB Nathaniel B. Palmer recovered fresh volcanic rocks in eight dredges in Bransfield Strait (Keller et al., 1994). All but one of the dredges also contained rounded erratics ice-rafted from the South Shetland Islands and the Antarctic Peninsula. At about the same time the British Antarctic Survey (BAS) ship RRS James Clark Ross recovered fresh volcanic rocks in four dredges (BSDR144, 145, 146, and 156) in BS. Samples from both cruises were carefully examined for weathered or rounded surfaces, and only those that appeared fresh and unequivocally *in situ* were selected for further analyses.

The samples, from southwest to northeast, are (Figure VI.2): dredges D145, D146, D156, and piston-core PD89.4.7 (PD7 in Figure VI.2) from a shallow elongate feature with a central ridge centered at 59.8°W just northeast of Deception Island; dredges D1 and D144 from a 30-km-long, axial ridge centered at 59.0°W; dredges D2, D3, and D4 from a large, caldera-topped seamount at 58.4°W; D10 from a small seamount at 58.1°W; D8 from a short, steep-sided linear feature at 57.1°W; D7 from the southwest

tip of a linear ridge coming off of the Bridgeman Island platform; and D6 from a small seamount just east of Bridgeman Island at 56.6°W. Also shown in Figure VI.2 (as filled triangles) are the locations of previously analyzed submarine and subaerial samples in BS (see Keller and Fisk, 1989; Fisk, 1990; Keller and Fisk, 1992; and Keller et al., 1992).

Rubbly chunks of pillows and flows were the most common form of sample recovered. Most samples have at least one glassy surface and contain abundant vesicles. Phenocrysts are rare, and include small plagioclase, olivine, and clinopyroxene. D144 included cryptocrystalline to glassy black rhyolite. Higher proportions of the basalts in dredges D1, D2, and D8 contained fresh glass, but fresh to only slightly palagonitized glass could be found in every dredge except D4 and D7, in which the glass was all slightly to moderately palagonitized. However, the lack of fresh glass in a dredge may not be a reliable measure of the age of the feature. Note that D4 contained little fresh glass, while D2 from the same volcano contained a high proportion of fresh glass. Other than the minor palagonitization in many of the samples, no alteration minerals nor zeolitization were observed.

In hand sample, many of the basalts are virtually-to-completely aphyric. A few samples from D1–D4 contained trace amounts of plagioclase microlites, while a few samples from D8 contained rare olivine microphenocrysts, and most samples from D6 contained a few percent olivine and plagioclase microphenocrysts. The only truly porphyritic samples were from D10, which contained up to 15% olivine, and a few samples from D7 that contained up to 5% plagioclase + clinopyroxene + olivine. The samples are unusually vesicular for basalts dredged from these depths (700–1950 m; Keller et al., 1994). A few of the samples in dredges D1, D2, and D7 contained <10% vesicles, but otherwise all samples contained 10–40% vesicles.

In thin section, most of the samples have rare microphenocrysts of plagioclase ± olivine ± clinopyroxene in a groundmass of plagioclase microlites + glassy mesostasis ± olivine ± clinopyroxene. The exceptions are D6 and D7, which contained a few percent plagioclase ± clinopyroxene ± olivine in a groundmass similar to the aphyric sections, and D10, which contained 15% olivine in a glassy groundmass.

## RESULTS

### Major Elements

We analyzed clean glass chips from 77 samples from dredges D1–D4, D6–D8, and D10 and the two piston-cores (DF86.32 and PD89.4.7) for major elements by electron microprobe (Table VI.1; see appendix for analytical techniques). The samples are subalkaline basalts and basaltic andesites, except for two analyses that just extend to andesitic compositions (Figure VI.3). MgO concentrations in the glasses range from 2.2 wt.% (D2J) to 8.1 wt.% (D2H) (Figure VI.3). Every major element except CaO has a range of concentrations at a given MgO, so the samples cannot all be related to a common parent by simple fractional crystallization.

All of the major elements except Al<sub>2</sub>O<sub>3</sub> and CaO increase with decreasing MgO across almost the entire sample suite. Al<sub>2</sub>O<sub>3</sub> decreases with decreasing MgO, meaning that plagioclase began fractionating at MgO of  $\geq 8$  wt.%. CaO increases slightly with decreasing MgO between 7 and 8 wt.% MgO, but then decreases with decreasing MgO at  $< 7$  wt.% MgO, so clinopyroxene was not an important fractionating phase until then. There appears to be a slight decrease in FeO\* and TiO<sub>2</sub> in the two samples from D2 that have MgO contents of 3.2 wt.%, suggesting that an Fe-Ti oxide began fractionating at 3.5–4.0 wt.% MgO.

TiO<sub>2</sub> contents tend to mimic FeO\* contents, with samples from D2–D4 (all from the large seamount at 58.4°W) having high TiO<sub>2</sub> and FeO\* at a given MgO, and D1, D6–D8, and D10 having lower TiO<sub>2</sub> and FeO\*. D2–D4 also have higher Na<sub>2</sub>O and lower K<sub>2</sub>O than D6–D8 and D10, while D1 extends to even higher Na<sub>2</sub>O and lower K<sub>2</sub>O. D2–D4 are slightly higher in total alkalies than D1, D6–D8, and D10, but are similar to published analyses from the small seamount at 57.5°W (Fisk, 1990). D6 and D7 are notable for their low TiO<sub>2</sub> and P<sub>2</sub>O<sub>5</sub>, and high Al<sub>2</sub>O<sub>3</sub> and CaO.

The chemical differences between the glasses are more obvious when they are plotted by element-ratios (Figure VI.3). The high Na<sub>2</sub>O and low K<sub>2</sub>O of D1–D4 give them a much higher Na<sub>2</sub>O/K<sub>2</sub>O than the other dredges. K<sub>2</sub>O/P<sub>2</sub>O<sub>5</sub> values are also obviously lower in D1–D4. FeO\*/TiO<sub>2</sub> is less definitive, with D6 and D7 being significantly higher than the other dredges, and D10 being perhaps transitional. The two piston-cored samples fall within the same area as D1–D4 on all of the plots.

Whole rock major element geochemistry (Table VI.2) grossly resembles the glass

**Table VI.1. Electron Microprobe Analyses of Bransfield Strait Glass Samples**

Sample	SiO <sub>2</sub>	TiO <sub>2</sub>	Al <sub>2</sub> O <sub>3</sub>	FeO*	MnO	MgO	CaO	Na <sub>2</sub> O	K <sub>2</sub> O	P <sub>2</sub> O <sub>5</sub>	SUM
DIA1	56.03	1.56	15.33	9.33	0.19	4.15	7.92	4.57	0.42	0.26	99.76
DIA2	57.56	1.49	15.08	9.52	0.22	3.70	6.85	4.50	0.51	0.31	99.74
DIB1	55.54	1.51	15.19	9.10	0.22	4.45	8.23	4.44	0.41	0.26	99.35
DIB2	55.14	1.46	15.17	9.39	0.20	4.47	8.26	4.29	0.40	0.30	99.08
DIB3	55.81	1.44	15.08	9.25	0.16	4.29	7.91	4.45	0.42	0.31	99.12
DIB4	56.10	1.48	15.33	9.19	0.20	4.06	7.85	4.42	0.45	0.30	99.38
DIB5	56.63	1.50	15.07	9.54	0.18	4.22	7.60	4.47	0.51	0.31	100.03
DIB6	55.24	1.35	15.58	8.57	0.15	4.46	8.42	4.32	0.39	0.21	98.69
DIC	52.30	1.89	15.20	10.38	0.22	5.14	9.73	3.79	0.23	0.21	99.09
DID	55.84	1.47	15.43	9.61	0.14	4.18	7.91	4.40	0.43	0.30	99.71
DIE	54.01	1.80	15.16	10.35	0.25	4.68	8.87	3.95	0.38	0.26	99.71
DIF	53.99	1.81	14.82	10.12	0.17	4.58	8.84	4.09	0.38	0.29	99.09
DIG	55.48	1.34	15.37	8.53	0.18	4.30	8.33	4.33	0.42	0.29	98.57
DIH	53.90	1.68	15.24	10.00	0.20	4.50	8.70	4.11	0.39	0.28	99.00
DII	55.84	1.34	15.46	8.84	0.17	4.48	8.27	4.51	0.43	0.27	99.61
DIJ	54.21	1.89	14.76	10.43	0.13	4.16	8.15	4.15	0.43	0.33	98.64
DIK	52.26	1.82	15.04	10.42	0.19	5.15	9.68	3.71	0.24	0.20	98.71
DIL1	55.93	1.38	15.69	9.14	0.16	4.41	8.16	4.49	0.39	0.29	100.04
DIL1	55.59	1.39	15.41	9.08	0.12	4.35	8.24	4.39	0.42	0.29	99.27
DIL2	55.49	1.30	14.89	9.14	0.14	4.11	7.82	4.51	0.42	0.30	98.13
D1M	54.74	1.84	14.85	10.37	0.20	4.18	8.10	4.07	0.42	0.37	99.14
D1N	52.24	1.82	15.02	10.45	0.19	5.35	9.63	3.74	0.23	0.20	98.87
D2A	53.47	2.20	14.24	11.88	0.17	4.13	8.19	4.29	0.44	0.31	99.31
D2B	56.39	2.18	14.81	11.29	0.17	3.21	6.56	4.29	0.60	0.43	99.93
D2C	52.66	2.40	14.83	11.93	0.12	4.09	8.16	4.34	0.38	0.32	99.23
D2D	55.87	2.08	14.69	11.08	0.15	3.20	6.59	4.65	0.60	0.40	99.30
D2E	54.46	2.28	13.67	12.36	0.16	3.72	6.96	4.16	0.54	0.39	98.70
D2G	49.63	1.33	16.50	9.01	0.10	7.58	11.66	3.03	0.15	0.13	99.13
D2H	49.28	1.35	16.00	9.18	0.12	8.06	11.63	3.01	0.14	0.12	98.89
D2I	48.89	1.22	16.60	8.52	0.09	8.00	11.63	2.87	0.14	0.11	98.07
D2J	59.92	1.67	15.07	9.44	0.21	2.15	5.16	4.59	0.76	0.47	99.44
D3A	51.97	1.63	14.95	9.89	0.13	5.46	10.13	3.72	0.31	0.22	98.40
D3B	52.14	1.61	14.91	9.82	0.10	5.53	10.27	3.70	0.30	0.20	98.59
D3C	51.12	1.54	14.78	9.68	0.11	5.86	10.46	3.58	0.28	0.18	97.59
D3D	52.12	2.72	13.56	13.04	0.20	3.71	7.90	4.03	0.43	0.35	98.07
D4A	52.15	2.08	13.98	11.77	0.16	4.85	9.01	4.08	0.37	0.20	98.64
D4B	52.64	2.14	14.07	11.51	0.16	4.90	9.02	4.03	0.36	0.20	99.04
D4C	54.06	2.78	13.38	12.90	0.19	3.66	7.31	4.03	0.52	0.39	99.22
D4D	52.40	2.13	13.93	11.77	0.19	4.89	8.99	4.02	0.37	0.24	98.92
D4E	52.60	2.15	14.14	11.64	0.15	4.89	8.98	4.12	0.35	0.23	99.24
D4F	53.78	2.78	13.64	12.79	0.17	3.87	7.68	3.97	0.50	0.35	99.53
D4G	52.67	2.26	14.08	11.78	0.17	4.88	8.84	4.04	0.37	0.27	99.35
D6C	51.31	0.81	16.18	8.21	0.08	7.17	12.04	2.57	0.38	0.11	98.86
D6D	51.82	0.84	16.08	8.45	0.12	7.12	12.00	2.55	0.39	0.06	99.42
D6F	51.15	0.82	16.44	8.32	0.10	7.45	12.02	2.52	0.39	0.07	99.27
D7B	54.76	1.36	14.69	10.44	0.16	4.58	8.92	3.55	0.57	0.12	99.14
D7D	54.40	1.27	14.97	10.06	0.19	4.74	9.13	3.48	0.56	0.12	98.92
D7E	53.79	1.09	15.36	9.54	0.16	5.07	9.59	3.40	0.53	0.10	98.61
D7F	54.95	0.85	15.38	8.68	0.11	5.45	10.00	3.11	0.52	0.10	99.14
D7G	54.59	0.89	15.30	9.15	0.17	5.29	9.87	3.09	0.54	0.10	98.98
D7H	53.28	1.29	14.73	10.32	0.16	4.45	8.81	3.52	0.57	0.13	97.26
D7I	52.77	1.18	15.02	9.70	0.16	5.05	9.47	3.42	0.54	0.09	97.38
D7K	52.54	1.24	14.44	10.14	0.16	4.45	8.88	3.43	0.60	0.11	95.98
D7N	54.86	1.33	14.92	10.18	0.21	4.49	8.87	3.55	0.58	0.12	99.08
D7O	52.71	1.00	15.28	8.84	0.16	5.58	10.41	3.17	0.45	0.09	97.68
D7P	53.05	1.12	15.25	9.32	0.15	5.15	9.76	3.42	0.51	0.09	97.81
D8A	51.48	1.32	15.69	8.58	0.16	6.46	11.22	3.13	0.37	0.17	98.56
D8B	51.60	1.42	15.25	9.01	0.20	6.46	11.10	3.07	0.39	0.18	98.67
D8C	51.70	1.36	15.86	8.49	0.16	6.84	10.87	3.03	0.34	0.13	98.79
D8D	51.72	1.28	16.38	8.30	0.12	6.70	11.17	3.02	0.34	0.13	99.16
D8E	51.31	1.29	16.48	8.15	0.15	6.71	10.95	3.02	0.33	0.14	98.52
D8F	50.52	1.23	16.45	8.15	0.14	6.73	10.98	3.01	0.32	0.13	97.66
D8I	51.47	1.25	16.43	8.29	0.14	6.73	11.12	3.07	0.33	0.15	98.99
D8J	51.09	1.24	16.48	8.16	0.15	6.78	11.16	3.08	0.32	0.13	98.59
D8L	51.25	1.36	16.12	8.48	0.11	6.67	11.10	3.06	0.33	0.15	98.63
D8O	51.50	1.30	16.68	8.17	0.15	6.69	11.14	2.98	0.34	0.13	99.07
D10A	51.20	1.14	15.59	7.95	0.10	6.62	11.80	2.74	0.63	0.29	98.06
D10B	51.30	1.10	15.84	7.88	0.18	6.06	11.59	2.81	0.65	0.16	97.55
D10C	51.54	1.21	15.64	8.49	0.20	6.15	11.53	2.91	0.70	0.20	98.56
D10D	51.84	1.12	15.61	8.18	0.14	6.16	11.38	2.86	0.66	0.21	98.15
D10F	51.56	1.13	15.82	8.11	0.13	6.07	11.53	2.81	0.65	0.20	97.99
D10G	51.59	1.20	15.79	8.65	0.14	6.22	11.57	2.99	0.66	0.24	99.05
D10H	51.83	1.12	15.76	8.41	0.18	6.17	11.43	2.84	0.66	0.19	98.59
D10J	52.13	1.09	15.85	8.32	0.12	6.14	11.48	2.91	0.67	0.24	98.95
D10K	52.10	1.08	15.65	8.09	0.15	6.18	11.50	2.84	0.64	0.15	98.37
PC7	54.80	1.85	15.59	9.76	0.15	4.21	8.08	4.63	0.52	0.28	99.86
DF32	54.79	2.18	14.20	10.78	0.20	4.40	8.07	3.99	0.43	0.33	99.37

Analyzed at OSU. See Techniques Appendix for details.

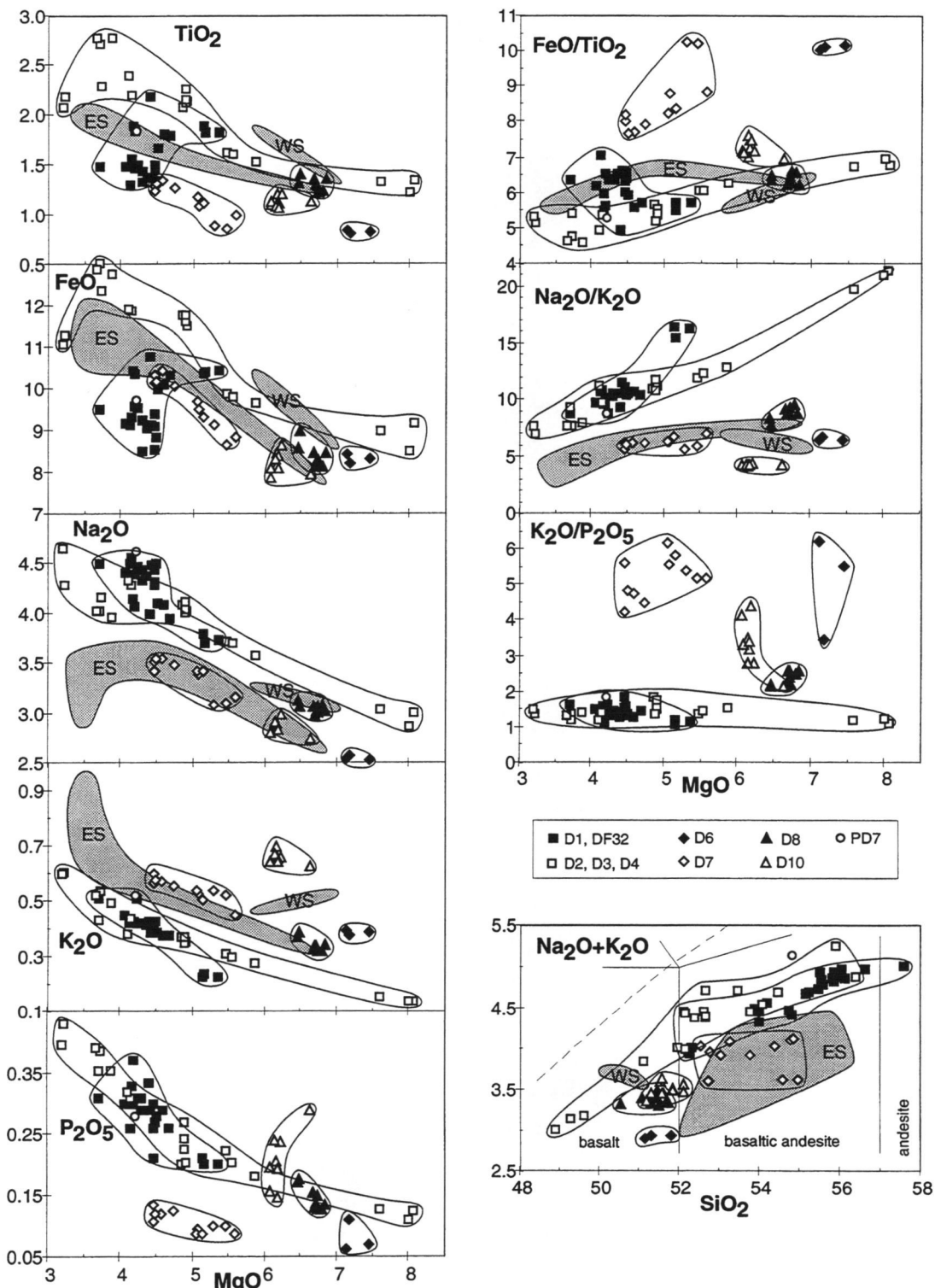


Figure VI.3. Major element plots of Bransfield Strait glass analyses by electron microprobe. WS and ES are Western Seamount and Eastern Seamount data from Fisk (1990).

**Table VI.2 Representative XRF Analyses of Whole Rock Samples from Bransfield Strait**

	D1A	D1F	D2G	D2N	D3C	D4D	D6D	D7A	D7F	D8F	D10A	D144.1	D144.4	D145.3	D146.1	D156.4
SiO <sub>2</sub>	54.05	52.91	49.04	52.15	51.14	51.91	50.11	51.51	52.63	50.81	48.29	70.28	50.06	51.50	50.97	50.02
TiO <sub>2</sub>	1.45	1.72	1.37	2.75	1.56	1.95	0.69	0.69	0.65	1.18	0.75	0.35	1.47	1.39	1.57	1.50
Al <sub>2</sub> O <sub>3</sub>	15.57	15.62	17.03	14.80	16.23	15.66	15.79	18.07	18.37	16.14	12.70	12.89	17.08	17.00	17.38	17.59
FeO*	9.70	10.56	9.75	13.27	10.35	11.71	8.99	7.67	7.53	9.54	9.51	4.95	9.66	9.45	9.30	9.12
MnO	0.18	0.18	0.16	0.22	0.17	0.19	0.14	0.12	0.13	0.16	0.15	0.13	0.16	0.16	0.16	0.15
MgO	4.52	5.27	7.61	3.93	6.03	4.80	11.21	7.33	5.82	8.84	17.57	0.12	6.40	5.85	5.94	6.34
CaO	8.40	9.12	11.61	7.83	10.87	9.23	10.60	11.95	11.49	10.19	8.58	1.26	10.71	10.61	10.42	11.12
Na <sub>2</sub> O	4.77	4.17	3.08	5.04	3.54	4.37	2.22	2.52	2.83	2.88	1.99	7.39	3.83	3.91	3.88	3.68
K <sub>2</sub> O	0.40	0.41	0.18	0.39	0.27	0.32	0.31	0.32	0.38	0.40	0.41	1.42	0.32	0.37	0.32	0.34
P <sub>2</sub> O <sub>5</sub>	0.24	0.23	0.11	0.34	0.14	0.20	0.03	0.04	0.05	0.10	0.10	0.01	0.17	0.16	0.18	0.20
LOI	0.28	-0.10	-0.26	-0.31	-0.25	-0.38	-0.13	0.04	0.19	0.10	-0.04	1.17	0.23	0.12	-0.20	-0.20
Total	99.56	100.09	99.68	100.41	100.05	99.96	99.96	100.26	100.07	100.34	100.01	99.97	100.09	100.52	99.92	99.86
V	189	244	212	340	272	344	221	195	209	267	238	10	269	249	218	225
Cr	43	35	219	3	49	6	631	174	56	462	1073	5	129	37	114	147
Ni	23	16	61	8	32	15	235	63	33	187	608	6	54	33	52	44
Cu	49	46	69	37	70	70	65	68	67	63	71	13	64	80	58	66
Zn	85	85	68	109	76	92	63	54	59	71	67	125	75	71	72	64
Ga	20	19	16	22	20	22	17	17	17	19	14	29	19	19	17	20
Rb	7	7	5	8	7	7	11	8	12	11	13	17	6	5	5	7
Sr	174	199	210	214	220	218	189	273	237	190	218	24	294	354	317	381
Y	62	48	28	55	34	45	16	16	17	25	17	152	33	26	31	27
Zr	260	204	109	219	127	171	51	58	67	86	70	856	125	115	128	136
Nb	7	6	4	9	6	7	2	2	2	3	3	18	5	5	5	6
Ba	29	25	2	41	22	30	46	36	52	51	115	113	72	57	24	42

Analyzed at NERC, UK. See Techniques Appendix for analytical details.

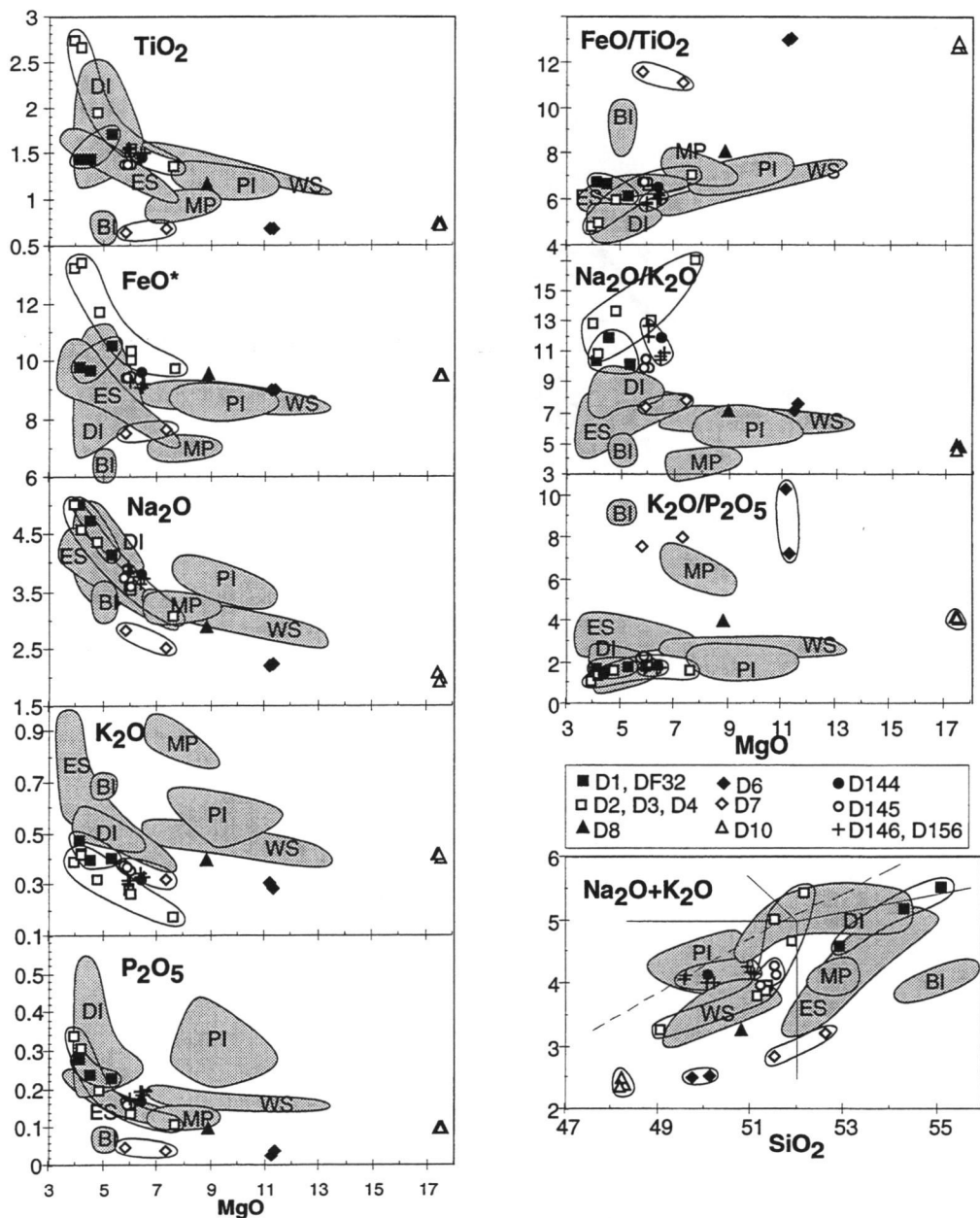


Figure VI.4. Major element plots of Bransfield Strait whole rock analyses by x-ray fluorescence. Shaded fields are published data (from Keller and Fisk, 1992; and Keller et al., 1992) for other Bransfield Strait locations (abbreviations as in Figure VI.2).

chemistry, with the notable exception that olivine causes MgO to be as much as 11 wt.% higher in the whole rocks (Figure VI.4), and SiO<sub>2</sub> tends to be 1–3 wt.% higher in the glass analyses. Sample locations that group together in their glass chemistry are also

similar in whole rock chemistry, e.g., the high Na<sub>2</sub>O/K<sub>2</sub>O and low K<sub>2</sub>O/P<sub>2</sub>O<sub>5</sub> of the D1–D4 glass data are also obvious in the whole rock data.

Sample locations for which we do not have glass analyses, i.e., the BAS dredges (D144–D146 and D156; Table VI.2) and the subaerial BS volcanoes (Weaver et al., 1979; Keller et al., 1992), do have XRF data. The BAS dredges have high Na<sub>2</sub>O and low K<sub>2</sub>O (Figure VI.4), similar to other samples from the southwest end of the rift (i.e., D1–D4 and the piston-cored samples). The rhyolite from D144 has low P<sub>2</sub>O<sub>5</sub> and must have experienced apatite fractionation, however it is not included in these plots to maintain a reasonable scale. For comparison, the subaerial Bransfield Strait volcanoes (Weaver et al., 1979; Keller et al., 1992) have as wide a range of compositions as do the dredged samples. Bridgeman Island has high Al<sub>2</sub>O<sub>3</sub>, FeO\*/TiO<sub>2</sub>, and K<sub>2</sub>O/P<sub>2</sub>O<sub>5</sub>, similar to the nearby dredges D6 and D7. Penguin Island and Melville Peak are on the northern margin of the rift basin, and do not consistently resemble any of the dredged samples, although they do both have low Na<sub>2</sub>O/K<sub>2</sub>O like other locations on the northeast end of the rift. The basalt-to-trachydacite suite (only samples with >4 wt.% MgO are shown here) on Deception Island has high Na<sub>2</sub>O like other samples from the southwest end of the rift.

### Trace Elements

Incompatible trace element concentrations (Table VI.2 and Table VI.3; Figure VI.5) vary at least as much as the incompatible major elements (Figure VI.4). (Note that our ICP-MS analysis of the rhyolite is semi-quantitative (see note in Table VI.3), and is not included in our discussion.) At any given MgO there is an assortment of trace element concentrations; far too much variation to be explained by simple fractional crystallization. Elements that are abundant and highly mobile in subduction zone magmas, such as Rb and Ba, show more variety than elements with higher field strengths, such as Zr and Nb (Figure VI.5). This is especially true when data from the earlier dredges (ES and WS in figures) and the BS subaerial samples are included in the comparison. Also, although there is some overlap, samples from the southwest end of the rift (D1–D4, piston-cores, BAS dredges, and Deception Island) tend to have lower Ba and Rb and higher Y, Zr, and Nb than the samples from the northeast end of the rift.

By plotting the trace element data on a MORB-normalized multi-element plot (Figure VI.6), it is readily apparent which elements are high ("enriched") and low ("depleted")

**Table VI.3. Representative ICP-MS Whole Rock Analyses of Bransfield Strait and South Shetland Islands Samples.**

	Rb	Sr	Y	Zr	Nb	Cs	Ba	La	Ce	Pr	Nd	Sm	Eu	Gd	Tb	Dy	Ho	Er	Tm	Yb	Lu	Hf	Ta	Pb	Th	U
DIA	3.5	174	60	272	6.0	0.27	38	9.52	29.48	4.83	22.98	6.94	2.03	7.87	1.45	9.28	2.02	5.99	0.92	5.66	0.86	6.75	0.45	2.17	0.56	0.31
D1F	3.3	192	47	207	5.1	0.24	35	7.92	23.85	3.95	18.53	5.62	1.76	6.47	1.18	7.53	1.62	4.82	0.74	4.54	0.70	5.09	0.36	2.08	0.51	0.24
D1J	4.1	199	53	235	5.9	0.23	38	8.95	26.34	4.22	21.11	6.47	1.98	7.45	1.34	8.34	1.78	5.18	0.78	5.06	0.80	5.56	0.43	1.87	0.53	0.27
D1N	3.6	220	36	142	3.2	0.12	29	5.35	15.75	2.61	13.31	4.18	1.49	5.16	0.92	5.93	1.27	3.64	0.55	3.50	0.56	3.47	0.25	1.32	0.27	0.17
D2G	1.6	204	30	106	2.4	0.09	20	4.02	12.17	2.22	10.81	3.44	1.30	3.92	0.74	4.67	1.02	2.90	0.47	2.71	0.40	2.60	0.19	0.95	0.22	0.13
D2J	8.6	163	82	407	10.9	0.46	95	16.57	46.61	7.24	35.77	10.13	2.96	12.11	2.15	12.97	2.93	8.24	1.25	8.01	1.25	9.65	0.79	4.62	1.34	0.63
D2N	4.2	213	55	226	7.0	0.28	58	9.39	28.07	4.75	22.59	6.65	2.32	7.71	1.38	8.81	1.90	5.46	0.86	5.14	0.77	5.38	0.52	2.30	0.64	0.33
D3C	3.2	219	34	127	3.6	0.18	39	5.23	15.14	2.47	12.76	4.02	1.50	4.93	0.89	5.57	1.20	3.42	0.49	3.24	0.48	3.10	0.26	1.74	0.39	0.24
D4D	3.6	219	44	175	4.8	0.22	47	7.06	20.00	3.35	16.81	5.06	1.78	6.23	1.11	6.90	1.52	4.39	0.64	4.15	0.66	4.22	0.34	2.04	0.50	0.25
D6D	7.4	193	15	40	0.7	0.46	53	2.45	6.17	1.05	5.09	1.68	0.63	1.95	0.37	2.40	0.53	1.54	0.24	1.48	0.22	1.22	0.07	2.29	0.57	0.24
D6G	12.2	380	12	42	0.6	0.53	79	2.77	6.88	1.06	5.07	1.60	0.66	1.93	0.32	1.94	0.40	1.16	0.17	1.10	0.18	1.26	0.04	3.14	0.74	0.34
D7A	5.5	277	16	48	0.7	0.29	44	2.50	6.73	1.17	5.66	1.89	0.74	2.18	0.39	2.53	0.55	1.61	0.25	1.47	0.23	1.49	0.07	1.93	0.51	0.21
D7F	8.2	237	17	58	1.0	0.48	67	3.32	8.45	1.38	6.45	1.91	0.73	2.33	0.42	2.71	0.59	1.76	0.27	1.75	0.24	1.66	0.08	2.40	0.79	0.30
D8F	7.2	190	25	82	1.5	0.38	57	3.92	11.21	1.91	9.23	2.90	1.07	3.35	0.61	3.93	0.86	2.53	0.39	2.39	0.34	2.20	0.11	2.27	0.58	0.41
D10A	10.0	223	15	61	1.6	0.34	138	6.67	15.68	2.24	9.20	2.29	0.78	2.43	0.41	2.55	0.53	1.57	0.23	1.46	0.22	1.70	0.13	2.84	1.59	0.41
D144.1*	15.2	22	153	998	17.8	1.18	125	28.27	79.98	12.07	56.60	15.74	2.32	17.75	3.51	22.39	5.02	15.71	2.54	16.37	2.59	22.91	1.29	7.10	2.63	1.14
D144.4	4.6	297	31	124	3.7	0.24	71	5.81	16.05	2.51	12.84	3.75	1.35	4.51	0.82	5.17	1.11	3.11	0.46	2.93	0.46	3.10	0.26	2.99	0.52	0.21
D145.3	2.9	352	25	112	4.0	0.26	66	6.53	16.74	2.54	12.55	3.51	1.23	3.85	0.71	4.20	0.89	2.49	0.38	2.34	0.36	2.67	0.27	2.32	0.51	0.20
D146.1	2.2	324	30	130	3.6	0.10	46	6.59	17.63	2.76	13.65	4.06	1.49	4.74	0.84	4.96	1.07	2.96	0.46	2.75	0.43	3.09	0.27	1.79	0.53	0.20
D156.4	2.7	376	27	139	5.0	0.18	60	7.92	20.17	3.03	14.63	3.93	1.41	4.36	0.75	4.48	0.94	2.62	0.39	2.42	0.39	3.03	0.36	2.06	0.50	0.43
DF32	3.9	196	53	230	5.7	0.30	45	8.37	26.02	4.35	20.35	6.21	1.91	7.25	1.29	8.22	1.78	5.13	0.81	4.90	0.72	5.41	0.40	2.22	0.50	0.39
PD7	3.8	244	48	256	5.5	0.22	61	10.30	28.65	4.52	22.11	5.99	1.93	6.95	1.27	7.67	1.67	4.76	0.74	4.57	0.71	5.68	0.39	2.52	0.73	0.40
P615.1	4.8	739	9	43	0.7	0.03	136	8.68	18.53	2.55	10.90	2.30	0.79	2.17	0.31	1.63	0.31	0.87	0.13	0.81	0.12	1.14	0.12	2.17	1.25	0.33
P842.9	4.6	678	20	97	4.5	0.06	240	14.15	31.64	4.37	19.46	4.47	1.38	4.01	0.61	3.35	0.68	1.83	0.28	1.72	0.26	2.22	0.25	5.72	1.73	0.46
P864.4	5.0	354	19	57	2.0	0.22	87	5.35	12.97	1.99	9.57	2.55	0.99	2.92	0.50	3.03	0.66	1.84	0.29	1.75	0.29	1.50	0.28	2.59	0.70	0.18
P845.9	3.1	527	17	40	1.1	0.44	86	4.78	12.33	2.03	10.27	2.84	1.06	3.16	0.50	2.86	0.61	1.63	0.24	1.46	0.22	1.20	0.07	8.08	0.45	0.14
P862.4	7.6	348	21	49	1.8	0.09	168	8.22	18.14	2.56	11.56	3.03	0.99	3.22	0.55	3.31	0.74	2.03	0.29	2.02	0.31	1.41	0.12	2.84	2.10	0.53

\*Concentrations of most trace elements in this rhyolite are >20% higher than our highest standard (AGV-1), and should be considered semi-quantitative.  
Analyzed at OSU. See Techniques Appendix for analytical details.

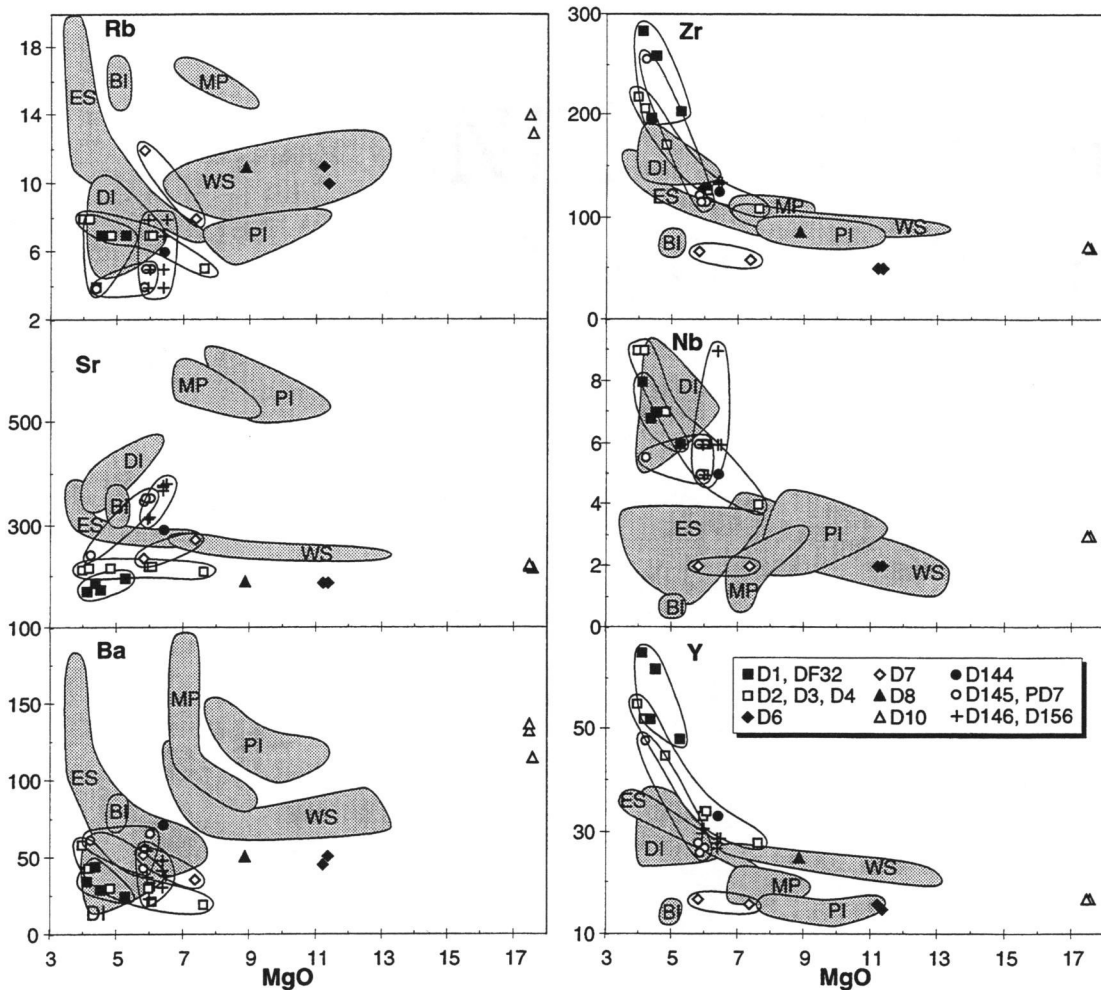


Figure VI.5. Whole rock MgO vs trace elements plots for Bransfield Strait volcanism. Shaded fields are published data (from Keller and Fisk, 1992; and Keller et al., 1992) for other Bransfield Strait locations (abbreviations as in Figure VI.2).

relative to MORB. If we assume that MORB values give an indication of what partial melting of the upper mantle produces when it is unaffected by subduction zone processes, we can readily determine how subduction has affected the magma sources and processes at the South Shetland Islands and BS. To characterize the subduction-related volcanism in this region, we analyzed five representative South Shetland Arc basalts (Table VI.3) from a range of locations and time periods (123–51 Ma; see Chapter 5), and added data from a 24 Ma arc basalt (Keller et al., 1992). Compared to normal MORB, or even enriched MORB (EMORB in Figure VI.6a), the arc volcanism has prominent spikes at Ba, Pb, and Sr, and possibly Cs, Th, U, and K (although Cs

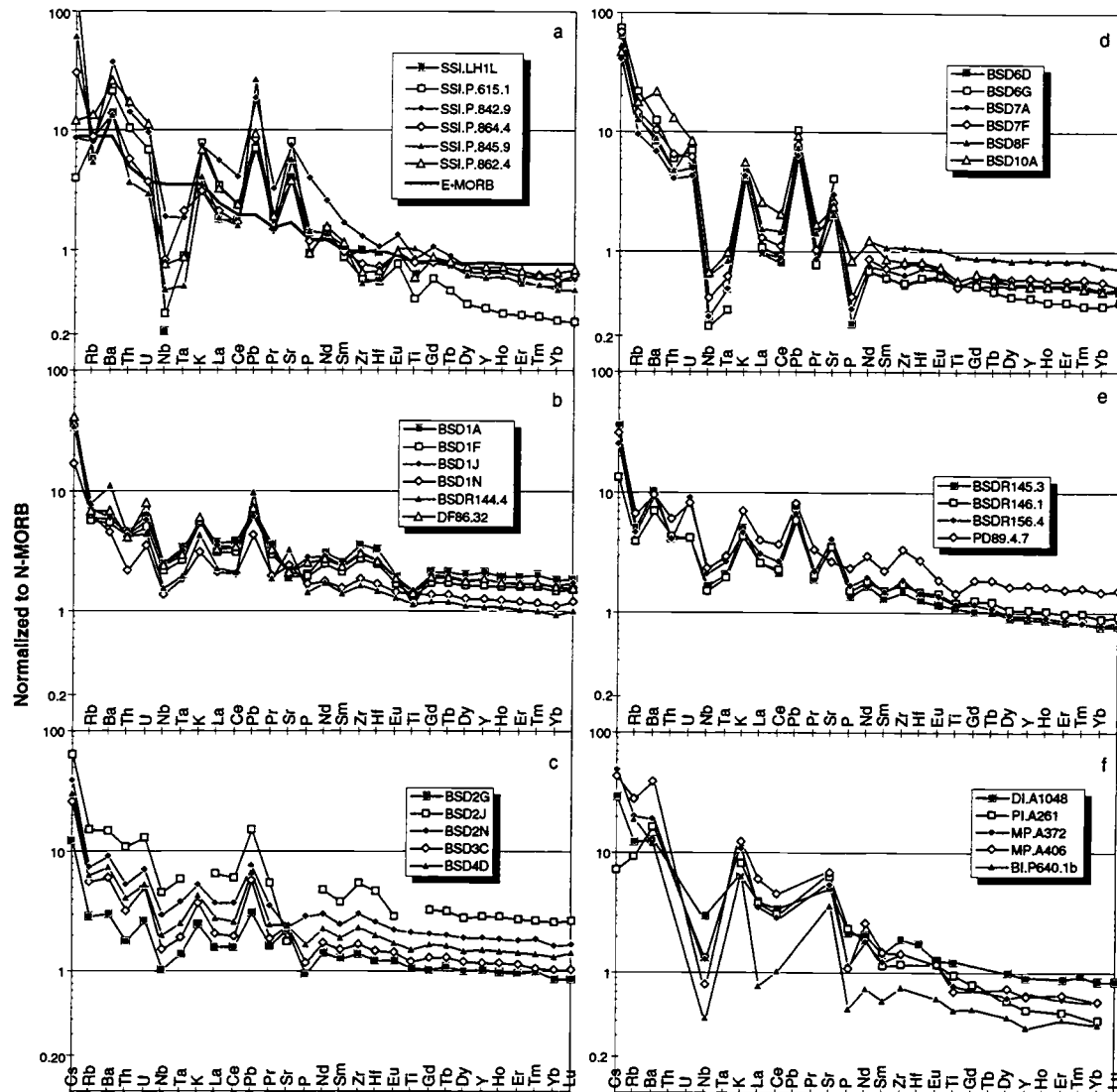


Figure VI.6. NMORB-normalized element-ratio plots of South Shetland Island Arc (panel a) and Bransfield Strait (panels b–f) samples (normalized to NMORB values of Sun and McDonough, 1989). The thick line in panel a is the EMORB of Sun and McDonough (1989). Abbreviations as in Figure VI.2. Data sources as in Figure VI.4, except some Bridgeman Island data from Weaver et al. (1979).

has been disturbed by alteration in some of the arc rocks), and sometimes divots at Nb and Ta, and possibly Zr and Hf. We attribute these deviations from MORB to the influences of the subduction zone.

The samples from D1 and the nearby piston-core DF86.32 (Figure VI.6b) have spikes at Cs, K, and Pb, and possibly U, but lack the Ba, Th, and Sr enrichments of the

arc samples. Their Nb-Ta depletion is noticeable, but not nearly as pronounced as that of the arc. D144 has a Nb-Ta depletion similar to D1, but has more pronounced K and Pb spikes, and has Ba and Sr spikes that D1 lacks. The higher Sr of D144 may be partially due to the fact that it is less evolved than any of the D1 samples, and experienced less plagioclase fractionation.

D2–D4 have Cs, Ba, K, Pb, and Sr enrichments and Nb-Ta depletions similar to D1 (Figure VI.6c), although Sr enrichments seen in the least evolved samples in D2–D4 do not continue into the more evolved samples due to plagioclase fractionation. D6–D8 and D10 have more of the arc characteristics than any of the other dredges (Figure VI.6d). D6 and D7 have the lowest REE concentrations of any dredged sample, yet have amongst the highest concentrations of the arc-characteristic elements: their Cs, K, Pb, and Sr enrichments and Nb-Ta depletions are unmatched by the other dredged samples, and in fact exceed some of the arc samples in relative magnitude. These two dredges are also enriched in Ba, but this is partially disguised by an enrichment in Rb that is unique amongst the dredged samples (except for D8, see below). The P depletion seen in D6 and D7 is only hinted at in some of the other dredged samples, but P depletion may not be an arc characteristic since it is only apparent in three of the six arc samples. D8 has enrichments in Cs, Rb, Ba, K, Pb, and Sr, and its depletion at Nb-Ta (Figure VI.6e) is more subdued than in D6 and D7, but more pronounced than the other dredged samples. D10, despite having relatively high MgO (6.5 wt.% in glass, 17.6 wt.% in whole rock) and low heavy REE concentrations, has the highest Rb, Ba, and Th, and amongst the highest Pb and K, and a steep REE pattern (Figure VI.6e). With the exception of its high Rb, it is quite similar to some of the arc samples. Dredges D145, D146, and D156, and piston-core PD89.4.7 (all from the same feature) have noticeable Cs, Ba, U, K, Pb, and Sr spikes (although the Sr spike on PD89.4.7 was presumably removed by plagioclase fractionation) and Nb-Ta depletions, although none of these characteristics are as pronounced as they are in D6 and D7.

It is difficult to compare the new samples to the subaerial volcanism in BS because comprehensive trace element data for the subaerial volcanoes are rare (Weaver et al., 1979; Keller et al., 1992). No Pb data exist, for example, so we cannot determine if these volcanoes have the characteristic Pb enrichment of the arc. From what data are available it is apparent that the subaerial volcanoes have a complex combination of arc and non-arc characteristics (Figure VI.6f). Deception Island has noticeable Cs and Sr spikes, but a subdued K spike, no Ba spike, and little or no Nb depletion. Penguin Island has spikes at Ba, K, and Sr, and a depletion at Nb, all of which are arc

**Table VI.4. Representative Isotopic Analyses of Bransfield Strait Samples**

	$^{87}\text{Sr}/^{86}\text{Sr}$	$^{143}\text{Nd}/^{144}\text{Nd}$	$^{206}\text{Pb}/^{204}\text{Pb}$	$^{207}\text{Pb}/^{204}\text{Pb}$	$^{208}\text{Pb}/^{204}\text{Pb}$	$\epsilon\text{Nd}$
D1F	0.702765	0.513058	18.771	15.592	38.426	8.2
D2G	0.702743	0.513068	18.763	15.564	38.332	8.4
D4D	0.702997	0.513061	18.769	15.602	38.473	8.3
D6D	0.703448	0.512936	18.746	15.595	38.520	5.8
D7A	0.703360	0.513005	18.724	15.585	38.455	7.2
D8F	0.703256	0.513018	18.744	15.587	38.473	7.4
D10A	0.703698	0.512930	18.748	15.602	38.533	5.7
D144.1	0.702897	0.513048	18.740	15.571	38.356	8.0
D145.3	0.703285	0.513031	18.696	15.584	38.387	7.7

Complete data set and details of the analytical technique can be found in Chapter 5.

characteristics, but its relative depletion at Cs is opposite to what is found in the arc. Penguin Island also has the steepest REE pattern of any BS volcano. Melville Peak has all of the chemical characteristics of the arc, such as the highest Cs, Ba, K, and Sr, and amongst the lowest Nb of any subaerial BS volcano, but its Rb, K, and LREE contents are higher than the arc. Bridgeman Island has higher Rb and lower  $\text{P}_2\text{O}_5$  and REE contents than the arc, but otherwise has the same incompatible trace element characteristics as the arc.

## Isotopes

Although a paucity of Nd and Pb isotopic data makes it impossible to paint a comprehensive picture of the isotopic characteristics of the arc, our Sr-Nd-Pb isotopic analyses of the six representative arc samples should be sufficient for a basic comparison to the BS data. Complete descriptions of the arc and BS isotopic data are published in Keller et al. (1992) and Chapter 5. Representative BS analyses are in Table VI.4. The youngest arc sample (24 Ma) is isotopically indistinguishable from some of the BS samples, but all of the other arc samples have lower  $^{143}\text{Nd}/^{144}\text{Nd}$ ,  $^{206}\text{Pb}/^{204}\text{Pb}$ , and  $^{207}\text{Pb}/^{204}\text{Pb}$ , and higher  $^{87}\text{Sr}/^{86}\text{Sr}$  (Figure VI.7).

Dredges D1–D4 have the lowest  $^{87}\text{Sr}/^{86}\text{Sr}$  and amongst the highest  $^{143}\text{Nd}/^{144}\text{Nd}$ , and are thus the most similar to the depleted upper mantle values found at mid-ocean ridges. These same samples have amongst the highest  $^{206}\text{Pb}/^{204}\text{Pb}$  values found in BS, although they are still within the reported range of MORB. The BAS dredges are mostly

similar to D1–D4, although not quite as depleted. Samples from the northeast end of the rift (e.g., D6–D8, D10) tend to have more enriched Sr and Nd isotopic ratios, i.e., displaced toward the arc values. D10, for example, has the highest  $^{87}\text{Sr}/^{86}\text{Sr}$  and lowest  $^{143}\text{Nd}/^{144}\text{Nd}$  of any dredged sample. The subaerial BS samples tend to have more of an arc signature than the dredged samples: Penguin Island has the highest  $^{87}\text{Sr}/^{86}\text{Sr}$ , Melville Peak has the lowest  $^{206}\text{Pb}/^{204}\text{Pb}$ , and Bridgeman Island has the lowest  $^{143}\text{Nd}/^{144}\text{Nd}$ . Deception Island falls in the middle of the range of the rest of the samples, except for its high  $^{207}\text{Pb}/^{204}\text{Pb}$  and  $^{208}\text{Pb}/^{204}\text{Pb}$ .

## DISCUSSION

### The 'Arc' Component

The tectonic setting of BABB above a mantle wedge that may have interacted with the dehydration/melting products coming off of the subducting slab can give them compositions somewhere between the depleted upper mantle signature of MORB and the subduction-zone signature of island arc basalts. The chemical signature of depleted upper mantle is easier to identify because MORBs have fairly consistent geochemical characteristics. The subducted component is harder to identify because there is more variation in the chemical characteristics of island arc volcanism. Our analyses of the six South Shetland Arc basalts provide a general sense of the chemical characteristics of the subduction zone volcanism in this area.

As noted earlier, the South Shetland Arc samples have high Ba and Pb, and low Nb (Figure VI.6a). These chemical characteristics are common features of arc volcanism in general (e.g., Pearce and Parkinson, 1993), and make high Ba/Nb and low Ce/Pb good indicators of the presence of an arc component in BS volcanism. The BS dredges and South Shetland Arc samples fall along a mixing curve in Ba/Nb-Ce/Pb space, with the arc samples at high Ba/Nb-low Ce/Pb and the most depleted BS samples at low Ba/Nb-high Ce/Pb (Figure VI.8a). Samples dredged from the northeast end of the Bransfield rift (D6–D8, D10) have Ba/Nb values that overlap the low end of the arc field, and Ce/Pb values the same as the arc. Samples dredged from elsewhere along the rift have lower Ba/Nb and higher Ce/Pb, and thus have less of the arc component than D6–D10. The two dredges with the least amount of arc signature are D1 and D2. They have low

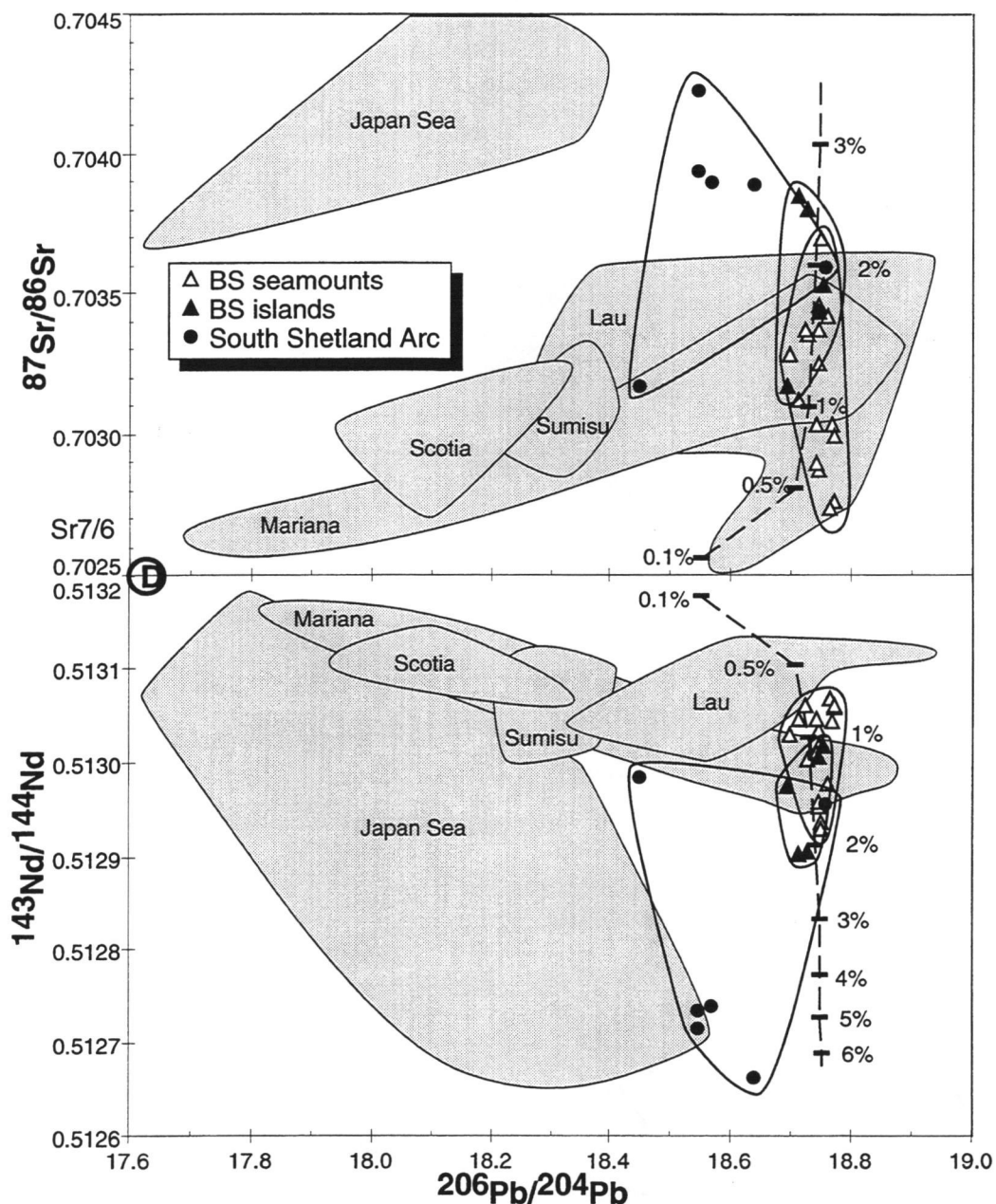


Figure VI.7.  $^{206}\text{Pb}/^{204}\text{Pb}$  vs.  $^{87}\text{Sr}/^{86}\text{Sr}$  and  $^{143}\text{Nd}/^{144}\text{Nd}$  of South Shetland Island Arc and Bransfield Strait samples (data from Chapter 5) compared to published data from other backarc basins (see text for data sources). Dashed line is a calculated mixing line between a depleted mantle component (shown by large D) and a subducted sediment component with high  $^{87}\text{Sr}/^{86}\text{Sr}$ , low  $^{143}\text{Nd}/^{144}\text{Nd}$  and  $\text{Sr/Pb} \leq 1$ , and very high Pb concentration ( $\geq 200$  ppm). Tick marks on the mixing lines are labeled with the percentage of the sediment component. A mixing line between depleted mantle with higher  $^{206}\text{Pb}/^{204}\text{Pb}$  and sediment with more typical Sr/Pb and Pb concentration would have similar form at sediment percentages  $>0.5\%$ . See Chapter 5 for details of the mixing model.

Ba/Nb and the highest Ce/Pb, and the lowest  $^{87}\text{Sr}/^{86}\text{Sr}$  and highest  $^{143}\text{Nd}/^{144}\text{Nd}$ . Their maximum Ce/Pb of 14 is less than the Ce/Pb of typical MORB (~25; Sun and McDonough, 1989) because the Bransfield samples have higher Pb contents (1–3 ppm vs. <1 ppm for MORB). Substituting U/Nb for Ba/Nb in Figure VI.8a produces a virtually identical plot.

The enrichment of the arc samples in Sr and Ba is obvious even in comparison to alkaline elements such as Rb. For example, at any given  $\text{K}_2\text{O}/\text{Rb}$ , the arc has higher Sr/Rb and Ba/Rb (Figure VI.8b) than do the dredged samples. Either the extra Sr and Ba in the arc volcanism was added by the subducted slab, or a mineral that retains K and Rb but not Sr and Ba (such as phlogopite) is present in the post-melting residual beneath the arc but not beneath BS.

If the elevated Pb concentrations of the BS basalts are from subducted Pb, their Pb isotopic compositions should reflect this subducted Pb. The BS Pb isotopes are in fact very similar to the Pb isotopes of the youngest South Shetland Arc basalt (Figure VI.7). Sr and Nd isotopic compositions of the BS basalts are affected to a lesser extent by the arc component, and at least in the case of the depleted basalts from the southwest end of BS, remain measurably different from the arc (Figure VI.7a). This causes the BS basalts (including the subaerial samples) to have a narrow range of Pb isotopic ratios compared to their ranges of Sr and Nd isotopic ratios, and also compared to the range of Pb isotopic ratios of other BABBs (Figure VI.7). This could be explained in one of two ways: (1) The depleted mantle beneath BS has Pb isotopic ratios that are at the high end of the MORB range, and happen to be similar to the Pb isotopic ratios of the subducted sediments. Other basaltic volcanism around West Antarctica tends to have high  $^{206}\text{Pb}/^{204}\text{Pb}$  (Hole et al., 1993; Hart et al., 1995), and the BS source may have incorporated some of this component (Chapter 5). Or (2), The depleted mantle beneath BS actually has low  $^{206}\text{Pb}/^{204}\text{Pb}$ , but the BS volcanism only samples sources that have some subducted sediment mixed in. Pb concentrations are so much higher in subducted sediments than in depleted mantle that mixing <1% sediment gives the mantle-sediment mixture the Pb isotopic composition of the sediments, while barely affecting the Sr and Nd isotopic compositions. Mixing in >1% sediment has little further affect on the Pb isotopic ratios, and only changes the Sr and Nd isotopic ratios. Keller et al. (1992) favored this latter explanation for the dredged and subaerial BS samples that they analyzed. However, the low- $^{87}\text{Sr}/^{86}\text{Sr}$  (0.7027) depleted basalts recently dredged from the SW end of the rift also have Pb isotopic compositions similar to the other BS samples. Modeling the isotopic compositions of these depleted basalts with a mixture of

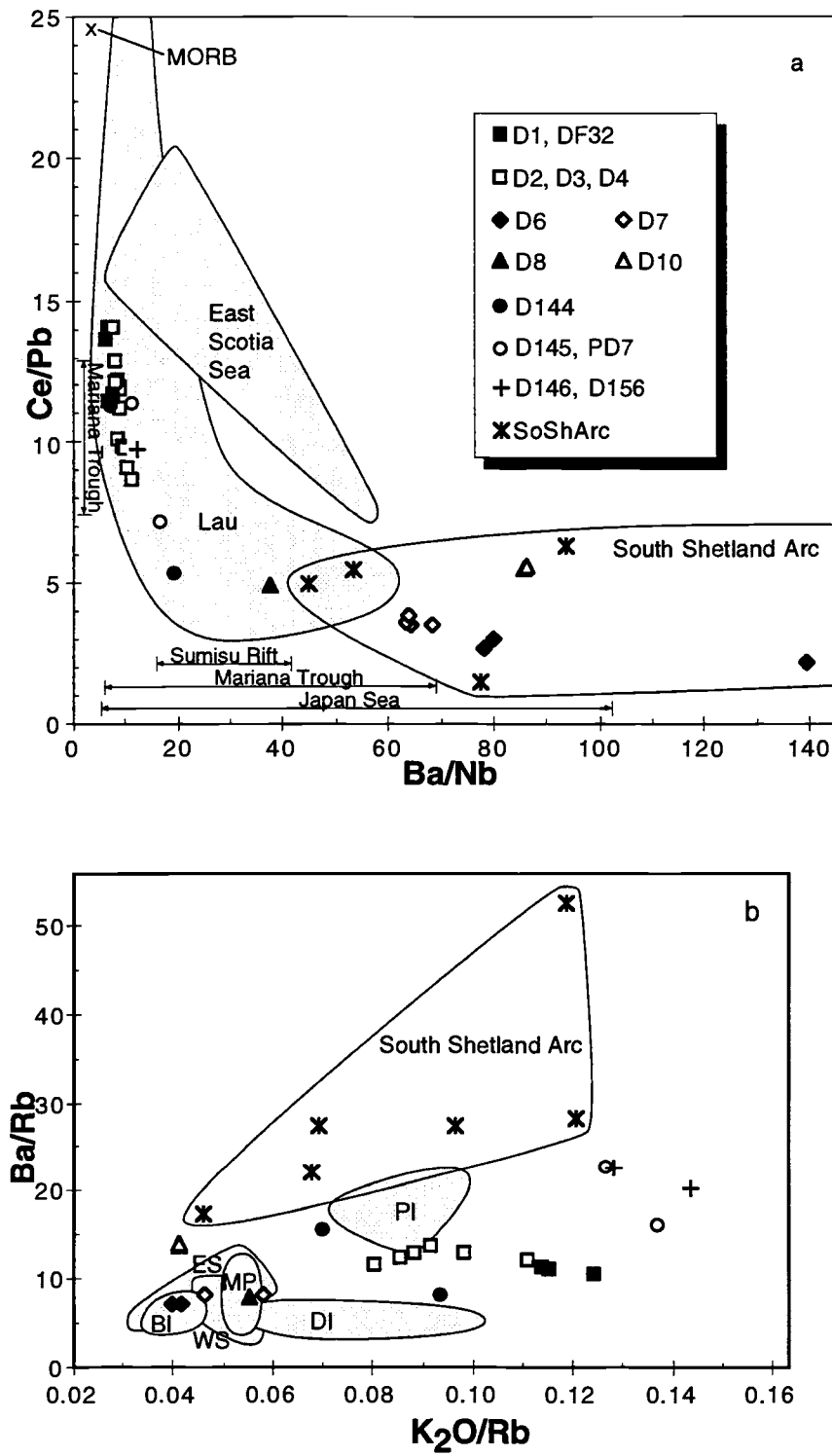


Figure VI.8. Ba/Nb vs. Ce/Pb (panel a), and  $K_2O/Rb$  vs. Ba/Rb (panel b) of South Shetland Island Arc and Bransfield Strait samples. Abbreviations as in Figure VI.2. Data from other backarc basins (see text for data sources) are shown for comparison. MORB value in panel a is from Sun and McDonough (1989).

sediments and low- $^{206}\text{Pb}/^{204}\text{Pb}$  depleted mantle requires sediments with higher Pb concentrations ( $\geq 200$  ppm) and lower Sr/Pb ( $\leq 1$ ) than any sediment except for Mn nodules (Chapter 5). Regardless of which of these two models we prefer, the arc component must have high  $^{87}\text{Sr}/^{86}\text{Sr}$  and low  $^{143}\text{Nd}/^{144}\text{Nd}$ , and Pb isotopic ratios similar to those of the BS samples. This explains why all of the BS samples have similar Pb isotopes, and also why the samples with the most arc signature in their trace elements also have the most enriched Sr and Nd isotopic ratios.

### Along-axis variations

Some BABs have systematic along-axis variations in rift morphology, grading from a diffuse rift, to a focused spreading center (e.g., Gulf of California - Saunders, 1983; Lau Basin - Hawkins, 1995). Bransfield rift does not have a well-developed spreading center, but the morphology of some of the Bransfield features has been interpreted as a developmental progression from seamount volcanism (the seamount at  $58.4^\circ\text{W}$ ), to a rifted seamount with a central ridge (the lineated feature at  $59.8^\circ\text{W}$ ), to a long ridge flanked by rifted seamount remnants (the ridge at  $59.0^\circ\text{W}$ ) (Gracia et al., in press). Note however, that the best-developed feature is located between two less-developed features, so this progression in rift morphology is not systematic from one end of the rift to the other.

BABs that have along-axis variation in rift morphology can also have along-axis variation in basalt chemistry, such that the more mature (wider) parts of the rift are erupting basalts more similar to MORB (Saunders et al., 1982; Hawkins, 1995). In BS, two additional factors must be kept in mind when attempting to match chemical variations to morphological variations: any along-axis variation may be complicated by the two anomalously large on-axis volcanoes of Deception and Bridgeman islands; and, the submarine samples from the southwest half of the rift are from large edifices, while the submarine samples from the northeast half of the rift are mostly from small features. Looking just at the submarine samples, there are variations in incompatible elements that suggest a greater contribution from a depleted source at the southwest end of the rift. The axial ridge at  $59.0^\circ\text{W}$  that is interpreted as the most mature rift feature was sampled by dredges D1 and D144 and piston core DF86.32, and has the most MORB-like (depleted) trace element concentrations and Sr-Nd isotopic ratios of any sampled feature. On average, dredges from the southwest end of the rift tend to have lower

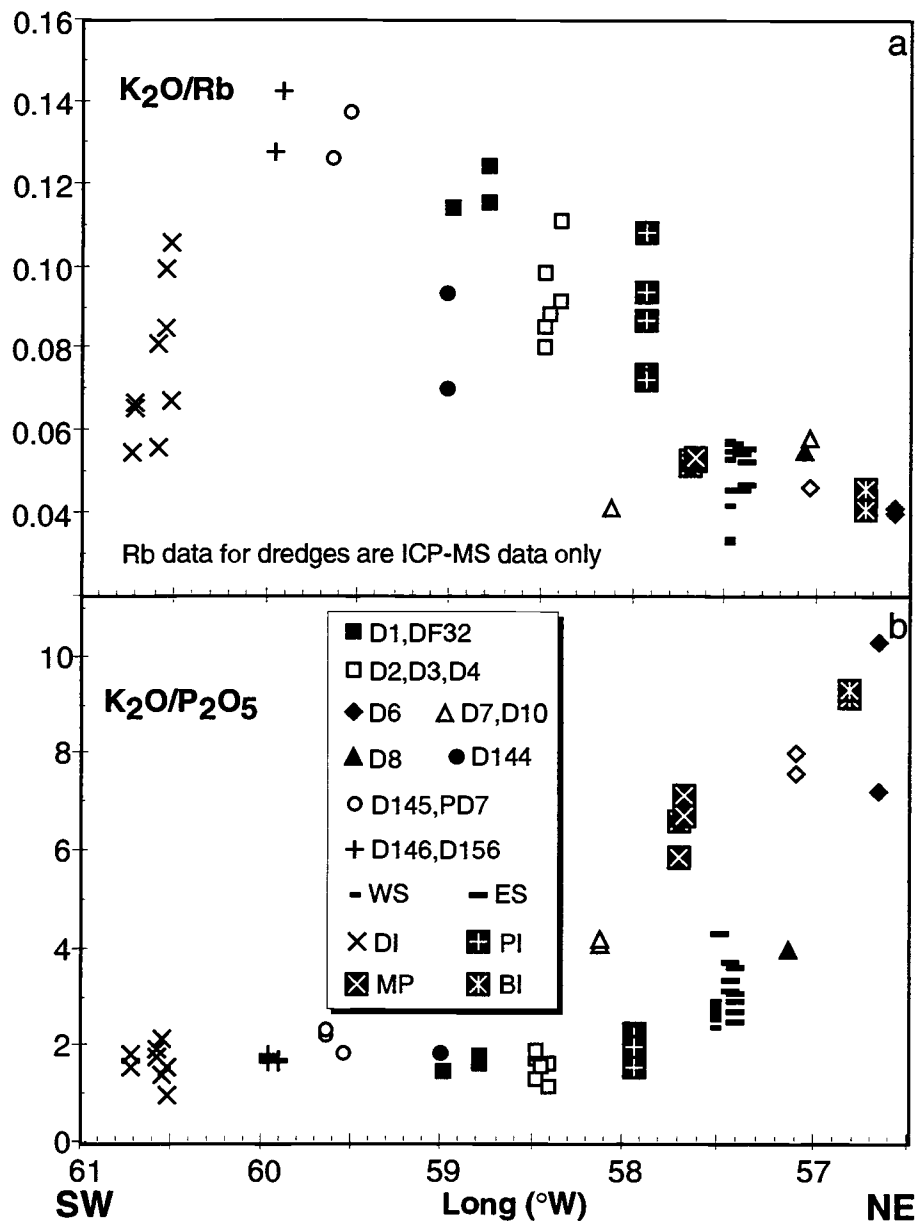


Figure VI.9. Longitude vs  $K_2O/Rb$  (panel a) and  $K_2O/P_2O_5$  (panel b) of Bransfield Strait samples. Abbreviations as in Figure VI.2. Data sources as in Figure VI.4.

$K_2O/P_2O_5$  and higher  $K_2O/Rb$  and  $Ba/Rb$  than the other dredges (Figure VI.9) (but  $Ba/Rb$  lower than the arc; Figure VI.8b). Neglecting Deception Island,  $K_2O$  contents actually decrease toward the southwest end of the rift, but Rb concentrations decrease even more, which raises  $K_2O/Rb$  values of the southwest dredges (0.10–0.14) to

typical values for NMORB (0.13; Sun and McDonough, 1989), suggesting that depleted mantle similar to the MORB source is important at the southwest end of the rift.

Seemingly contradictory to the high K<sub>2</sub>O/Rb of the southwest dredged samples is their low K<sub>2</sub>O/P<sub>2</sub>O<sub>5</sub>, but this is caused by increasing P<sub>2</sub>O<sub>5</sub> to the southwest despite constant or decreasing K<sub>2</sub>O. The low K<sub>2</sub>O/P<sub>2</sub>O<sub>5</sub> values are again similar to NMORB (0.62; Sun and McDonough, 1989). Additional features of the southwest dredged samples that are similar to MORB are their high Na<sub>2</sub>O/K<sub>2</sub>O and <sup>143</sup>Nd/<sup>144</sup>Nd, and low Rb/Sr, <sup>87</sup>Sr/<sup>86</sup>Sr, <sup>207</sup>Pb/<sup>204</sup>Pb, and <sup>208</sup>Pb/<sup>204</sup>Pb. Although some of the depleted trace element ratios could be due to in situ depletion of the Bransfield Strait source by repeated melting during rifting, the depleted isotopic ratios require that a long-term-depleted reservoir, such as oceanic upper mantle, be making a larger contribution to the BS source in the southwest.

One feature of along-axis variation that does not seem to simply be a trend toward MORB-like values is the higher Nb in the southwest. In this case Deception Island fits in with the trend, and has Nb as high as 9 ppm at MgO contents similar to the dredged samples. This increase in Nb to the southwest could be a feature of the source change required by the isotopic data, or it could be a change in melting conditions. H<sub>2</sub>O is known to increase the distribution coefficient of Nb in mafic systems (Tatsumi et al., 1986), so higher H<sub>2</sub>O in the source in the northeast would cause Nb to be less incompatible there, and thus in lower concentrations in the melts. Evidence for a more hydrous source region in the northeast also includes the higher degree of melting at Bridgeman Island and the NE dredged samples (evidenced by lower Ce/Y; Weaver et al., 1979; Keller et al., 1992), and the fact that very few of the samples dredged in the northeast contain <10% vesicles.

#### Comparisons to other areas

Much of what we know about how BABs form has come out of recent geophysical and geological surveys of BABs in the western Pacific, e.g., detailed studies of the Japan Sea, Lau Basin, Mariana Trough, and Sumisu Rift. Comparing BS to these other BABs may help us understand how BS's continental tectonic setting and rift-to-drift transitional nature affect the volcanism there.

The Japan Sea (JS) is similar to BS in that it is also ensialic, but JS differs in that it is wider, better-developed, and no longer active (Tamaki et al., 1992). Some trace

element characteristics of the JS are similar to those of BS (e.g., Ba/Nb 6–103 for JS vs. 6–140 for BS), but the two areas have significantly different isotopic characteristics. Pb isotopic ratios of JS basalts extend from values similar to BS, down to values much more depleted than anything in BS (Figure VI.7). Sr isotopic ratios of JS basalts, including those with depleted Pb isotopic ratios, are more enriched than those of BS basalts. JS Nd isotopic ratios extend to both more enriched and more depleted values. The enriched isotopic endmember in JS basalts has been identified as devolatilized subducted sediments (Cousens and Allan, 1992; Cousens et al., 1994), but these sediments must be different from those of the enriched BS endmember. The relatively enriched Sr isotopic ratios of JS basalts require that the subducted component at JS has higher Sr concentrations and/or  $^{87}\text{Sr}/^{86}\text{Sr}$ , and/or is present in greater percentages in the JS source than in the BS source.

Because of the rarity of continental BABs, we must turn to oceanic BABs in the western Pacific to find rifts that are at various stages of development: from a very young backarc rift that has not yet developed an axial neovolcanic ridge (Sumisu Rift (SR) at 31°N; Taylor et al., 1990), to a more mature BAB that has been spreading for at least 3 m.y. and has an axial neovolcanic ridge with segments up to 65 km long (Mariana Trough (MT) at 18°N; Hawkins et al., 1990), to an even more mature BAB that has been spreading for 5 m.y. (Lau Basin (LB) at 20°S; Hawkins, 1995). The <30 km-long axial ridges in BS appear to place it somewhere between SR and MT in this spectrum of tectonic development. How the relative tectonic development of BS is reflected in the volcanism there, compared to the other BABs, may shed some light on the differences between oceanic and continental BABs.

Simusu Rift (SR) basalts fall in the middle of the BS range of trace element characteristics, and are neither as depleted nor as enriched. For example, SR Ba/Nb ranges from 16–42 (Hochstaedter et al., 1990), compared to the BS range of 6–140. No Pb concentration data are available for SR, but Pb isotopic ratios are all markedly lower in the SR (Hochstaedter et al., 1990) than in BS. The two areas have similar  $^{143}\text{Nd}/^{144}\text{Nd}$ , but SR has a narrower range of  $^{87}\text{Sr}/^{86}\text{Sr}$  at mid-BS values (Figure VI.7). Pb isotopic compositions of the SR samples are more depleted than anything found in BS.

Trace element ratios in Mariana Trough (MT) basalts (Hawkins et al., 1990; Stern et al., 1990) are similar to the most depleted (southwestern) BS dredges: the maximum Ce/Pb in MT (13) is similar to the BS maximum (14), but MT Ba/Nb does not extend above 70, while northeastern BS samples have Ba/Nb as high as 140. Isotopic ratios of

the enriched ends of the MT isotopic fields (Hawkins et al., 1990; Stern et al., 1990; Volpe et al., 1990) are similar to BS isotopes, but the depleted end of MT isotopic fields extend to more depleted Sr and Nd isotopic ratios, and far more depleted Pb isotopic ratios than BS (Figure VI.7). Just as in the SR, the isotopically depleted MT samples are more depleted than the most depleted BS samples.

Some of the basalts in the Lau Basin (LB) are more depleted than anything found in BS, and are essentially indistinguishable from MORB (Hawkins, 1995). Ba/Nb does not exceed 60 in LB (Hergt and Farley, 1994; Pearce et al., 1995), which is lower than the northeastern BS dredged samples. LB Ce/Pb values range from similar to MORB (>20), to similar to the northeastern BS dredged samples (<5) (Figure VI.8a). The most enriched Sr, Nd, and Pb isotopic ratios of LB basalts (Volpe et al., 1988; Hergt and Farley, 1994; Hergt and Hawkesworth, 1994) overlap the BS field (Figure VI.7), but once again, the LB fields extend to ratios more depleted than anything in BS.

The very well-developed BAB in the East Scotia Sea (ESS) is geographically the closest to BS, and has been spreading for 8 m.y. (Barker and Hill, 1981).

Unfortunately, the ESS has not been thoroughly sampled, and comprehensive trace element data and Pb isotopic data are very rare (Saunders and Tarney, 1979; Cohen and O'Nions, 1982). From what data are available, it appears that the ESS has more depleted trace element ratios (Ce/Pb up to 20, and Ba/Nb <60) than BS. Sr and Nd isotopic ratios in ESS extend to more depleted values, and do not include values as enriched as some of the BS values. Pb isotopic ratios in ESS are significantly more depleted than, and do not overlap with, BS ratios. The ESS spreading center obviously is sampling a depleted endmember that is not evident in the BS samples. The depleted endmember in the ESS is also different from the depleted endmember of the western Pacific BABs, especially in its lower  $^{208}\text{Pb}/^{204}\text{Pb}$ .

Only the MT and LB include basalts with  $^{87}\text{Sr}/^{86}\text{Sr}$  more depleted than anything found in BS, but all of the other BABs include basalts with Pb isotopic ratios more depleted than anything in BS. The JS data show that we cannot attribute the higher Pb isotopic ratios in BS to the fact that it is ensialic. It is more likely that the depleted mantle endmember beneath BS has inherently higher Pb isotopic ratios (although still within the MORB range) than does depleted mantle beneath other BABs. However, we cannot rule out the possibility that the depleted endmember beneath BS has low Pb isotopic ratios, but the subducted component beneath BS has such high Pb concentrations and low Sr/Pb values that it can affect the Pb isotopes of BS volcanism without having much effect on the Sr and Nd isotopes (Chapter 5, and mixing line in Figure VI.7).

## CONCLUSION

Bransfield Strait is unique amongst backarc basins in that it is actively forming within continental crust, and appears to be at the transition from rifting to spreading. Trace element characteristics of newly dredged samples range from very similar to the nearby arc volcanism, to very similar to mid-ocean ridge basalt volcanism. Relative depletion of the BS basalts roughly correlates with the maturity of the features from which they were collected. However, the maturity/depletion correlation is not systematic along-axis, and we find no evidence for propagation of rifting or spreading. In the most depleted Bransfield Strait basalts, only high Cs and Pb concentrations are outside of the MORB range. Sr, Nd, and Pb isotopic ratios extend from enriched values similar to the arc, to depleted values within the range of MORB, although Pb isotopic ratios are at the high end of the MORB range.

Compared to other BABs, BS has a narrow range of Pb isotopic ratios for its range of Sr and Nd isotopic ratios, and either the depleted mantle isotopic component beneath BS has relatively high  $^{206}\text{Pb}/^{204}\text{Pb}$  that is similar to the arc  $^{206}\text{Pb}/^{204}\text{Pb}$ , or the depleted component has low  $^{206}\text{Pb}/^{204}\text{Pb}$ , but the subducted component has very high Pb concentration ( $\geq 200$  ppm) and low Sr/Pb ( $\leq 1$ ).

## ACKNOWLEDGMENTS

We are grateful to R. Nielsen for assisting with the microprobe analyses, and to A. Ungerer for assisting with the ICP-MS analyses. Dredging in Bransfield Strait was supported by NSF grant DPP90-19247 to LAL. Analytical work was supported by NSF grants DPP88-17126 and DPP93-17307 to MRF.

## ANALYTICAL TECHNIQUES APPENDIX

The glass analyses presented here were determined by electron microprobe at OSU using a four-spectrometer Cameca SX-50. Makaopuhi basalt glass from the Smithsonian reference collection was the standard. Software provided with the microprobe corrected for atomic number, absorption, and fluorescence effects. Glass was analyzed with 15-kV accelerating voltage, 30-nA beam current, and 10-s counting

times, except Ti and Al were counted for 20 s. Na was always analyzed first, and showed no evidence for loss under these conditions. Precision based upon multiple analyses of the Makaopuhi basalt glass is reported in Forsythe and Fisk (1994).

The whole rock major and trace element data presented in Table VI.2 were determined by x-ray fluorescence (XRF) at NERC-BAS, Cambridge, UK, using techniques described in Smellie et al. (1995).

Trace element and rare earth element data were analyzed by inductively coupled plasma mass spectrometry (ICP-MS) at Oregon State University. Approximately 70 mg of <1 mm, clean chips were hand-picked, rinsed in deionized water, and dried in an 80°C oven. The chips were then digested overnight in a mixture of redistilled GFS HF and doubly distilled 8N HNO<sub>3</sub> in sealed Savilex™ capsules in a 80°C oven. The capsules were then opened and the solutions allowed to dry on a 70°C hotplate in an exhaust hood. When dry, 0.5 mL of 6N HCl was added and allowed to dry down. Then 0.5 mL of 8N HNO<sub>3</sub> was added and allowed to dry down, and this step was then repeated. The residue was then taken up in 10 mL of 2N HNO<sub>3</sub>. This solution was then diluted 20:1 with 1% HNO<sub>3</sub> and placed in a run tube with a Be-In-Re-Bi spike.

The ICP-MS at OSU is a VG PlasmaQuad. Before running rock solutions, a sample rock solution is used to tune the machine for maximum response to the elements sought. The unknown solutions are then run in suspected order of increasing trace element concentrations. The analysis procedure used is a 75-s uptake, 60-s acquire, and 150-s wash. Three consecutive replicates are done on each sample solution. The PlasmaQuad calculates and prints out integrated counts per second (cps) for each element. The cps from each of these three replicates are then checked for flyers and averaged.

Instrument drift is monitored and corrected using the Be-In-Re-Bi spike and a monitor solution that is analyzed eight to ten times during the course of a run. Matrix affects are minimized by using consistent sample weights, but can also be monitored via the Be-In-Re-Bi spike. Corrected counts are then converted to concentrations using a linear regression of at least four international rock standards (e.g., AGV-1, BCR-1, BHVO-1, JB-1, and W-2).

## Chapter 7

### Summary and Conclusions

The widely-held relationship between the geochemistry of a volcanic rock and the tectonic setting in which it erupted is supported by the results in this thesis, although the fidelity of the relationship is variable. Hotspot volcanism can have depleted compositions more similar to divergent-plate-boundary signatures (MORB) than to intraplate signatures (hotspots). Also, volcanic rocks erupted 360 km from a trench can have a component of subducted sediments in their isotopic compositions, even though their trace element compositions lack evidence for a subducted component. Thus, the enriched components that set intraplate and subduction zone volcanism apart from each other and from mid-ocean ridge volcanism can become obscured or ambiguous in tectonically complex areas, such as a hotspot near a spreading ridge, or a rift near a subduction zone. A specific example of this is that the Hawaiian hotspot erupted unusually depleted basalts in the Late Cretaceous (Figure VII.1) when it was close to an active spreading ridge (Chapters 2 and 3; Keller et al., 1994), but since then, the primitive-mantle-like signature of the hotspot has become obvious (Stille et al., 1986). We interpret this history to be an effect of larger amounts of entrainment of depleted upper mantle while the hotspot was close to the spreading ridge, rather than a real change in the composition of the mantle plume.

The Cobb hotspot in the northeast Pacific, in contrast, erupted relatively depleted basalts throughout its history (Figure VII.1; Chapters 2 and 4). This is typical of hotspots in the northeast Pacific, so a regional explanation is appropriate. One possibility is that the northeast Pacific hotspots are weak, thermal, rather than compositional, mantle plumes (Desonie and Duncan, 1990). This would explain the lack of enriched compositions of the hotspots, and the discontinuity of the hotspot tracks. The only suggestion of an enrichment in the Cobb hotspot over time is the fact that the oldest basalt (33 Ma) has the lowest  $^{206}\text{Pb}/^{204}\text{Pb}$  value (Chapter 4, and Keller et al., 1995). The difference in  $^{206}\text{Pb}/^{204}\text{Pb}$  is small though, and may reflect a sampling bias. If the Cobb hotspot did become more enriched with time, this certainly cannot be explained by the proximity-to-a-spreading-ridge argument used for the Hawaiian hotspot because the Cobb hotspot was farther from a spreading ridge early in its history.

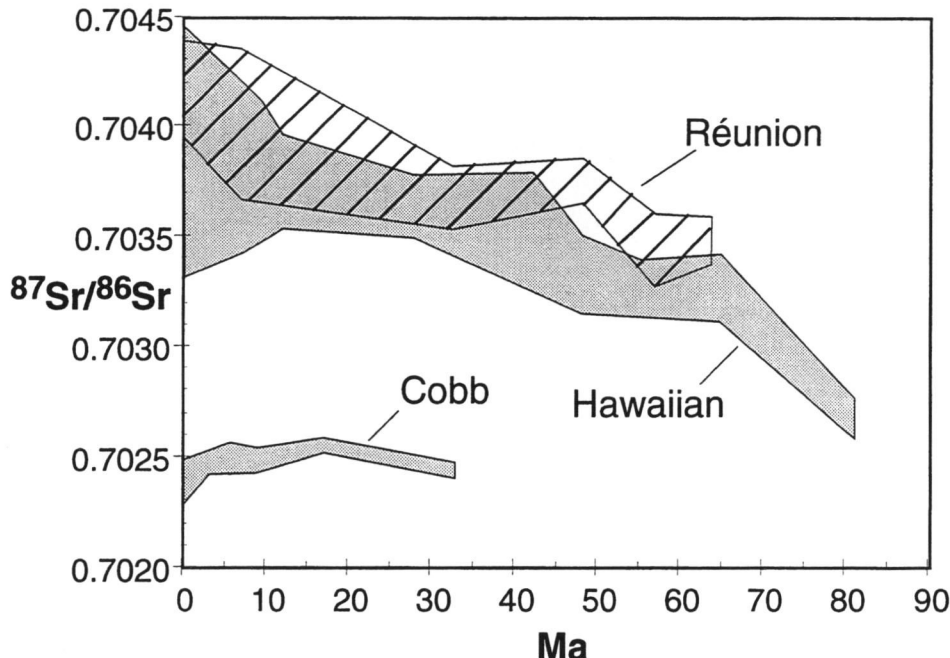


Figure VII.1. Evolution of Sr isotopic ratios of hotspots over time. The Réunion and Hawaiian hotspots show increasing enrichment with time. The Cobb hotspot has had depleted isotopic compositions throughout its known history. The only other hotspot track with sufficient data for this plot is Kerguelen, and it has a complex evolution that appears to have been disturbed by its passage under a spreading ridge (Weis and Frey, 1991). Réunion data from Fisk et al. (1988), Mahoney et al. (1989), and White et al. (1990). Hawaiian data from Lanphere et al. (1980), Unruh et al. (1987), Keller et al. (1994 and Chapter 3), Tatsumoto (1994), and numerous references for the Hawaiian Islands. Cobb data from Desonie and Duncan (1990), Rhodes et al. (1990), and Keller et al. (1995 and Chapter 4).

Other hotspot tracks that have been sampled in sufficient detail to determine their long-term chemical evolution also became more enriched with time (Weis et al., 1992). The Réunion hotspot produced lavas with progressive enrichments in Sr (Figure VII.1), Nd, and Pb isotopic compositions. Evolution of the Kerguelen hotspot was complicated by its passage under a spreading ridge, but the Ninetyeast Ridge part of the hotspot track shows a progressive increase in  $^{206}\text{Pb}/^{204}\text{Pb}$  with time (Weis and Frey, 1991). The progressive enrichment of both of these hotspots was explained by a model wherein the head of a newly ascending mantle plume entrains and melts more of the depleted upper mantle than does an established plume conduit (White et al., 1990; Weis et al., 1992). This required the assumption that the flood basalts (Deccan and Rajmahal) at the old ends of the Réunion and Kerguelen hotspot tracks were caused by plume heads

(Richards et al., 1989). A similar model cannot be applied with confidence to the two hotspots we studied because the old ends of the Hawaiian and Cobb hotspot tracks end at trenches. We have no way of knowing if the oldest remaining seamounts in these two hotspot tracks are among the earliest products of the hotspots, or if substantial portions of the hotspot tracks have been subducted. Also, there is no recognized evidence that either of these hotspots created flood basalts early in their histories.

Exactly how the enriched component makes its way into a mantle plume that creates a hotspot remains unclear. The relatively depleted compositions of the hotspot basalts studied here suggest that compositional buoyancy is not required to sustain a mantle plume. Although this does not rule out the possibility that the initial source of some mantle plumes is deeply subducted crust (Hofmann and White, 1982), the lack of a recycled crustal signature in either of the hotspots studied here suggests that at least some plumes can be initiated and sustained by thermal events alone. Plumes that are initiated by thermal contrasts may then acquire enriched compositions as they ascend and encounter enriched regions of the mantle (e.g., Hanan and Graham, submitted).

Another curious result of our Patton-Murray seamounts work is that volcanism can occur along a hotspot track as much as 16 m.y. after that part of the track has moved away from the hotspot. Such a late pulse of volcanism can, at most, be only indirectly related to the hotspot. The subduction zones that virtually surround the northeast Pacific may put that area of the Pacific plate under tension. Intraplate extension could be focused at pre-existing weaknesses in the plate, such as where it had previously passed over a hotspot. Since there is still subduction going on around the northeast Pacific, it is possible that even younger phases of volcanism occurred on the Patton-Murray seamount lineament, or on any other hotspot track in the northeast Pacific.

Convergent-margin volcanism can be distinguished from within-plate volcanism by the former's lack of enrichment in Nb and Ta, despite its similar or greater enrichment in Sr, Cs, Ba, and Pb. This style of enrichment is well-expressed in the South Shetland Arc (Chapters 5 and 6), and can be modeled by mixing depleted mantle with 1–4% marine sediment. The subduction zone signature is more subtle in Bransfield Strait backarc volcanism, and can be modeled by mixing depleted mantle with 0.5–2.5% marine sediment. In the extreme backarc, the James Ross Island Volcanic Group has trace element signatures similar to intraplate basalts rather than convergent margin basalts, but its isotopic compositions contain evidence for subducted sediments. The fact that we have found evidence for a small, but isotopically significant, amount of

subducted component in basalts erupted 360 km from a trench means that incompatible elements from the subducted slab interact with a widespread region of the upper mantle.

Numerous opportunities for future work exist in all of the areas studied in this thesis:

a) Additional trace element, isotopic, and geochronological data from the oldest Emperor seamounts other than Detroit could make it possible to carefully model the Late Cretaceous history of interaction between the Hawaiian hotspot and a spreading ridge. Meiji Guyot has not been isotopically dated, and our one sample from DSDP Site 192 on Meiji is the only one with full trace element and isotopic analyses. Suiko Guyot has been dated, but our one sample from DSDP Site 433 on Suiko is the only one with full trace element and isotopic data.

b) More isotopic data from the oldest products of the Cobb hotspot would determine if there has been an isotopic enrichment of the hotspot, how significant that enrichment was, and how it could be explained. Also, in light of our results from Patton-Murray seamount platform showing that anomalously young volcanism can occur on a hotspot seamount, anomalous ages from other hotspot seamounts that had been dismissed as spurious because they were 'too young', should be reexamined. The young volcanism does not conform to the hotspot model, and could be present on any northeast Pacific seamount regardless of its position relative to a hotspot. These late-stage volcanic events may ultimately be tied to periods of intraplate extension related to changes in forces acting on the Pacific plate.

c) With additional trace element and isotopic data, and sufficient geochronological control, it may eventually be possible to quantify the crust-to-mantle fluxes at the northern Antarctic Peninsula subduction zone. The rate of subduction into the South Shetland Trench over the past 30 m.y. is extraordinarily well-constrained (Maldonado et al., 1994), so we know how much crust has gone into the subduction zone during that time. If we can quantify the amount of enriched component from the subducted crust that returns to the surface as volcanic activity, we can determine, by difference, the amount of enriched component that remains in the mantle. This has important implications for the chemical evolution of the mantle, as well as the possibility that deeply subducted crust can contribute an enriched component to hotspot volcanism (White and Patchett, 1984). We are not yet at a point where we can calculate the volume flux of subduction zone volcanism. Although the Tertiary-Quaternary arc/backarc volcanism in the South Shetland Islands/Bransfield Strait/James Ross Island Volcanic Group is well-sampled, only the Bransfield Strait backarc samples have been

sufficiently dated and analyzed for trace element and isotopic compositions. Geochronological data and comprehensive trace element and isotopic analyses are rare from the arc and extreme backarc, and ice cover in the arc and extreme backarc makes it difficult to determine volumes of volcanism without geophysical surveying.

d) Additional geological and geophysical data are necessary from Bransfield Strait to answer questions about how this nascent backarc basin is developing. Does rift-related volcanism in Bransfield Strait extend to the northeast past Bridgeman Island and to the southwest past Deception Island? This question could be answered by additional dredging and multibeam bathymetric surveying in the basins northeast of Bridgeman and southwest of Deception. Are there additional volcanic features between the two islands that remain hidden beneath sediments? Answering this question requires either a major improvement in the penetration depth of seismic reflection data from the strait, or an Ocean Drilling Program drilling leg. Only drilling could sample the rocks hidden beneath the sediments, and determine if basement in the deepest part of the strait is the most similar to depleted MORB. Does the subducted component that is so subtle in the trace elements of the most-depleted Bransfield Strait samples (evident only in slightly elevated Cs and Pb concentrations) show up in trace elements that we have not measured? Among the best tracers of the quantity of subducted component in arc/backarc volcanism are incompatible elements such as Li, Be, and B. The behavior of these elements and H<sub>2</sub>O is also a reflection of whether the enriched component is removed in a hydrous phase created by dehydration reactions or by partial melting. Changes in the behavior of these elements with distance from the trench could be a reflection of variations in these processes acting on the subducting slab. Also, measuring Be isotopic compositions can determine how long it has been since the sediment component was subducted.

These questions make it clear that this thesis is a starting point as much as an ending point — our work on hotspot seamounts in the North Pacific and arc/backarc volcanism on the northern Antarctic Peninsula has posed as many new questions as it has answered.

## Bibliography

- Allan, J.F., R.L. Chase, B. Cousens, P.J. Michael, M.P. Gorton, and S.D. Scott, 1993, The Tuzo Wilson volcanic field, NE Pacific: Alkaline volcanism at a complex, diffuse, transform-trench-ridge triple junction. *J. Geophys. Res.*, 98:22367–22387.
- Anderson, J.B., D.J. DeMaster, and C.A. Nittrover, 1987, Preliminary results from marine geological cruises aboard the U. S. Coast Guard icebreaker Glacier. *Antarctic Journal U. S.*, 1986 Review, p.144–148.
- Armstrong, R.L., 1971, Isotopic and chemical constraints on models of magma genesis in volcanic arcs. *Earth Planet. Sci. Lett.*, 12:137–142.
- Barbieri, M., K. Birkenmajer, M.C. Delitala, L. Francalanci, W. Narebski, M. Nicoletti, A. Peccerillo, C. Petrucciani, M.L. Todaro, L. Tolomeo, and C. Trudu, 1989, Preliminary petrological, geochemical and Sr isotopic investigation on Mesozoic to Cainozoic magmatism of King George Island, South Shetland Islands (West Antarctica). *Mineral. Petrogr. Acta (Bologna)*, 37:37–49.
- Barker, P.F., 1982, The Cenozoic subduction history of the Pacific margin of the Antarctic Peninsula: ridge crest-trench interactions. *J. geol. Soc. London*, 139:787–801.
- Barker, P.F., and I.A. Hill, 1981, Back-arc extension in the Scotia Sea. *Phil. Trans. R. Soc. London*, 300:249–262.
- Barreiro, B., 1983, Lead isotopic compositions of South Sandwich Island volcanic rocks and their bearing on magmagenesis in intra-oceanic island arcs. *Geochim. Cosmochim. Acta*, 47:817–822.
- Basu, A.R., and B.E. Faggart, 1994, Temporal Isotopic Variations in the Hawaiian Mantle Plume, the Lanai Anomaly, the Molokai Fracture Zone and a Seawater-Altered Lithospheric Component in Hawaiian Volcanism (ICOG abs.). *U.S.G.S. Circular* 1107, p.23.
- Ben Othman, D., W.M. White, and J. Patchett, 1989, The geochemistry of marine sediments, island arc magma genesis, and crust-mantle recycling, *Earth Planet. Sci. Lett.*, 94:1–21.
- Birkenmajer, K., 1980, Age of the Penguin Island volcano, South Shetland Islands (West Antarctica), by the lichenometric method. *Bull. Polish Acad. Sci., Earth Sci.*, 27:69–76.
- Birkenmajer, K., 1992, Volcanic succession at Deception Island, West Antarctica: A revised lithostratigraphic standard. *Studia Geol. Polonica*, 101:27–82.
- Birkenmajer, K., and R.A. Keller, 1990, Pleistocene age of the Melville Peak volcano, King George Island, West Antarctica, by K-Ar dating. *Bull. Polish Acad. Sci., Earth Sci.*, 38:17–24.

- Castillo, P., R. Batiza, and R.J. Stern, 1986, Petrology and geochemistry of Nauru Basin igneous complex: Large-volume, off-ridge eruptions of MORB-like basalt during the Cretaceous. In Moberly, R., Schlanger, S.O., et al., *Init. Rep. DSDP*, 89: Washington (U.S. Govt. Printing Office), 555–576.
- Chapman, D., R. Allis, W. Bentowski, M. Bone, V. Cermak, T. Hamilton, T. Lewis, R. McDonald, K. Rohr, D. Seeman, G. Spence, S. Willett, and J. Wright, 1987, A geophysical investigation at the southeast terminus of the Kodiak-Bowie seamount chain. *Eos, Transactions, Am. Geophys. Union*, 68(44):1498. (Abstract)
- Chen, C.-Y., and F.A. Frey, 1985, Trace element and isotopic geochemistry of lavas from Haleakala volcano, East Maui, Hawaii: Implications for the origin of Hawaiian basalts. *J. Geophys. Res.*, 90:8743–8768.
- Cheng, Q., K.-H. Park, J.D. Macdougall, A. Zindler, G.W. Lugmair, H. Staudigel, J. Hawkins, and P. Lonsdale, 1987, Isotopic evidence for a hotspot origin of the Louisville Seamount Chain, in B.H. Keating, P. Fryer, R. Batiza, and G.W. Boehlert (eds.), *Seamounts, Islands, and Atolls*. Geophys. Monograph 43, AGU, Washington, DC, p. 283–296.
- Church, S.E., and M. Tatsumoto, 1975, Lead isotope relations in oceanic ridge basalts from the Juan de Fuca-Gorda Ridge area, NE Pacific Ocean. *Contrib. Mineral. Petrol.*, 53:253–279.
- Clague, D.A., G.B. and Dalrymple, 1987, The Hawaiian-Emperor volcanic chain, Part I, Geologic evolution. In R.W. Decker, T.L. Wright, and P.H. Stauffer, (eds.), *Volcanism in Hawaii*. U.S. Geol. Survey Prof. Paper, 1350(1):5–54.
- Clague, D.A., M.R. Fisk, A.E. and Bence, 1983, Mineral chemistry of basalts from Ojin, Nintoku, and Suiko Seamounts, Leg 55 DSDP. In Jackson, E.D., Koizumi, I., et al., *Init. Rep. DSDP*, 55: Washington (U.S. Govt. Printing Office), 607–637.
- Class, C., S.L. Goldstein, S.J.G. Galer, and D. Weis, 1993, Young formation age of a mantle plume source. *Nature*, 362:715–721.
- Cloetingh, S., and M. Wortel, 1985, Regional stress field of the Indian plate. *Geophys. Res. Letts.*, 12:77–80.
- Cohen, R.S. and R.K. O'Nions, 1982. Identification of recycled continental material in the mantle from Sr, Nd and Pb isotopic investigations. *Earth Planet. Sci. Lett.*, 61:73–84.
- Cousens, B.L., 1988, Isotopically depleted, alkalic lavas from Bowie seamount, northeast Pacific Ocean. *Can. J. Earth Sci.*, 25:1708–1716.
- Cousens, B.L., and J.F. Allan, 1992, A Pb, Sr, and Nd isotopic study of basaltic rocks from the Sea of Japan, ODP Leg 127/128. *Proc. ODP, Sci. Res.*, 127/128:805–817.
- Cousens, B.L., J.F. Allan, and M.P. Gorton, 1994, Subduction-modified pelagic sediments as the enriched component in back-arc basalts from the Japan Sea: Ocean Drilling Program Sites 797 and 794. *Contrib. Mineral. Petrol.*, 117:421–434.

- Dalrymple, G.B., D.A. Clague, and T. Vallier, and H.W. Menard, 1987,  $^{40}\text{Ar}/^{39}\text{Ar}$  age, petrology, and tectonic significance of some seamounts in the Gulf of Alaska. In Keating, B.H., and Batiza, R., (eds.), *Seamounts, Islands, and Atolls*. Geophys. Monogr. Srs., Am. Geophys. Union, Washington, DC, 43:297–315.
- Dalrymple, G.B., M.A. Lanphere, and D.A. Clague, 1980, Conventional and  $^{40}\text{Ar}/^{39}\text{Ar}$  K-Ar ages of volcanic rocks from Ojin (Site 430), Nintoku (Site 432), and Suiko (Site 433) seamounts and the chronology of volcanic propagation along the Hawaii-Emperor chain. in E.D. Jackson, I. Koisumi, et al., *Initial Reports of the Deep Sea Drilling Project*, 55:659–676.
- Dalrymple, G.B., M.A. Lanphere, and J.H. Natland, 1980, K-Ar minimum age for Meiji Guyot, Emperor seamount chain. in E.D. Jackson, I. Koisumi, et al., *Initial Reports of the Deep Sea Drilling Project*, 55:677–683.
- Davies, G.F., 1988, Ocean bathymetry and mantle convection 1. Large scale flow and hotspots. *J. Geophys. Res.*, 93:10467–10480.
- Desonie, D.L., and R.A. Duncan, 1990, The Cobb-Eickelberg seamount chain: Hotspot volcanism with mid-ocean ridge basalt affinity. *J. Geophys. Res.*, 95:12697–12711.
- Duncan, R.A., 1991, Age distribution of volcanism along aseismic ridges in the eastern Indian Ocean. In J. Weissel, J. Pierce, E. Taylor, J. Alt, et al. (eds.), *Proc. ODP, Sci. Results*, 121: College Station TX (Ocean Drilling Program), 507–517.
- Duncan, R.A., and D.A. Clague, 1985. Pacific plate motion recorded by linear volcanic chains. In A.E.M. Narin, F.G. Stehi, and S. Uyeda (eds.), *The Ocean Basins and Margins* (vol. 7A): *The Pacific Ocean*: New York (Plenum), 89–121.
- Duncan, R.A., and I. McDougall, 1976, Linear volcanism in French Polynesia. *J. Volcan. Geotherm. Res.*, 1:197–227.
- Elderfield, H., C.J. Hawkesworth, M.J. Greaves, and S.E. Calvert, 1981, Rare earth element geochemistry of oceanic ferromanganese nodules and associated sediments. *Earth Planet. Sci. Lett.*, 45:513–528.
- Fartnetani, D.G., and M.A. Richards, 1995, Thermal entrainment and melting in mantle plumes. *Earth Planet. Sci. Lett.*, 136:251–267.
- Fisk, M.R., 1990, Volcanism in the Bransfield Strait, Antarctica. *J. South Am. Earth Sci.* 3:91–101.
- Fisk, M.R., B.G.J. Upton, C.E. Ford, and W.M. White, 1988, Geochemical and experimental study of the genesis of magmas of Réunion Island, Indian Ocean. *J. Geophys. Res.*, 93:4933–4950.
- Fisk, M.R., R.A. Duncan, A.N. Baxter, J.D. Greenough, R.B. Hargraves, Y. Tatsumi, and Shipboard Scientific Party, 1989, Reunion hotspot magma chemistry over the past 65 m.y.: Results from Leg 115 of the Ocean Drilling Program. *Geology*, 17:934–937.

- Fleck, R.J., J.F. Sutter, and D.H. Elliott, 1977, Interpretation of discordant  $^{40}\text{Ar}/^{39}\text{Ar}$  age spectra of Mesozoic tholeiites from Antarctica. *Geochim. Cosmochim. Acta*, 41:15–32.
- Forsythe, L.M., and M.R. Fisk, 1994, Comparison of experimentally crystallized and natural spinels from Leg 135. In Hawkins, J., Parson, L., Allan, J., et al., *Proc. ODP, Sci. Results*, 135, College Station TX (Ocean Drilling Program), 585–594.
- Futa, K. and W.E. Le Masurier, 1983, Nd and Sr isotopic studies on Cenozoic mafic lavas from West Antarctica: Another source for continental alkali basalts. *Contrib. Mineral. Petrol.*, 29:275–289.
- Geist, D.J., A.R. McBirney, and R.A. Duncan, 1986, Geology and petrogenesis of lavas from San Cristobal Island, Galápagos Archipelago. *Geol. Soc. Am. Bull.*, 97:555–566.
- Geist, D.J., W.M. White, and A.R. McBirney, 1988, Plume-asthenosphere mixing beneath the Galapagos Archipelago. *Nature*, 333:657–660.
- Gracia, E., M. Canals, M. Farran, M.J. Prieto, J. Sorribas, and GEBRA Team, in press, Morphostructure and evolution of the Central and Eastern Bransfield Basins (NW Antarctic Peninsula). *Mar. Geophys. Res.*
- Grad, M., A. Guterch, T. and Janik, 1993, Seismic structure of the lithosphere across the zone of subducted Drake plate under the Antarctic plate, West Antarctica, *Geophys. J. International*, 115:586–600.
- Gripp, A.E., and R.G. Gordon, 1990, Current plate velocities relative to the hotspots incorporating the NUVEL-1 global plate motion model. *Geophys. Res. Lett.*, 17:1109–1112.
- Hart, R.B., 1994, Kula-Farallon Ridge Origin for the Great Valley (abs.). *Eos* supplement, November 1, 1994, p. 609.
- Hart, S.R., 1988, Heterogeneous mantle domains: signatures, genesis, and mixing chronologies. *Earth Planet. Sci. Lett.*, 90:273–296.
- Hart, S.R., J. Blusztajn, and C. Craddock, 1995, Cenozoic volcanism in Antarctica: Jones Mountains and Peter I Island. *Geochim. Cosmochim. Acta*, 59:3379–3388.
- Hauri, E.H., J.A. Whitehead, and S.R. Hart, 1994, Fluid dynamic and geochemical aspects of entrainment in mantle plumes, *J. Geophys. Res.*, 99:24275–24300.
- Hawkesworth, C.J., R.K. O'Nions, R.J. Pankhurst, P.J. Hamilton, and N.M. Evensen, 1977, A geochemical study of island arc and back-arc tholeiites from the Scotia Sea. *Earth Planet. Sci. Lett.*, 36:253–262.
- Hawkins, J.W., 1995, Evolution of the Lau Basin—Insights from ODP Leg 135, in B. Taylor and J. Natland (eds.), *Active Margins and Marginal Basins of the Western Pacific*. AGU Geophys. Monogr. 88:125–173.

- Hawkins, J.W., P.F. Lonsdale, J.D. Macdougall, and A.M. Volpe, 1990, Petrology of the axial ridge of the Mariana Trough backarc spreading center. *Earth Planet. Sci. Lett.*, 100, 226–250.
- Hegner, E., and M. Tatsumoto, 1987, Pb, Sr, and Nd isotopes in basalts and sulfides from the Juan de Fuca Ridge. *J. Geophys. Res.*, 92:11380–11386.
- Hegner, E., and M. Tatsumoto, 1989, Pb, Sr, and Nd isotopes in seamount basalts from the Juan de Fuca Ridge and Kodiak-Bowie Seamount Chain, NE Pacific. *J. Geophys. Res.*, 94:17839–17846.
- Hergt, J.M. and K.N. Farley, 1994, Major, trace element, and isotope (Pb, Sr, and Nd) variations in Site 834 basalts: implications for the initiation of backarc opening, in J.W. Hawkins, L.M. Parson, J.F. Allan, et al. (eds.), *Proc. ODP, Sci. Results*, 135, College Station, TX (Ocean Drilling Program), 471–486.
- Hergt, J.M. and C.J. Hawkesworth, 1994, The Pb, Sr, and Nd isotopic evolution of the Lau Basin: implications for mantle dynamics during backarc opening, in J.W. Hawkins, L.M. Parson, J.F. Allan, et al. (eds.), *Proc. ODP, Sci. Results*, 135, College Station, TX (Ocean Drilling Program), 505–518.
- Hickey, R.L., F.A. Frey, D.C. Gerlach, and L. Lopez-Escobar, 1986, Multiple sources for basaltic arc rocks from the Southern Volcanic Zone of the Andes (34°–41°S): Trace element and isotopic evidence for contributions from subducted oceanic crust, mantle, and continental crust. *J. Geophys. Res.*, 91:5963–5983.
- Hickey-Vargas, R., J.M. Hergt, and P. Spadea, 1995, The Indian Ocean-type isotopic signature in western Pacific marginal basins: Origin and significance, in B. Taylor and J. Natland (eds.), *Active Margins and Marginal Basins of the Western Pacific*. AGU Geophys. Monogr. 88:175–197.
- Hochstaedter, A.G., J.B. Gill, and J.D. Morris, 1990, Volcanism in the Sumisu Rift, II. Subduction and non-subduction related components. *Earth Planet. Sci. Lett.*, 100:195–209.
- Hofmann, A.W., and W.M. White, 1982, Mantle plumes from ancient oceanic crust. *Earth Planet. Sci. Lett.*, 57:421–436.
- Hole, M.J., 1990, Geochemical evolution of Pliocene-Recent post-subduction alkalic basalts from Seal Nunataks, Antarctic Peninsula. *J. Volcan. Geotherm. Res.*, 40:149–167.
- Hole, M.J., A.D. Saunders, G. Rogers, and M.A. Sykes, 1995, The relationship between alkaline magmatism, lithospheric extension and slab window formation along destructive plate margins, in J.L. Smellie (ed.), *Volcanism Associated with Extension at Consuming Plate Margins*. Geol. Soc. Spec. Pub., 81:265–285.
- Hole, M.J., G. Rogers, A.D. Saunders, and M. Storey, 1991, Relation between alkalic volcanism and slab-window formation. *Geology* 19:657–660.

- Hole, M.J., P.D. Kempton, and I.L. Millar, 1993, The isotopic and trace element composition of small-degree melts of the asthenosphere: evidence from the alkalic basalts of the Antarctic Peninsula. *Chemical Geology*, 109:51–68.
- Hooper, P.R., 1981, The role of magnetic polarity and chemical analysis in establishing the stratigraphy, tectonic evolution, and petrogenesis of the Columbia River Basalts. *Mem. Geol. Soc. India*, 3:362–376.
- Hurford, A.J., and K. Hammerschmidt, 1985,  $^{40}\text{Ar}/^{39}\text{Ar}$  and K-Ar dating of the Fish Canyon Tuff: Calibration ages for fission-track dating standards. *Chem. Geol.*, 58:23–32.
- Ionov, D.A., and A.W. Hofmann, 1995, Nb-Ta-rich mantle amphiboles and micas: Implications for subduction-related metasomatic trace element fractionations. *Earth Planet. Sci. Lett.*, 131:341–356.
- Jin Qingmin, Kuang Fuxiang, Ruan Honghong, and Xing Guangfu, 1991, Island arc volcanism and magmatic evolution in Fildes Peninsula, King George Island, Antarctica. Abstracts, *Sixth International Symp. Antarctic Earth Sci.*, Ranzan, Japan, 250–255.
- Karsten, J.L., and J.R. Delaney, 1989, Hot spot-ridge crest convergence in the northeast Pacific. *J. Geophys. Res.*, 94:700–712.
- Kay, R.W., 1980, Volcanic arc magmas: Implications of a melting-mixing model for element recycling in the crust-upper mantle system. *J. Geol.*, 88:497–522.
- Keller, R.A., and M.R. Fisk, 1989, Rifting and volcanism in the Bransfield Strait and South Shetland Islands. *Antarctic J. U. S.*, 1988 Review, 23:102–104.
- Keller, R.A., and M.R. Fisk, 1992, Quaternary marginal basin volcanism in the Bransfield Strait as a modern analogue of the southern Chilean ophiolites, in L.M. Parson, B.J. Murton, and P. Browning (Eds.) *Ophiolites and Their Modern Oceanic Analogues*. Geological Society Special Publication No. 60, London, p.155–170.
- Keller, R.A., and Leg 145 Shipboard Scientific Party, 1993, Ages and geochemistry of basaltic basement recovered during ODP Leg 145 (North Pacific Transect). *Eos* supplement, October 26, 1993, p. 355.
- Keller, R.A., M.R. Fisk, and J.A. Strelin, 1993, Correlating distance from a trench with subducted component in recent basalts from the northern Antarctic Peninsula. *Eos* supplement, October 26, 1993, p. 663.
- Keller, R.A., M.R. Fisk, and W.M. White, 1994, Sr, Nd, and Pb Isotopic Characteristics of Cretaceous Volcanism From the Hawaiian Mantle Plume. *Eos* supplement, November 1, 1994, p. 723.
- Keller, R.A., M.R. Fisk, W.M. White, and K. Birkenmajer, 1992, Isotopic and trace element constraints on mixing and melting models of marginal basin volcanism, Bransfield Strait, Antarctica. *Earth Planet. Sci. Lett.*, 111:287–303.

- Keller, R.A., R.A. Duncan, and M.R. Fisk, 1995, Geochemistry and  $^{40}\text{Ar}/^{39}\text{Ar}$  Geochronology of Basalts from ODP Leg 145 (North Pacific Transect), in D.K. Rea, I.A. Basov, D.W. Scholl, and J.A. Allan (Eds.), *Proc. ODP, Sci. Results*, 145, College Station, TX (Ocean Drilling Program), 333–344.
- Keller, R.A., J.A. Strelin, L.A. Lawver, and M.R. Fisk, 1994, Dredging young volcanic rocks in Bransfield Strait. *Antarctic Journal U.S.*, 1993 Review, 100–102.
- Klepeis, K.A., and L.A. Lawver, 1994, Bathymetry of the Bransfield Strait, southeastern Shackleton Fracture Zone and South Shetland Trench, *Antarctic J. U. S.*, 28:103–104.
- Lanphere, M.A., and G.B. Dalrymple, 1978, The use of  $^{40}\text{Ar}/^{39}\text{Ar}$  data in evaluation of disturbed K-Ar systems. In Zartman, R.E., (Ed.), *Short Papers of the Fourth International Conference on Geochronology, Cosmochronology, and Isotope Geology*. Open-File Rep. U.S. Geol. Surv., 78-701:241–243.
- Lanphere, M.A., G.B. Dalrymple, D.A. Clague, 1980, Rb-Sr systematics of basalts from the Hawaii-Emperor volcanic chain, in E.D. Jackson, I. Koizumi, et al., *Initial Reports of the Deep Sea Drilling Project*, 55:695–706.
- Lawver, L.A., R.A. Keller, M.R. Fisk, and J.A. Strelin, 1995, Bransfield Strait, Antarctic Peninsula: Active extension behind a dead arc, in B. Taylor (Ed.), *Back-Arc Basins: Tectonics and Magmatism*. Plenum Press, 315–342.
- LeMasurier, 1990, Overview in LeMasurier, W.E., and J.W. Thomson, (Eds.), *Volcanoes of the Antarctic Plate and Southern Oceans*. Antarct. Res. Srs., 48, Am. Geophys. Union, Wash., DC, 487 pp.
- Lonsdale, P., J. Dieu, and J. Natland, 1993, Posterosional Volcanism in the Cretaceous part of the Hawaiian Hotspot Trail. *J. Geophys. Res.*, 98:4081–4098.
- MacDonald, D.I.M., P.F. Barker, S.W. Garrett, et al., 1988, A preliminary assessment of the hydrocarbon potential of the Larsen Basin, Antarctica. *Marine and Petrol. Geol.*, 5:34–52.
- Macdonald, G.A., and T. Katsura, 1964, Chemical composition of Hawaiian lavas. *J. Petrol.*, 5:82–133.
- Mahoney, J.J., J.H. Natland, W.M. White, R. Poreda, R.L. Fisher, and A.N. Baxter, 1989, Isotopic and geochemical provinces of the western Indian Ocean spreading centers. *J. Geophys. Res.*, 94:4033–4052.
- Maldonado, A., R.D. Larter, and F. Aldaya, 1994, Forearc tectonic evolution of the South Shetland margin, Antarctic Peninsula. *Tectonics*, 13:1345–1370.
- Mammerickx, J. and G.F. Sharman, 1988, Tectonic Evolution of the North Pacific During the Cretaceous Quiet Period. *J. Geophys. Res.*, 93:3009–3024.
- McDougall, I., and T.M. Harrison, 1988, *Geochronology and Thermochronology by the  $^{40}\text{Ar}/^{39}\text{Ar}$  Method*. Oxford (Oxford Univ. Press).

- Morris, J.D., W.P. Leeman, and F. Tera, 1990, The subducted component in island arc lavas: constraints from Be isotopes and B-Be systematics. *Nature*, 344:31–36.
- Nelson, P.H.H., 1966, The James Ross Island Volcanic Group of north-east Graham Land. *British Antarct. Sci. Reports*, No.54, 62 pp.
- O'Nions, R.K., S.R. Carter, R.S. Cohen, N.M. Evensen, and P.J. Hamilton, 1978, Pb, Nd and Sr isotopes in oceanic ferromanganese deposits and ocean floor basalts. *Nature*, 273:435–438.
- Pearce, J.A., and J.R. Cann, 1973, Tectonic setting of basic volcanic rocks determined using trace element analyses. *Earth Planet. Sci. Lett.*, 19:290–300.
- Pearce, J.A., and I.J. Parkinson, 1993, Trace element models for mantle melting: application to volcanic arc petrogenesis, in H.M. Prichard, T. Alabaster, N.B.W. Harris, and C.R. Neary (eds.), *Magmatic Processes and Plate Tectonics*. Geol. Soc., London, Spec. Pub., 76:373–403.
- Pearce, J.A., M. Ernewein, S.H. Bloomer, L.M. Parson, B.J. Murton, and L.E. Johnson, 1995, Geochemistry of Lau Basin volcanic rocks: influence of ridge segmentation and arc proximity, in J.L. Smellie (ed.), *Volcanism Associated with Extension at Consuming Plate Margins*. Geol. Soc. Spec. Pub., 81:53–75.
- Pelayo, A.M., and D.A. Wiens, 1989, Seismotectonics and relative plate motions in the Scotia Sea region. *J. Geophys. Res.*, 94:7293–7320.
- Pollitz, F.F., 1988, Episodic North American and Pacific plate motions. *Tectonics*, 7:711–726.
- Pouclet, A., J-S. Lee, P. Vidal, B. Cousens, and H. Bellon, 1995, Cretaceous to Cenozoic volcanism in South Korea and in the Sea of Japan: magmatic constraints on the opening of the back-arc basin, in J.L. Smellie (ed.), *Volcanism Associated with Extension at Consuming Plate Margins*. Geol. Soc. Spec. Pub., 81:169–191.
- Rea, D.K., and J.M. Dixon, 1983, Late Cretaceous and Paleogene tectonic evolution of the North Pacific Ocean. *Earth Planet. Sci. Lett.*, 65:145–166.
- Rea, D.K., I.A. Basov, T.R. Janacek, A. Palmer-Julson, et al., 1993, *Proc. ODP, Init. Repts.*, 145: College Station, TX (Ocean Drilling Program).
- Rhodes, J.M., C. Morgan, and R.A. Llias, 1990, Geochemistry of Axial Seamount lavas: Magmatic relationship between the Cobb hotspot and the Juan de Fuca Ridge. *J. Geophys. Res.*, 95:12713–12733.
- Richards, M.A., R.A. Duncan, and V. Courtillot, 1989, Flood basalts and hotspot tracks: plume heads and tails. *Science*, 246:103–107.
- Ringwood, A.E., 1990, Slab—mantle interactions 3. Petrogenesis of intraplate magmas and structure of the upper mantle. *Chemical Geology*, 82:187–207.
- Ringwood, A.E., and T. Irifune, 1988, Nature of the 650-km seismic discontinuity: implications for mantle dynamics and differentiation. *Nature*, 331:131–136.

- Rocholl, A., M. Stein, M. Molzahn, S.R. Hart, and G. Worner, 1995, Geochemical evolution of rift magmas by progressive tapping of a stratified mantle source beneath the Ross Sea Rift, Northern Victoria Land, Antarctica. *Earth Planet. Sci. Lett.*, 131:207–224.
- Sager, W.W., and M.S. Pringle, 1988, Mid-Cretaceous to early Tertiary apparent polar wander path of the Pacific plate. *J. Geophys. Res.* 93(B10):11753–11771.
- Sandwell, D.T., E.L. Winterer, J. Mammerickx, R.A. Duncan, M.A. Lynch, D.A. Levitt, and C.L. Johnson, 1995, Evidence for diffuse extension of the Pacific plate from the Pukapuka ridges and cross-grain gravity lineations. *J. Geophys. Res.*, 100(B8):15087–15100.
- Saunders, A.D., 1983, Geochemistry of basalts recovered from the Gulf of California during Leg 65 of the Deep Sea Drilling Project, in B.T.R. Lewis, P. Robinson, et al., *Init. Rpts DSDP*, 65:591–621.
- Saunders, A. D., and J. Tarney, 1979, The geochemistry of basalts from a back-arc spreading centre in the East Scotia Sea. *Geochim. Cosmochim. Acta*, 43:555–572.
- Saunders, A. D., and J. Tarney, 1984, Geochemical characteristics of basaltic volcanism within back-arc basins. In, B. P. Kokelaar and M. F. Howells (Eds.), *Marginal Basin Geology: Volcanic and associated sedimentary and tectonic processes in modern and ancient marginal basins*, Geol. Soc. Sp. Pub. No. 16:59–76.
- Saunders, A.D. , D.J. Fornari, and M. A. Morrison, 1982, The composition and emplacement of basaltic magmas produced during the development of continent-margin basins: the Gulf of California, Mexico. *J. geol. Soc. London*, 139:335–346.
- Scientific Event Alert Network, 1993, *Bulletin* for 31 March 1993, Smithsonian Institute, Washington, DC, p.8.
- Silver, E.A., R. von Huene, and J.K. Crouch, 1974, Tectonic significance of the Kodiak-Bowie Seamount chain, northeastern Pacific. *Geology*, 2:147–150.
- Sleep, N.H., 1990, Hotspots and mantle plumes: Some phenomenology. *J. Geophys. Res.*, 95:6715–6736.
- Smellie, J.L., A. Hofstetter, and G. Troll, 1992, Fluorine and boron geochemistry of an ensialic marginal basin volcano: Deception Island, Bransfield Strait, Antarctica. *J. Volcan. Geotherm. Res.*, 49:255–267.
- Smellie, J.L., R.J. Pankhurst, M.J. Hole, and J.W. Thomson, 1988, Age, distribution and eruptive conditions of late Cenozoic alkaline volcanism in the Antarctic Peninsula and eastern Ellsworth land: Review. *British Antarct. Surv. Bull.*, No.80:21–49.
- Smellie, J.L., R.J. Pankhurst, M.R.A. Thomson, and R.E.S. Davies, 1984, The Geology of the South Shetland Islands: VI. Stratigraphy, Geochemistry and Evolution. *British Antarct. Surv. Sci. Reports*, No.87, 85 pp.

- Smellie, J.L., P. Stone, and J. Evans, 1995, Petrogenesis of boninites in the Ordovician Ballantrae Complex ophiolite, southwestern Scotland. *J. Volcan. Geotherm. Res.*, 69:323–342.
- Stern, C.R., F.A. Frey, K. Futa, R.E. Zartman, Z. Peng, and T.K. Kyser, 1990, Trace-element and Sr, Nd, Pb, and O isotopic composition of Pliocene and Quaternary alkali basalts of the Patagonian Plateau lavas of southernmost South America. *Contrib. Mineral. Petrol.*, 104:294–308.
- Stern, R.J., P.-N. Lin, J.D. Morris, M.C. Jackson, P. Fryer, S.H. Bloomer, and E. Ito, 1990, Enriched back-arc basin basalts from the northern Mariana Trough: Implications for the magmatic evolution of back-arc basins. *Earth Planet. Sci. Lett.*, 100:210–225.
- Stewart, R.J., J.H. Natland, and W.R. Glassley, 1973, Petrology of volcanic rocks recovered on DSDP Leg 19 from the North Pacific Ocean and the Bering Sea. in J.S. Creager, D.W. Scholl, et al., *Initial Reports of the Deep Sea Drilling Project*, 19:615–627.
- Stille, P., D.M. Unruh, and M. Tatsumoto, 1986, Pb, Sr, Nd, and Hf isotopic constraints on the origin of Hawaiian basalts and evidence for a unique mantle source. *Geochim. Cosmochim. Acta*, 50:2303–2319.
- Stolper, E., and S. Newman, 1994, The role of water in the petrogenesis of Mariana Trough magmas. *Earth Planet. Sci. Lett.*, 121:293–325.
- Strelin, J.A., H. Carrizo, A. Lopez, and C. Torielli, 1993, Actividad volcánica holocena en la Isla James Ross. *Segundas Jornadas de Comunicaciones Sobre Investigaciones Antárticas, Actes*, 335–340, Buenos Aires.
- Sun, S.-S., 1980, Lead isotopic study of young volcanic rocks from mid-ocean ridges, ocean islands and island arcs. *Phil. Trans. R. Soc. London*, 297:409–445.
- Sun, S.-S., and W.F. McDonough, 1989, Chemical and isotopic systematics of oceanic basalts: implications for mantle composition and processes, in A.D. Saunders and M.J. Norry (eds.), *Magmatism in the Ocean Basins*. Geological Society Special Publication No. 42:313–345.
- Sykes, M.A., 1988, New K-Ar age determinations on the James Ross Island Volcanic Group, north-east Graham Land, Antarctica. *British Antarct. Surv. Bull.*, No.80:51–56.
- Tamaki, K., K. Suyehiro, J. Allan, J.C. Ingle, and K.A. Pisciotto, 1992, Tectonic synthesis and implications of Japan Sea ODP drilling, in K. Tamaki, K. Suyehiro, J. Allan, M. McWilliams, et al., (eds.), *Proc. ODP, Sci. Results*, 127/128, Pt.2, College Station, TX (Ocean Drilling Program), 1333–1348.
- Tatsumi, Y., D.L. Hamilton, and R.W. Nesbitt, 1986, Chemical characteristics of fluid phase released from a subducted lithosphere and origin of arc magmas: Evidence from high-pressure experiments and natural rocks. *J. Volcan. Geotherm. Res.*, 29:293–309.

- Tatsumoto, M., 1994, Origin of Hawaiian Basalts Inferred From Isotopes (ICOG abs.). *U.S.G.S. Circular* 1107, p.316.
- Taylor, B., and G.D. Karner, 1983, On the evolution of marginal basins. *Rev. Geophys. Space Phys.*, 21:1727–1741.
- Taylor, B., G. Brown, P. Fryer, J.B. Gill, A.G. Hochstaedter, H. Hotta, C.H. Langmuir, M. Leinen, A. Nishimura, and T. Urabe, 1990, ALVIN-SeaBeam studies of the Sumisu Rift, Izu-Bonin arc. *Earth Planet. Sci. Lett.*, 100:127–147.
- Turner, D.L., R.D. Jarrard, and R.B. Forbes, 1980, Geochronology and origin of the Pratt-Welker seamount chain, Gulf of Alaska: A new pole of rotation for the Pacific Plate. *J. Geophys. Res.*, 85:6547–6556.
- Unruh, D.M., P. Stille, and M. Tatsumoto, 1987, Pb, Sr, and Nd Isotopic Study of Basalts from the Hawaiian-Emperor Chain (abs.). in *Hawaiian Symposium on How Volcanoes Work*, 260.
- Volpe, A.M., J.D. Macdougall, J.W. and Hawkins, 1988, Lau basin basalts (LBB): trace element and Sr-Nd isotopic evidence for heterogeneity in backarc basin mantle. *Earth Planet. Sci. Lett.*, 90:174–186.
- Volpe, A.M., J.D. Macdougall, G.W. Lugmair, J.W. Hawkins, and P.F. Lonsdale, 1990, Fine-scale isotopic variation in Mariana Trough basalts: evidence for heterogeneity and a recycled component in backarc basin mantle. *Earth Planet. Sci. Lett.*, 100:251–264.
- Walker, D.A., and I. McDougall, 1982,  $^{40}\text{Ar}/^{39}\text{Ar}$  and K–Ar dating of altered volcanic glassy rocks: the Dabi Volcanics. *Geochim. Cosmochim. Acta*, 46:2181–2190.
- Weaver, B.L., 1991, The origin of ocean island basalt end-member compositions: trace element and isotopic constraints. *Earth Planet. Sci. Lett.*, 104:381–397.
- Weaver, S.D., A.D. Saunders, R.J. Pankhurst, and J. Tarney, 1979, A geochemical study of magmatism associated with the initial stages of back-arc spreading. The Quaternary volcanics of Bransfield Strait, from South Shetland Islands. *Contrib. Mineral. Petrol.*, 68:151–169.
- Weis, D., and F.A. Frey, 1991, Isotope geochemistry of Ninetyeast Ridge basalts: Sr, Nd, and Pb evidence for the involvement of the Kerguelen hotspot, In, J.K. Weissel, J. Pearce, E. Taylor, J. Alt, et al. (eds.) *Proc. ODP, Sci. Results*, 121:591–610.
- Weis, D., W.M. White, F.A. Frey, R. Duncan, J. Dehn, M. Fisk, J. Ludden, A. Saunders, and M. Storey, 1992, The influence of mantle plumes in generation of Indian Ocean crust. In, R.A. Duncan, D.K. Rea, R.B. Kidd, U. von Rad, and J.K. Weissel, (eds.) *The Indian Ocean: A Synthesis of Results from the Ocean Drilling Program*, Geophysical Monograph 70:57–89.
- White, W.M., 1985, Sources of oceanic basalts: Radiogenic isotopic evidence. *Geology*, 13:115–118.

- White, W.M., 1993,  $^{238}\text{U}/^{204}\text{Pb}$  in MORB and open system evolution of the depleted mantle. *Earth Planet. Sci. Lett.*, 115:211–226.
- White, W.M. and A.W. Hofmann, 1982, Sr and Nd isotope geochemistry of oceanic basalts and mantle evolution. *Nature*, 296:821–825.
- White, W.M., and J. Patchett, 1984, Hf-Nd-Sr isotopes and incompatible element abundances in island arcs: implications for magma origins and crust-mantle evolution. *Earth. Planet. Sci. Letters*, 67:167–185.
- White, W.M., B. Dupré and Ph. Vidal, 1985, Isotope and trace element geochemistry of sediments from the Barbados Ridge—Demerara Plain region, Atlantic Ocean. *Geochim. Cosmochim. Acta*, 49:1875–1886.
- White, W.M., M.M. Cheatham, and R.A. Duncan, 1990, Isotope geochemistry of Leg 115 basalts and inferences on the history of the Reunion mantle plume, in: *Proc. Ocean Drilling Prog., Sci. Results*, 115:53–61.
- White, W.M., A.R. McBirney, and R.A. Duncan, 1993, Petrology and geochemistry of the Galapagos Islands: Portrait of a pathological mantle plume. *J. Geophys. Res.*, 98:19533–19563.
- Wilson, J.T., 1963, A possible origin of the Hawaiian Islands. *Can. J. Phys.*, 41:863–870.
- Wood, D.A., J.-L. Joron, and M. Treuil, 1979, A re-appraisal of the use of trace elements to classify and discriminate between magma series erupted in different tectonic settings. *Earth Planet. Sci. Letters*, 45:326–336.
- Woodhead, J.D., 1989, Geochemistry of the Mariana arc (western Pacific) source compositions and processes. *Chem Geol.*, 76:1–24.
- Woodhead, J.D., and R.W. Johnson, 1993, Isotopic and trace-element profiles across the New Britain island arc, Papua New Guinea. *Contrib. Mineral. Petrol.*, 113:479–491.
- Worsley, J.R., 1973, Calcareous nannofossils from Leg 19 of the Deep Sea Drilling Project. In Creager, J.S., Scholl, D.W., et al., *Init. Rep. DSDP*, 19: Washington (U.S. Govt. Printing Office), 741–750.
- York, D., 1969, Least-squares fitting of a straight line with correlated errors. *Earth Planet. Sci. Lett.*, 5:320–324.
- Zindler, A., and S. Hart, 1986, Chemical Geodynamics. *Ann. Rev. Earth Planet. Sci.*, 14:493–571.